Solution Properties and Chiral Separation Ability of Cyclic Amylose Carbamates

A Doctoral Thesis

by

Akiyuki Ryoki

Submitted to
the Graduate School of Science, Osaka University
February, 2019

Acknowledgement

This thesis work was carried out from 2013 to 2019 under the direction of Professor Takahiro Sato at the Department of Macromolecular Science, Graduate School of Science, Osaka University. First, I would like to express my sincerest gratitude to Professor Takahiro Sato and Associate Professor Ken Terao for their kindest guidance, valuable suggestion, and discussion during this work. I also would like to extend my gratitude to Professor Akihito Hashidzume for his helpful advice and valuable discussions. I would like to express my deep gratitude to Professor Katsumi Imada and Professor Tadashi Inoue for their careful review and valuable comments.

I would like to express my deep gratitude to Professor Shinichi Kitamura at Osaka Prefecture University for his kindly providing of cyclic amylose samples and fruitful discussion. I am grateful to Dr. Shiho Suzuki and Dr. Makoto Nakaya at Osaka Prefecture University for their kindest teaching for preparation of cyclic amylose samples, and Mr. Yoshihiro Umetani at Osaka Prefecture University, and Associate Professor Masaki Nojiri, Mr. DongChan Kim, Mr. Yuto Kimura and Mr. Daigo Kabata at Osaka University for their kindest help on the preparation. Mr. DongChan Kim and Mr. Yuto Kimura also perform preparation of amylose carbamates and measurements on this work. I would like to extend my gratitude to Professor Katsuhiro Maeda at Kanazawa University and Dr. Yuuya Nagata at Kyoto University for their kindest help on the preparation of chiral columns and valuable discussion. I also would like to express my gratitude to Professor Yoshio Okamoto at Harbin Engineering University for his provision of a part of experimental results obtained previously for chiral columns rerated with this work. I would like to extend my gratitude to Professor Takenao Yoshizaki and Associate Professor Daichi Ida at Kyoto University for allowing us to

use a simulation program for scattering function of the wormlike ring, and their valuable suggestion, and also other members of the NKO academy, Dr. Yoshiyuki Einaga, Professor Yo Nakamura, Associate Professor Atsushi Takano, and Associate Professor Masashi Osa for their fruitful discussion during this work. I am grateful to Ms. Hiromi Yokobatake for her great contribution to this work. I am grateful Dr. Hirokazu Hasegawa at Toray Research Center Inc., Dr. Rintaro Takahashi and Mr. Masaki Kondo for their help on measurements. I also thank Dr. XinYue Jiang for related research of this work and her kind help.

The small angle X-ray scattering experiments in this work were conducted on SPring-8 under the approval of the Japan Synchrotron Radiation Research Institute (JASRI) with the help by Dr. Noboru Ohta, and on KEK-PF under the approval of the Photon Factory Program Advisory Committee with the help by Dr. Noriyuki Igarashi and Dr. Nobutaka Shimizu. This work was financially supported by Grant-in-Aid for JSPS Research Fellow (Proposal No. 18J10648) and Graduate School Honor Program sponsored by the Graduate School of science at Osaka University.

I thank all members of Sato laboratory for their helpful advice and their friendships. Finally, I express my sincerest thanks to my family members and friends for their constant support and warmest encouragements.

February 2019

Akiyuki Ryoki

Contents

Chapter I.

General introduction

I-1. Dilute solution properties of cyclic polymers

Solution properties of polymers are significantly related to their architecture including linear, branched, and cyclic chains. Among them, cyclic chain has one of the simplest architectures since the corresponding linear chain can be obtained from the scission of the cyclic chain. Biological systems indeed utilize some cyclic chains, that is, DNAs, RNAs, peptides, and polysaccharides. High molar mass samples can be obtained for cyclic DNA, of which conformational properties were therefore widely investigated experimentally and theoretically[1,2] while twisting of double helical DNA yields writhe or supercoiled structure even in solution. Cyclic polymers were synthesized by using the end linking reaction of the telechelic polymers,[3–5] or a specially designed enzymatically synthesis of polysaccharide.[6,7] Owing to the difficulties to obtain highly purified cyclic polymers, early studies for dilute solution properties of cyclic polymers were limited to cyclic DNA and relatively filexible ring polymers, *e.g.*, cyclic poly(dimethylsiloxane),[8] cyclic polystyrene,[8] and cyclic amylose.[6,9,10] Such flexible cyclic polymers should have substantially identical local conformation with that of the corresponding linear polymer, although the cyclization introduces the topological constraints which may influence theoretically the dimensions of the chain.[11–14] Furthermore, it was shown both theoretically[12,15–19] and experimentally[20–22] that the intermolecular interaction between cyclic chains also be affectable by the topological interactions arising

from the chain connectivity which inhibits rings from interlocking each other.

On the other hand, cyclic polymers with stiff main chains were hardly synthesized by the end linking reaction, while some theoretical works were reported.[2,23,24] This is owing to the extremely small end-closure probability of rigid linear polymers to synthesize cyclic chains from linear precursor.[2] Except for cyclic DNA, no work has been reported for solution properties of rigid ring polymers. Another strategy to obtain a rigid ring is to stiffen a flexible ring by using some appropriate chemical modification. Recently synthesized grafted ring polymers[25–28] may have stiff main chain. However, the stiffening efficiency for grafted polymers was not so high even though the grafting density is considerably high.[29,30] Very recently, our group[31–33] proposed cyclic amylose carbamate derivatives behave as rigid rings in solution. This thesis work focuses on cyclic amylose carbamates with different side-chain groups.

I-2. Side-chain- and solvent-dependent chain conformation of amylose carbamates

Amylose is a polymer in which glucose units are linked by α-1,4-linkage as shown in Figure I-1. The main-chain conformation of amylose and its derivatives is mainly determined by the two internal rotation angles ψ = O(5)–C(1)–O(1)–C(4′) and ϕ = C(1)–O(1)–C(4′)–C(5′). Both ψ and ϕ have asymmetric distribution for rotation due to the chirality of glucose residues. Thus, the main chain of amylose forms left-handed helix in solution.

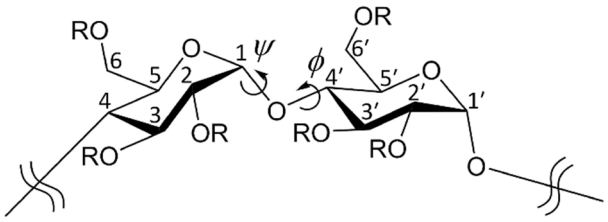

Figure I-1. Chemical structure of amylose (R = H) and its carbamate derivatives (R = CONHR′). Rotation angles ψ and ϕ are defined as the dihedral angles formed by the atoms O(5)–C(1)–O(1)–C(4′) and C(1)–O(1)–C(4′)–C(5′), respectively.

Fully substituted amylose carbamates can be synthesized by reactions of amylose with the corresponding isocyanate. Dilute solution properties of amylose tris(phenylcarbamate) (ATPC) have been widely investigated since 1960s, owing to its good solubility for various organic solvents.[34-47] In these reports, analyses of molar mass dependence of the radius of gyration $\langle S^2\rangle^{1/2}$ and of the intrinsic viscosity $[\eta]$ revealed that ATPC in solution has relatively high chain stiffness, which is characterized in terms of the Kuhn segment length λ^{-1} or the persistence length. However, since the local helical conformation of amylose backbone sensitively depends on solvents, it was not easy to determine λ^{-1} without uncertainty in contrast with most of stiff chains including cellulose of which local conformation in solution is approximately identical with that in crystal.[48]

Recent development of synchrotron-radiation small angle X-ray scattering (SAXS) allows us to determine highly accurate particle scattering function $P(q)$ of polymer chains in solution, which makes it possible to characterize the chain conformation without uncertainty. Recently, Terao *et al.* characterized the chain conformation of ATPC,[49–52] amylose tris(3,5-dimethylphenilcarbamate) (ADMPC),[52] amylose tris(ethylcarbamate) (ATEC)[53], amylose

tris(*n*-butylcarbamate) (ATBC)[54–56], and amylose tris(*n*-hexylcarbamate) (ATHC)[53] in various solvents, using $P(q)$ obtained by SAXS as well as $\langle S^2 \rangle^{1/2}$ and $[\eta]$ to determine λ^{-1} and the helix pitch (or helix rise) per residue h (Figure I-2); the latter parameter is related to the local helical structure. The resultant h values for the amylose derivatives varied from 0.25 to 0.42 nm depending on the side chain and solvent, and such variable h value had to be considered in characterizing the conformation of amylose derivatives. The determined λ^{-1} value also significantly depends on the side chain and solvent.

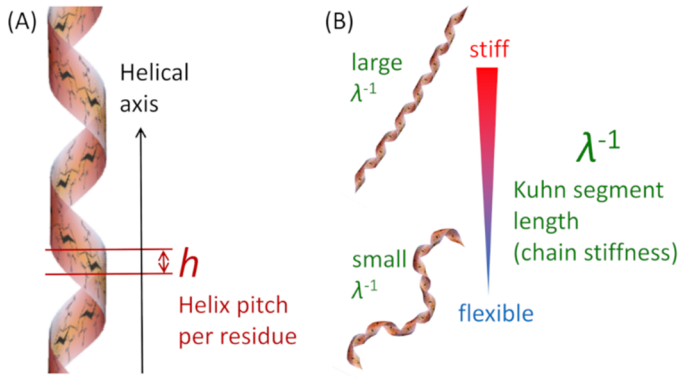

Figure I-2. Schematic representation of helix pitch per residue h (A) and the Kuhn segment length λ^{-1} (B).

From infrared absorption and optical rotation measurements, it turned out that solvent dependence of the main-chain conformation of ATEC and ATBC is related to the intramolecular hydrogen bonding between NH and C=O groups on the adjacent carbamate groups, indicating that the hydrogen bonds significantly restricts the internal rotation of the amylosic main chain as illustrated in Figure I-3A. The chain stiffness of these amylose derivatives was the highest in THF in which 50 – 60 % of C=O groups form intramolecular

hydrogen bonding with NH groups, and concentrated THF solutions of ATEC, ATBC, and ATHC exhibited lyotropic liquid crystallinity.[57]

On the other hand, solvent molecules forming hydrogen bonding with the carbamate groups of the amylose derivatives (Figure I-3B) also play an important role for the main chain conformation. Both h and λ^{-1} of ATPC increase with increasing the molar volume of the solvent having C=O group, suggesting that hydrogen-bonding solvent molecules restrict the internal rotation to extend and stiffen the main chain.[51] This solvent-dependent chain stiffness is more significantly observed for ADMPC.[52]

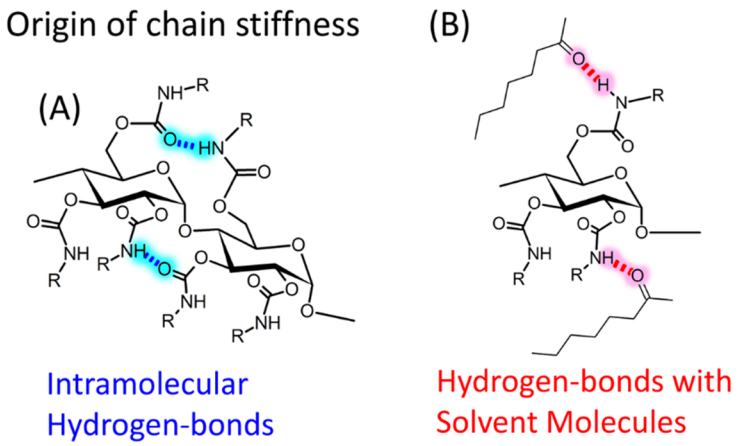

Figure I-3. Origin of the chain stiffness of amylose carbamates in solution. (A) Intramolecular hydrogen bonds. (B)Hydrogen bonding solvent molecules.

I-3. Conformational characterization of cyclic amylose carbamates

As indicated in Figure I-4, the direct cyclization of linear amylose carbamates is difficult because of the low ring-closure probability, nevertheless the cyclic amylose may be

able to make stiffen by full substitution with the corresponding isocyanate. Recently, Terao *et al.* synthesized cyclic ATPC (cATPC)[31] and cyclic ATBC (cATBC)[33] from enzymatically synthesized cyclic amylose samples by substituting phenyl isocyanate and *n*-butyl isocyanate, respectively. Dimensional and hydrodynamic properties of the cATPC and cATBC samples demonstrated the stiff ring nature in solution. However, the dilute solution properties for cATPC in a ketone cannot be explained by the wormlike ring model with h and λ^{-1} for the linear ATPC chain over the whole molar mass range studied.[32]

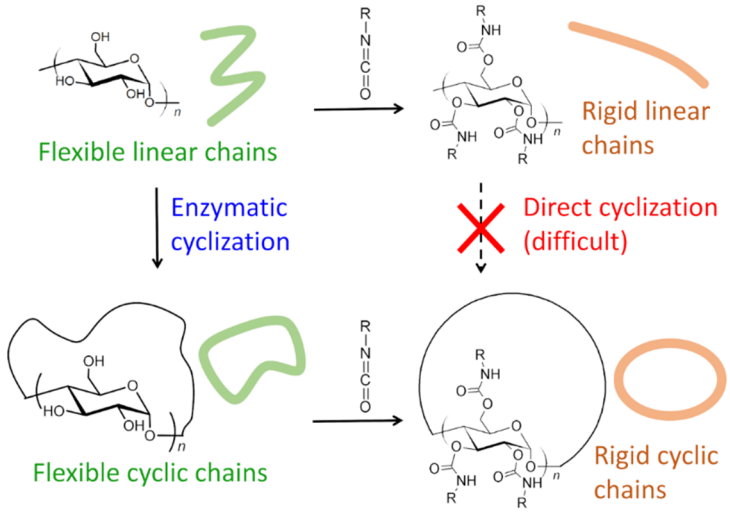

Figure I-4. Schematic illustration of the synthetic pathway for cyclic amylose carbamates, of which main chains have high stiffness in solution.

For rigid amylose derivatives, the local helix conformation of the cyclic chain is not necessarily identical with that of the linear chain, due to the ring closure restriction. This restriction is more severe for lower molar mass cyclic chain, so that the wormlike chain parameters h and λ^{-1} may depend on the molar mass of the cyclic chain. Molar mass

dependences of $\langle S^2 \rangle^{1/2}$, $[\eta]$, and the hydrodynamic radius are analyzed using the wormlike chain model usually on the assumption that both h and λ^{-1} do not depend on the molar mass. This assumption may not hold for rigid cyclic amylose derivatives. Consequently, the conventional wormlike chain analysis cannot be applied to them. One might determine the wormlike chain parameters by comparing experimental SAXS particle scattering function $P(q)$ for a single molar mass sample with the theoretical $P(q)$, but no theoretical $P(q)$ for the wormlike ring had been available so far.

Very recently, Ida *et al.* developed a Monte-Carlo simulation method[58] to calculate theoretical $P(q)$ of the wormlike ring model. This method allows us to determine the two parameters, h and λ^{-1}, for each cyclic amylose carbamate sample. The main purpose of the present thesis work is to determine the wormlike chain parameters for cyclic amylose carbamates with different side-chain groups in different solvents using this theoretical $P(q)$ to be compared with the parameters of the linear analogues.

I-4. Chiral separation of amylose carbamates

Owing to the chirality of polysaccharides, many polysaccharide derivatives, including amylose carbamates, are utilized as chiral stationary phases of liquid chromatography.[59–63] The chiral recognition ability to racemates may arise from the local helical structure of polysaccharide chains which can fit to one enantiomer of the racemates (Figure I-5). Thus, the local helical structure plays an important role. Chiral separation ability of amylose and cellulose carbamates were investigated by ^{1}H NMR, infrared spectroscopy, X-ray diffraction,

and computer simulation.[64–67] However, the effect of the local helical structure on the chiral separation ability is still unclear, because of the above-mentioned variable local helical structures of the amylosic chain and of weak chiral interactions.

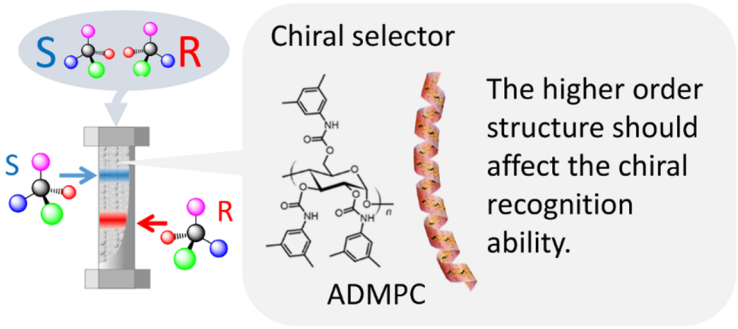

Figure I-5. Chemical structure and schematic illustration of local helical structure and chiral columns.

As mentioned above, the local helical structure of cyclic amylose carbamates is different from that of the linear analogues. Furthermore, we also found that the helical structure of ATBC in chiral solvents depends on the chirality of solvent, that is, $_{D}$- and $_{L}$-ethyl lactates.[56] Therefore, we expected that the chiral recognition ability of the cyclic amylose carbamates may be different from that of the linear analogues. Another purpose of the present thesis work is to investigate the recognition ability of the cyclic amylose carbamates to be compared with that of the linear analogues. In this study, we chose ADMPC and cADMPC because ADMPC is widely used as a chiral selector of chiral columns of high performance liquid chromatography (HPLC).

I-5. Scope of this research

The aim of this dissertation is to clarify conformations of semiflexible and/or rigid cyclic amylose carbamate derivatives, and to compare the conformations with their chiral separation ability.

Chapter II explains the Monte Carlo simulation method recently reported by Tsubouchi[58] *et al.* to calculate theoretical $P(q)$ of the wormlike rings, which is important to analyze the conformations of cyclic amylose carbamate derivatives. This method is applied to $P(q)$ for cATBC[33] and cATPC[31,32] recently obtained by SAXS in order to investigate their molar mass dependence of the local conformation (h and λ^{-1}) in solution.

Chapter III concerns the local helical structure of cADMPC. Five cADMPC samples ranging in the weight-average molar mass M_w from 1.4×10^4 to 9.1×10^4 g mol^{-1} were obtained from enzymatically synthesized cyclic amylose. SAXS measurements were performed for the cADMPC samples in MEA, MIBK, and THF at 25 °C to determine $P(q)$ and $\langle S^2 \rangle^{1/2}$. The $P(q)$ data were analyzed in terms of the wormlike ring model to determine h and λ^{-1}, as in Chapter II. These parameters for the cyclic chains were compared with those for the linear chains.

It may be interesting to study whether the bulkiness of the substituent affects the difference in the local conformation between linear and cyclic amylose carbamates. Chapter IV describes the local conformation of linear and cyclic amylose tris(*n*-octadecylcarbamate)s (cATODC and ATODC) in solution. Seven ATODC samples ranging in M_w from 2.4×10^4 to 1.5×10^6 g mol^{-1} and seven cATODC samples of which M_w are from 3.6×10^4 to

1.9×10^5 g mol^{-1} were prepared to characterize their conformation in THF, in 2-octanone (MHK), and in *tert*-butyl methyl ether (MTBE). Light and small-angle X-ray scattering and viscosity measurements in dilute solution were employed to determine the $P(q)$, $\langle S^2 \rangle^{1/2}$, and $[\eta]$. The obtained data were analyzed in terms of the wormlike chain and wormlike ring models to determine h and λ^{-1}.

Chapter V deals with the chiral separation ability of cADMPC. Three cADMPC samples and ADMPC samples were coated on macro-porous silica gel as a carrier to obtain coated-type chiral stationary phases. The resultant silica gel samples were packed into stainless steel columns. ADMPC and cADMPC having 3-(triethoxysilyl)propyl linkers (cADMPCi and ADMPCi) were synthesized in order to prepare immobilized-type columns of cADMPC and ADMPC. The cADMPCi and ADMPCi samples were cross-linked on the silica gel and packed into stainless steel columns. Each column was connected with conventional HPLC system. Racemate samples were separated on each column to evaluate the chiral separation ability of the column using hexane/2-propanol, which mixing ration is 90/10 and 99/1 in the original volume, as the eluent. Chiral separation ability of cADMPC and cADMPCi columns were compared with that of ADMPC and ADMPCi columns.

The main findings and conclusions from this research are summarized in Chapter VI.

Reference

(1) Bates, A. D.; Maxwell, A. *DNA Topology*; Oxford University Press: New York, U.S.A., 2005.

(2) Yamakawa, H.; Yoshizaki, T. *Helical Wormlike Chains in Polymer Solutions*, 2nd ed.; Springer: Berlin, Heidelberg, 2016.

(3) Laurent, B. A.; Grayson, S. M. *Chem. Soc. Rev.* **2009**, *38*, 2202.

(4) Tu, X.-Y.; Liu, M.-Z.; Wei, H. *J. Polym. Sci. Part A Polym. Chem.* **2016**, *54*, 1447–1458.

(5) Josse, T.; De Winter, J.; Gerbaux, P.; Coulembier, O. *Angew. Chemie Int. Ed.* **2016**, *55*, 13944–13958.

(6) Nakata, Y.; Amitani, K.; Norisuye, T.; Kitamura, S. *Biopolymers* **2003**, *69*, 508–516.

(7) Takaha, T.; Yanase, Mi.; Takata, H.; Okada, S.; Smith, S. M. *J. Biol. Chem.* **1996**, *271*, 2902–2908.

(8) *Cyclic Polymers*; Semlyen, J. A., Ed.; Elsevier: London; New York, 1986.

(9) Kitamura, S.; Isuda, H.; Shimada, J.; Takada, T.; Takaha, T.; Okada, S.; Mimura, M.; Kajiwara, K. *Carbohydr. Res.* **1997**, *304*, 303–314.

(10) Shimada, J.; Kaneko, H.; Takada, T.; Kitamura, S.; Kajiwara, K. *J. Phys. Chem. B* **2000**, *104*, 2136–2147.

(11) Abe, H.; Ida, D. *Polymers (Basel).* **2016**, *8*, 271.

(12) des Cloizeaux, J. *J. Phys. Lettres* **1981**, *42*, 433–436.

(13) Grosberg, A. Y. *Phys. Rev. Lett.* **2000**, *85*, 3858–3861.

(14) Moore, N. T.; Lua, R. C.; Grosberg, A. Y. *Proc. Natl. Acad. Sci.* **2004**, *101*, 13431–13435.

(15) Edwards, S. F. *Proc. Phys. Soc.* **1967**, *91*, 513–519.

(16) Edwards, S. F. *J. Phys. A Gen. Phys.* **1968**, *1*, 303.

(17) Iwata, K.; Kimura, T. *J. Chem. Phys.* **1981**, *74*, 2039–2048.

(18) Iwata, K. *Macromolecules* **1985**, *18*, 115–116.

(19) Tanaka, F. *J. Chem. Phys.* **1987**, *87*, 4201–4206.

(20) Roovers, J.; Toporowski, P. M. *Macromolecules* **1983**, *16*, 843–849.

(21) Huang, J.; Shen, J.; Li, C.; Liu, D. *Makromol. Chemie* **1991**, *192*, 1249–1254.

(22) Takano, A.; Kushida, Y.; Ohta, Y.; Masuoka, K.; Matsushita, Y. *Polymer (Guildf).* **2009**, *50*, 1300–1303.

(23) Ida, D. *Polym. J.* **2014**, 1–6.

(24) Ida, D. *React. Funct. Polym.* **2018**, *130*, 111–117.

(25) Schappacher, M.; Deffieux, A. *J. Am. Chem. Soc.* **2008**, *130*, 14684–14689.

(26) Doi, Y.; Iwasa, Y.; Watanabe, K.; Nakamura, M.; Takano, A.; Takahashi, Y.; Matsushita, Y. *Macromolecules* **2016**, *49*, 3109–3115.

(27) Lahasky, S. H.; Serem, W. K.; Guo, L.; Garno, J. C.; Zhang, D. *Macromolecules* **2011**, *44*, 9063–9074.

(28) Zhang, K.; Tew, G. N. *ACS Macro Lett.* **2012**, *1*, 574–579.

(29) Zhang, B.; Gröhn, F.; Pedersen, J. S.; Fischer, K.; Schmidt, M. *Macromolecules* **2006**, *39*, 8440–8450.

(30) Nakamura, Y.; Norisuye, T. In *Soft Matter Characterization*; Springer Netherlands: Dordrecht, 2008; pp 235–286.

(31) Terao, K.; Asano, N.; Kitamura, S.; Sato, T. *ACS Macro Lett.* **2012**, *1*, 1291–1294.

(32) Asano, N.; Kitamura, S.; Terao, K. *J. Phys. Chem. B* **2013**, *117*, 9576–9583.

(33) Terao, K.; Shigeuchi, K.; Oyamada, K.; Kitamura, S.; Sato, T. *Macromolecules* **2013**, *46*, 5355–5362.

(34) Burchard, W. *Zeitschrift für Phys. Chemie* **1964**, *42*, 293–313.

(35) Cowie, J. M. G. *Biopolymers* **1965**, *3*, 69–78.

(36) Burchard, W. *Die Makromol. Chemie* **1965**, *88*, 11–28.

(37) Bittiger, H.; Keilich, G. *Biopolymers* **1969**, *7*, 539–556.

(38) Banks, W.; Greenwood, C. T.; Sloss, J. *Makromol. Chemie* **1970**, *140*, 109–118.

(39) Banks, W.; Greenwood, T.; Sloss, J. *J. Chem. Phys.* **1970**, *140*, 119–129.

(40) Banks, W.; Greenwood, C. T.; Sloss, J. *Eur. Polym. J.* **1971**, *7*, 263–273.

(41) Banks, W.; Greenwood, C. T.; Sloss, J. *Eur. Polym. J.* **1971**, *7*, 879–888.

(42) Banks;, W.; Greenwood, C. T. *Makromol. Chemie* **1971**, *144*, 135–153.

(43) Burchard, W. *Br. Polym. J.* **1971**, *3*, 214–221.

(44) Sutter, W.; Burchard, W. *Makromol. Chemie* **1978**, *179*, 1961–1980.

(45) Gupta, A. K.; Marchal, E.; Burchard, W.; Pfannemüller, B. *Macromolecules* **1979**, *12*, 281–284.

(46) Pfannemüller, B.; Schmidt, M.; Ziegast, G.; Matsuo, K. *Macromolecules* **1984**, *17*, 710–716.

(47) Muroga, Y.; Hayashi, K.; Fukunaga, M.; Kato, T.; Shimizu, S.; Kurita, K. *Biophys. Chem.* **2006**, *121*, 96–104.

(48) Norisuye, T. *Prog. Polym. Sci.* **1993**, *18*, 543–584.

(49) Terao, K. *J. Phys. Conf. Ser.* **2009**, *184*, 012006.

(50) Terao, K.; Fujii, T.; Tsuda, M.; Kitamura, S.; Norisuye, T. *Polym. J.* **2009**, *41*, 201–207.

(51) Fujii, T.; Terao, K.; Tsuda, M.; Kitamura, S.; Norisuye, T. *Biopolymers* **2009**, *91*, 729–736.

(52) Tsuda, M.; Terao, K.; Nakamura, Y.; Kita, Y.; Kitamura, S.; Sato, T. *Macromolecules* **2010**, *43*, 5779–5784.

(53) Terao, K.; Maeda, F.; Oyamada, K.; Ochiai, T.; Kitamura, S.; Sato, T. *J. Phys. Chem. B* **2012**, *116*, 12714–12720.

(54) Sano, Y.; Terao, K.; Arakawa, S.; Ohtoh, M.; Kitamura, S.; Norisuye, T. *Polymer (Guildf).* **2010**, *51*, 4243–4248.

(55) Terao, K.; Murashima, M.; Sano, Y.; Arakawa, S.; Kitamura, S.; Norisuye, T. *Macromolecules* **2010**, *43*, 1061–1068.

(56) Arakawa, S.; Terao, K.; Kitamura, S.; Sato, T. *Polym. Chem.* **2012**, *3*, 472–478.

(57) Oyamada, K.; Terao, K.; Suwa, M.; Kitamura, S.; Sato, T. *Macomolecules* **2013**, *46*, 4589–4595.

(58) Tsubouchi, R.; Ida, D.; Yoshizaki, T.; Yamakawa, H. *Macromolecules* **2014**, *47*, 1449–1454.

(59) Shen, J.; Okamoto, Y. *Chem. Rev.* **2016**, *116*, 1094–1138.

(60) Yashima, E. *J. Chromatogr. A* **2001**, *906*, 105–125.

(61) Ikai, T.; Okamoto, Y. *Chem. Rev.* **2009**, *109*, 6077–6101.

(62) Okamoto, Y. *J. Polym. Sci. A Polym. Chem.* **2009**, *47*, 1731–1739.

(63) Okamoto, Y.; Kaida, Y. *J. Chromatogr. A* **1994**, *666*, 403–419.

(64) Yamamoto, C.; Yashima, E.; Okamoto, Y. *J. Am. Chem. Soc.* **2002**, *124*, 12583–12589.

(65) Kasat, R. B.; Zvinevich, Y.; Hillhouse, H. W.; Thomson, K. T.; Wang, N.-H. L.; Franses, E. I. *J. Phys. Chem. B* **2006**, *110*, 14114–14122.

(66) Kasat, R. B.; Wang, N.-H. L.; Franses, E. I. *J. Chromatogr. A* **2008**, *1190*, 110–119.

(67) Kasat, R. B.; Franses, E. I.; Wang, N.-H. L. *Chirality* **2010**, *22*, 565–579.

Chapter II.

Scattering function of semi-rigid cyclic polymers analyzed in terms of wormlike rings: cyclic amylose tris(phenylcarbamate) and cyclic amylose tris(*n*-butylcarbamate)

II-1. Introduction

The local conformation of ring or cyclic chains is substantially the same as that of their linear analogs if the chain length is sufficiently longer than the Kuhn segment length λ^{-1}, which is the chain stiffness parameter of the Kratky–Porod wormlike chain.[1] The discrepancy between cyclic and linear polymers may become significant upon shortening or stiffening the main chain because the difference in the curvature distribution becomes prominent owing to the topological constraint. Little is known, however, about the chain stiffness (or length) -dependent local conformational change, except for the case of the super-helical structure of cyclic DNA,[2] although abundant studies have examined the physical properties of rather flexible cyclic polymers including polystyrene,[3–9] polydimethylsiloxane[10,11] and polysaccharides.[12–15] A variety of novel cyclic polymers have recently been reported not only for fundamental synthetic studies, but also for building blocks of higher order structures consisting of amphiphilic block copolymers.[16–19] Considering that dense macrocyclic comb polymers that should have relatively stiff main chains form tube-like complexes,[20] the chain stiffness effect on the dimensional properties and intermolecular interactions should be an important topic.

Semi-flexible and rigid cyclic polymers were recently obtained by means of 'stiffening' the main chain of rather flexible cyclic chains. Cyclic amylose tris(phenylcarbamate) (cATPC)[21] and cyclic amylose tris(*n*-butylcarbamate) (cATBC)[22] prepared from enzymatically synthesized cyclic amylose[23] behave as semi-flexible and/or rigid cyclic macromolecules in solution. The molar mass dependence of the mean square radius of gyration $\langle S^2 \rangle$ for cATPC and cATBC in various solvents is fairly explained by current theories for the cyclic wormlike chain[24] with the parameters, λ^{-1} and the helix pitch (or helix rise) h per unit chain length, determined for the corresponding linear chains.[21,22] The h and λ^{-1} values for cATPC in some ketones and esters are, however, appreciably smaller than the theoretical values calculated with the parameters so determined.[25] This suggests that both the local helical structure and the chain stiffness depend on the molar mass of the cyclic polymer chains. Although the particle scattering function $P(q)$ was determined as a function of the magnitude q of the scattering vector for the two cyclic polymers in different solvents,[21,22] appropriate theories or simulation data were not yet available for semi-rigid cyclic chains. Recently, Ida and colleagues[26,27] calculated $P(q)$ for wormlike rings with a variety of reduced chain lengths, that is, the ratio of the contour length L to λ^{-1} or the Kuhn segment number N_K, allowing us to compare them with experimental $P(q)$ data. We thus reanalyzed the previously published $P(q)$ data to discuss the difference between the molecular structures of linear and cyclic amylose derivatives in solution.

II-2. Materials and Methods

II-2-1. $P(q)$ for cATPC and cATBC

The previously reported $P(q)$ data for cATPC[21,25] in 1,4-dioxane (DIOX), 2-ethoxyethanol (2EE), methyl acetate (MEA), ethyl acetate (EA), and 4-methyl-2-pentanone (MIBK) and cATBC[22] in methanol (MeOH), 2-propanol (2PrOH), and tetrahydrofuran (THF) were obtained at the BL40B2 beamline in SPring-8 and the BL-10C beamline in KEK-PF. They were obtained for five cATPC and nine cATBC samples ranging in weight-average molar mass M_w between 1.25×10^4 g mol^{-1} and 1.49×10^5 g mol^{-1} for cATPC and 1.60×10^4 g mol^{-1} and 1.11×10^5 g mol^{-1} for cATBC, corresponding to numbers of saccharide units between 24 and 290 for the former polymer, and between 35 and 240 for the latter. The dispersity index $Đ$ defined as the ratio of M_w to the number-average molar mass was estimated to be 1.05–1.23.

II-2-2. Calculation for theoretical $P(q)$ for semi-flexible rings

Monte Carlo simulations were performed using the method reported by Ida *et al.*[27,28] to calculate the particle scattering function $P_0(q)$ of wormlike rings without chain thickness as a function of N_K ($\equiv \lambda L$). A discrete wormlike chain model originally proposed by Frank-Kamenetskii *et al.*[29] was used with the bond number being 200. For each N_K, 10^5 configurations were generated to obtain an ensemble average with the appropriate monitoring steps. According to our previous study,[21,22] the chain thickness significantly affects $P(q)$ at a relatively high q range. The relationship can be considered by means of the touched bead

model[30,31] as follows:

$$P(q) = 9\left(\frac{2}{qd_b}\right)^6 \left(\sin\frac{qd_b}{2} - \frac{qd_b}{2}\cos\frac{qd_b}{2}\right)^2 P_0(q) \qquad \text{(II-1)}$$

where d_b denotes bead diameter. Since actual cATPC and cATBC samples have finite molar mass distributions, the z-average particle scattering function $P_z(q)$ with a log-normal distribution was calculated numerically to compare the experimental data.

II-3. Results and discussions

II-3-1. Comparison between the experimental $P(q)$ data and the theoretical values of the wormlike ring model

The calculated $P_z(q)$ or $P(q)$ values with the best fit parameters λ^{-1} and h for cATBC in three solvents are plotted in Figure II-1. The calculated values of $P_z(q)$ with appropriate $Đ$ =1.05 (blue) and $Đ$ = 1.20 (red) well explain the behavior of the experimental data, while those of $P(q)$ for the monodisperse ring (green) slightly deviate downward in the middle-q range from the experimental values for the lower-M_w samples. Good agreement was observed between the simulation and experimental data for cATPC in six solvent systems (Figure II-2). We note that the values of λ^{-1} can be determined without ambiguity only for the samples with high M_w, for which the theoretical values for the rigid ring calculated with the appropriate h value (black dot-dashed curves) underestimate $P(q)$ at approximately q = 0.2 nm^{-1}. We then adopted the λ^{-1} value determined for the samples with high M_w to calculate $P_z(q)$ or $P(q)$ for the samples with low M_w. We also note that

$P_z(q)$ and $P(q)$ become insensitive to changes in λ^{-1} with decreasing M_w. The other two parameters, h and d_b, were uniquely determined for more samples, except for the two lowest M_w samples, for both cATBC and cATPC. The latter parameter d_b was consistent with those for the corresponding linear chain within ±11% if we estimate d_b for the linear polymer from the literature chain diameter d values[32–35] for the cylinder model by means of the known relationship $d_b = 1.118\ d$.[36] The negligible difference between the $P(q)$ data for the discrete wormlike chain and those for the continuous rigid cyclic chain in the high q region supports that the current simulation results are substantially the same as those for the continuous chain.

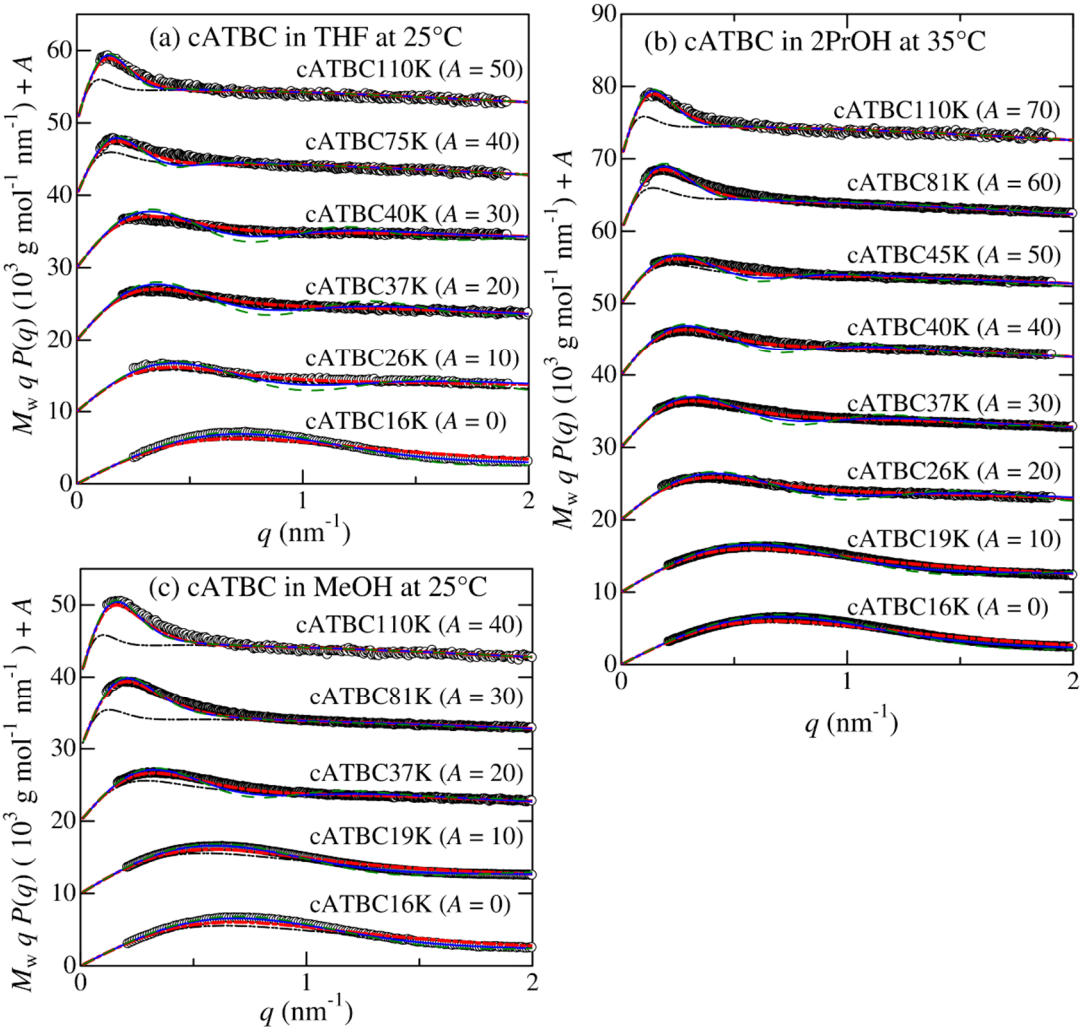

Figure II-1. Comparison between the experimental $P(q)$ data[22] (unfilled circles) and the theoretical values for the indicated cATBC samples in tetrahydrofuran (THF) at 25 °C (a), in 2-propanol (2PrOH) at 35 °C (b) and in methanol (MeOH) at 25 °C (c). Dashed green, solid blue and dot-dashed red curves are the simulation values for the wormlike ring model with the dispersity index $Đ$ = 1.00, 1.05 and 1.20, respectively. The double-dot-dashed black curve represents the theoretical values for the rigid ring ($Đ$ = 1.2). The ordinate values are shifted by A for clarity.

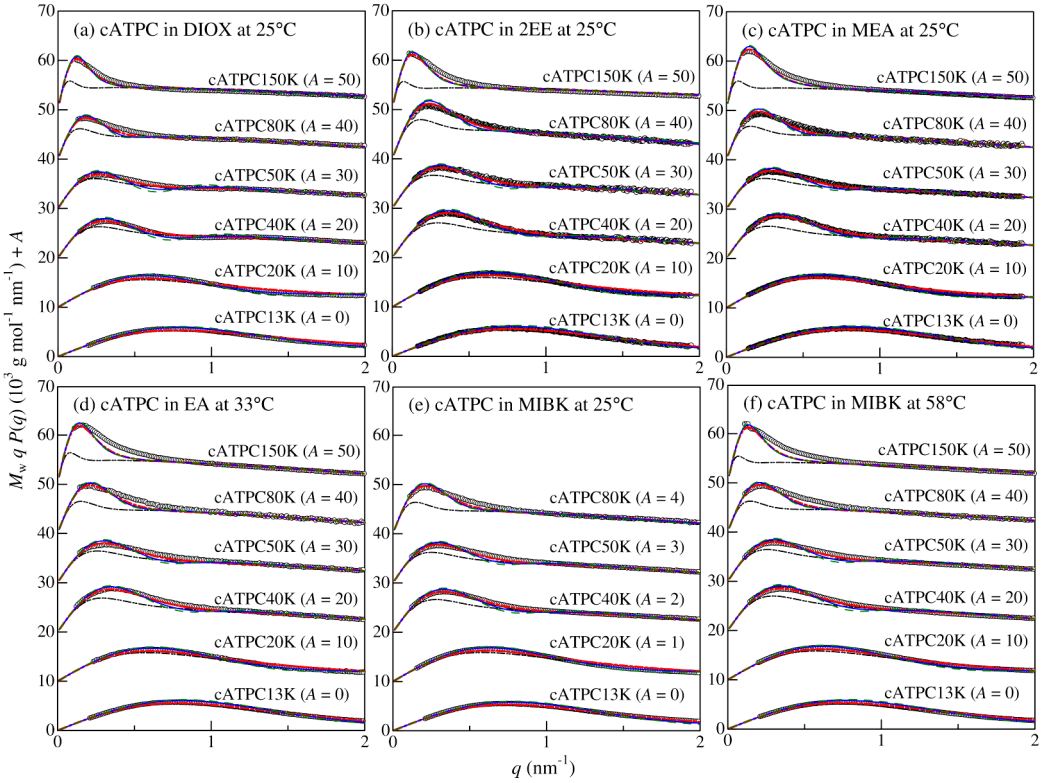

Figure II-2. Comparison between the experimental $P(q)$ data[21,25] (black unfilled circles) and the calculated values for the indicated cATPC samples in 1,4-dioxane (DIOX) at 25 °C (a), in 2-ethoxyethanol (2EE) at 25 °C (b), in methyl acetate (MEA) at 25 °C (c), in ethyl acetate (EA) at 33 °C (d), and in 4-methyl-2-pentanone (MIBK) at 25 °C (e) and at 58 °C (f). Dashed green, solid blue and dot-dashed red curves, simulation values for the wormlike ring model with the dispersity index $Đ$ = 1.00, 1.05, and 1.20, respectively. Double-dots-dashed black curve, theoretical values for rigid ring. The ordinate values are shifted by A for clarity.

II-3-2. Molar mass dependence of the wormlike parameters

The determined λ^{-1} and h values are plotted against M_w in Figure II-3. The λ^{-1} value for cATBC in THF is much smaller than that for the linear ATBC. This difference is clearly recognized from the fact that the calculated values of $P_z(q)$ and $P(q)$ for cATBC in THF with

the parameters determined for linear ATBC (h = 0.28 nm and λ^{-1} = 75 nm) are appreciably smaller than the experimental values, as shown in Figure II-4. On the other hand, the theoretical values of $\langle S^2 \rangle$ for wormlike rings calculated from the Shimada–Yamakawa equation[24] with the parameters determined currently for cATBC (h=0.33 nm and λ^{-1}=20 nm) and those calculated using the previously estimated values (h=0.28 nm and λ^{-1}=75 nm)[22] assuming λ^{-1} for linear ATBC[34] are indistinguishable in the investigated M_w range, as shown in Figure II-5. This indicates that the wormlike chain parameters for this system cannot be determined from the reported $\langle S^2 \rangle$ data alone. When we consider that the wormlike chain parameters of infinitely long cyclic chains should be the same as those for the corresponding linear chains, as mentioned in the Section II-1, it is expected that a molar mass-dependent chain stiffness could be observed in the higher molar mass range. In the case of h, its values for most cases of cyclic chains are fairly identical to those of the corresponding linear chains, except for cATPC in MIBK, cATPC in EA, cATBC in THF and cATBC in 2PrOH. The former two polymer-solvent systems are rather specific because hydrogen bonding solvent molecules extend and stiffen the linear ATPC, while in the latter cases, the rigid helical main chain of ATBC in THF (or 2PrOH) is extended by the cyclization similarly to the case with bended helical springs. This local structural change also reduces the chain stiffness of the main chain of cATBC. It is however noted that this local structural change is insensitive to the solution infrared absorption, which reflects the intramolecular hydrogen bonds.[22]

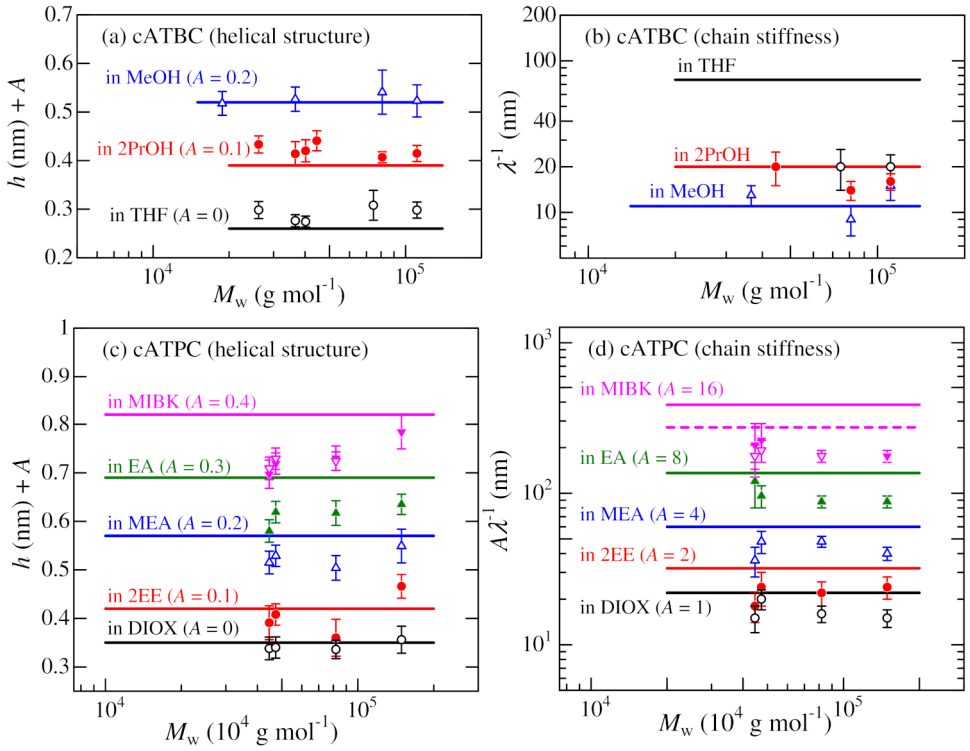

Figure II-3. Weight-average molar mass M_w dependence of the wormlike chain parameters for cATBC and cATPC in solution. In (a, b), the unfilled circles, filled circles and triangles indicate the parameters for cATBC in THF at 25 °C, in 2PrOH at 33 °C and in MeOH at 25 °C, respectively. The solid lines are h or λ^{-1} for the corresponding linear chain. In (c, d), the unfilled circles, filled circles, unfilled triangles, filled triangles, unfilled inverted triangles and filled inverted triangles represent the parameters for cATPC in DIOX at 25 °C, in 2EE at 25 °C, in MEA at 25 °C, in EA at 33 °C, and in MIBK at 25 and 58 °C, respectively. The solid and dashed magenta lines in (d) are the λ^{-1} values for linear ATPC in MIBK at 25 and 58 °C, respectively. The ordinate values are shifted by A for clarity.

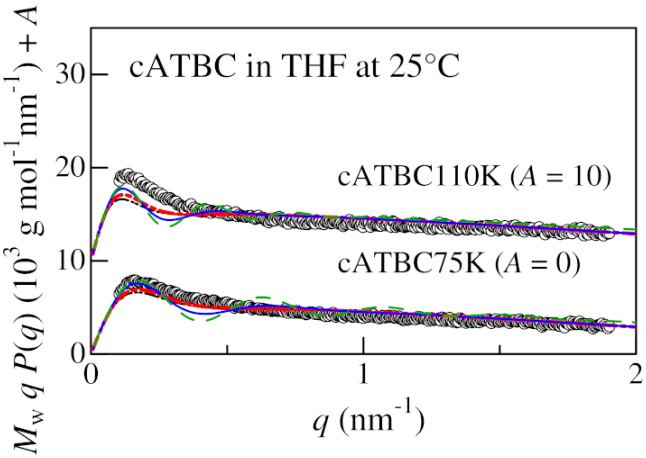

Figure II-4. Comparison between the experimental $P(q)$ data[22] (black unfilled circles) and the calculated values for the indicated cATBC samples in tetrahydrofuran (THF) at 25 °C. Dashed green, solid blue and dot-dashed red curves, simulation values for the wormlike ring model with the chain stiffness parameters of linear ATBC (λ^{-1} = 75 nm and h = 0.28 nm) and with the dispersity index $Đ$ = 1.00, 1.05, and 1.20, respectively. Double-dots-dashed black curve, theoretical values for rigid ring. The ordinate values are shifted by A for clarity.

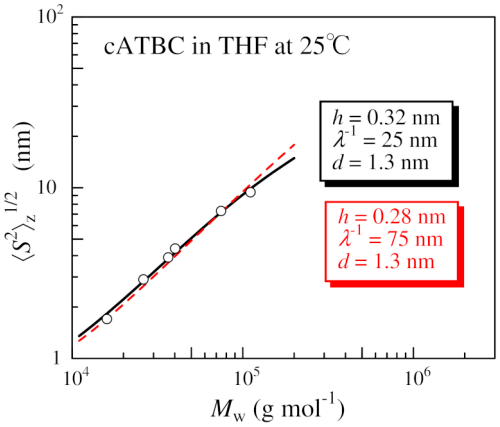

Figure II-5. Weight-average molar mass M_w dependence of the z-average mean square radius of gyration $\langle S^2 \rangle_z$ for cATBC in THF at 25 °C.[22] Solid (black) and dashed (red) curves, theoretical values for cylindrical wormlike ring calculated with the indicated parameters in terms the Shimada-Yamakawa scheme.[24]

II-3-3. Comparison between the Kuhn segment number of linear and cyclic chains

The Kuhn segment numbers $N_{K,ring}$ for cATBC and cATPC are plotted against that for the corresponding linear chain $N_{K,linear}$ in Figure II-6. Note that $N_{K,linear}$ was calculated from the wormlike chain parameters reported for the corresponding linear chain with the same M_w. This number is well-known as a universal parameter that mainly reflects the chain conformation of unperturbed linear polymer chains in solution.

Interestingly, in the range of $N_{K,linear} > 1.5$, $N_{K,ring}$ is fairly close to $N_{K,linear}$, in contrast to the case of cATBC in THF in the range of $N_{K,linear} < 1$, for which λ^{-1} is clearly smaller than that of the linear ATBC (Figure II-3b). The threshold value 1.0 – 1.5 of N_K is close to the value at which the (angle-independent) ring closure probability for the (linear) wormlike chain significantly increases.[37] It is however noted that $N_{K,ring}$ for ATPC in EA and MIBK is incidentally close to $N_{K,linear}$, although h and λ^{-1} for cATPC are smaller than those for linear ATPC (Figure II-3c and d). As mentioned above and in previous papers,[25,38] the origin of the chain stiffness of these systems is different from that of other systems. We may thus conclude that some strain effects for cyclic chains arising from the relaxation of the internal-rotation-angle distribution in their main chain become appreciable for shorter (stiffer) cyclic chains with small N_K. In contrast, λ^{-1} for the cyclic chain is substantially the same as that for the corresponding linear chain when N_K is larger, and the local helical structure of the cyclic chain is almost identical to that of the corresponding linear chain. Although such a threshold value of N_K may depend on the polymer-solvent system and/or the origin of the chain stiffness, for example, differences in h and λ^{-1} between cyclic and linear chains were reported for ATPC

in EA and MIBK (Figure II-3c and d) in the range of N_K from 0.42 to 6.6,[25] such strain effects seem to make cyclic chains more flexible than linear chains as far as amylose carbamates are concerned. Unfortunately, however, it is still not clear whether rigid cyclic chains should have a smaller λ^{-1} compared to the corresponding linear chains. It is desirable to test other rigid cyclic chain systems to clarify this issue.

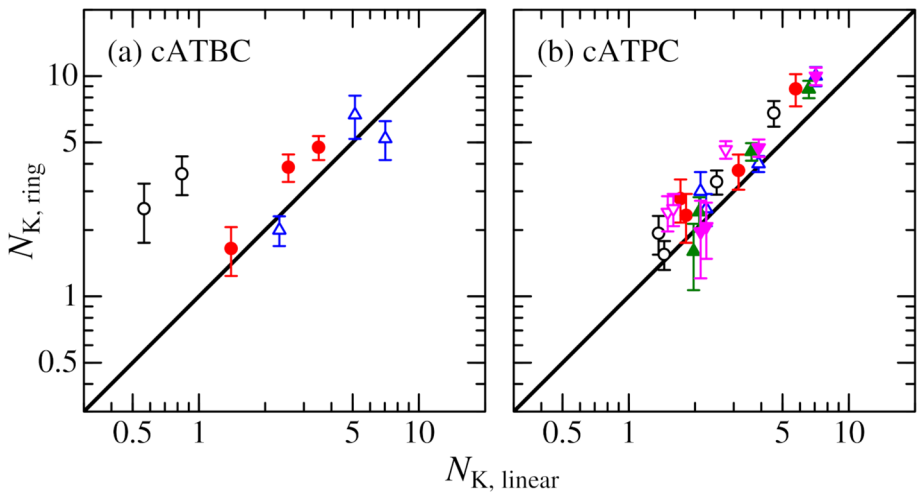

Figure II-6. Double logarithmic plots of $N_{K,ring}$ vs $N_{K,linear}$ for (a) cATBC and (b) cATPC in various solvents. The symbols are the same as those used in Figure II-3. The solid lines indicate $N_{K,ring} = N_{K,linear}$.

II-4. Conclusion

We reanalyzed recently published scattering function data for cATBC in three and cATPC in five solvent systems in terms of the cyclic wormlike chain to determine the contour length per residue h and the Kuhn segment length λ^{-1} (stiffness parameter). While there was

no significant molar mass dependence of the wormlike chain parameters, a clearly small λ^{-1} was estimated for cATBC in THF, even though the difference cannot be distinguishable from the radius of gyration, showing that the analysis of the particle scattering function of the cyclic chain is important to determining the chain shape of the rigid cyclic chains in solution.

Reference

(1) Kratky, O.; Porod, G. *Recl. des Trav. Chim. des Pays-Bas* **2010**, *68*, 1106–1122.

(2) Vologodskii, A. V; Cozzarelli, N. R. *Annu. Rev. Biophys. Biomol. Struct.* **1994**, *23*, 609–643.

(3) Roovers, J.; Toporowski, P. M. *Macromolecules* **1983**, *16*, 843–849.

(4) Ragnetti, M.; Geiserb, D.; Hd, H.; Oberthiir, R. C. *Makromol. Chemie* **1985**, *186*, 1701–1709.

(5) Lutz, P.; McKenna, G. B.; Rempp, P.; Strazielle, C. *Makromol. Chemie, Rapid Commun.* **1986**, *7*, 599–605.

(6) Hadziioannou, G.; Cotts, P. M.; ten Brinke, G.; Han, C. C.; Lutz, P.; Strazielle, C.; Rempp, P.; Kovacs, A. J. *Macromolecules* **1987**, *20*, 493–497.

(7) McKenna, G. B.; Hostetter, B. J.; Hadjichristidis, N.; Fetters, L. J.; Plazek, D. J. *Macromolecules* **1989**, *22*, 1834–1852.

(8) Takano, A.; Ohta, Y.; Masuoka, K.; Matsubara, K.; Nakano, T.; Hieno, A.; Itakura, M.; Takahashi, K.; Kinugasa, S.; Kawaguchi, D.; et al. *Macromolecules* **2012**, *45*, 369–373.

(9) Gooßen, S.; Brás, A. R.; Pyckhout-Hintzen, W.; Wischnewski, A.; Richter, D.; Rubinstein, M.; Roovers, J.; Lutz, P. J.; Jeong, Y.; Chang, T.; et al. *Macromolecules* **2015**, *48*, 1598–1605.

(10) Dodgson, K.; Sympson, D.; Semlyen, J. a. *Polymer (Guildf).* **1978**, *19*, 1285–1289.

(11) Higgins, J. S.; Dodgson, K.; Semlyen, J. A. *Polymer (Guildf).* **1979**, *20*, 553–558.

(12) Kitamura, S.; Isuda, H.; Shimada, J.; Takada, T.; Takaha, T.; Okada, S.; Mimura, M.; Kajiwara, K. *Carbohydr. Res.* **1997**, *304*, 303–314.

(13) Shimada, J.; Kaneko, H.; Takada, T.; Kitamura, S.; Kajiwara, K. *J. Phys. Chem. B* **2000**, *104*, 2136–2147.

(14) Nakata, Y.; Amitani, K.; Norisuye, T.; Kitamura, S. *Biopolymers* **2003**, *69*, 508–516.
(15) Suzuki, S.; Yukiyama, T.; Ishikawa, A.; Yuguchi, Y.; Funane, K.; Kitamura, S. *Carbohydr. Polym.* **2014**, *99*, 432–437.
(16) Deffieux, A.; Schappacher, M. In *Polymer Science: A Comprehensive Reference*; Elsevier, 2012; Vol. 6, pp 5–28.
(17) Pangilinan, K.; Advincula, R. *Polym. Int.* **2014**, *63*, 803–813.
(18) Williams, R. J.; Dove, A. P.; O'Reilly, R. K. *Polym. Chem.* **2015**, *6*, 2998–3008.
(19) Yamamoto, T.; Tezuka, Y. *Soft Matter* **2015**, *11*, 7458–7468.
(20) Schappacher, M.; Deffieux, A. *Science (80-.).* **2008**, *319*, 1512–1515.
(21) Terao, K.; Asano, N.; Kitamura, S.; Sato, T. *ACS Macro Lett.* **2012**, *1*, 1291–1294.
(22) Terao, K.; Shigeuchi, K.; Oyamada, K.; Kitamura, S.; Sato, T. *Macromolecules* **2013**, *46*, 5355–5362.
(23) Takaha, T.; Yanase, Mi.; Takata, H.; Okada, S.; Smith, S. M. *J. Biol. Chem.* **1996**, *271*, 2902–2908.
(24) Shimada, J.; Yamakawa, H. *Biopolymers* **1988**, *27*, 657–673.
(25) Asano, N.; Kitamura, S.; Terao, K. *J. Phys. Chem. B* **2013**, *117*, 9576–9583.
(26) Tsubouchi, R.; Ida, D.; Yoshizaki, T.; Yamakawa, H. *Macromolecules* **2014**, *47*, 1449–1454.
(27) Ida, D. *Polym. J.* **2014**, 1–6.
(28) Ida, D.; Nakatomi, D.; Yoshizaki, T. *Polym. J.* **2010**, *42*, 735.
(29) Frank-Kamenetskii, M. D.; Lukashin, A. V.; Anshelevich, V. V.; Vologodskii, A. V. *J. Biomol. Struct. Dyn.* **1985**, *2*, 1005–1012.
(30) Burchard, W.; Kajiwara, K. *Proc. R. Soc. A* **1970**, *316*, 185–199.
(31) Nagasaka, K.; Yoshizaki, T.; Shimada, J.; Yamakawa, H. *Macromolecules* **1991**, *24*, 924–931.
(32) Terao, K.; Fujii, T.; Tsuda, M.; Kitamura, S.; Norisuye, T. *Polym. J.* **2009**, *41*, 201–207.
(33) Fujii, T.; Terao, K.; Tsuda, M.; Kitamura, S.; Norisuye, T. *Biopolymers* **2009**, *91*, 729–736.
(34) Terao, K.; Murashima, M.; Sano, Y.; Arakawa, S.; Kitamura, S.; Norisuye, T. *Macromolecules* **2010**, *43*, 1061–1068.
(35) Sano, Y.; Terao, K.; Arakawa, S.; Ohtoh, M.; Kitamura, S.; Norisuye, T. *Polymer*

(Guildf). **2010**, *51*, 4243–4248.

(36) Nakamura, Y.; Norisuye, T. *J. Polym. Sci. Part B Polym. Phys.* **2004**, *42*, 1398–1407.

(37) Yamakawa, H.; Yoshizaki, T. *Helical Wormlike Chains in Polymer Solutions*, 2nd ed.; Springer: Berlin, Heidelberg, 2016.

(38) Tsuda, M.; Terao, K.; Nakamura, Y.; Kita, Y.; Kitamura, S.; Sato, T. *Macromolecules* **2010**, *43*, 5779–5784.

Chapter III.

Topology-dependent chain stiffness and local helical structure of cyclic amylose tris(3,5-dimethylphenylcarbamate) in solution

III-1. Introduction

Polysaccharide carbamate derivatives were first utilized to characterize the original polysaccharides[1,2] in solution. Some of them are widely used as a stationary phase of chiral columns,[3–6] and therefore molecular mechanisms of the chiral separation has been investigated by NMR, IR, X-ray diffraction, and computer simulation.[7–9] Tsuda *et al.* recently determined the molecular conformation of amylose tris(3,5-dimethylphenylcarbamate) (ADMPC), which is one of the most useful polysaccharide derivatives for chiral columns and found that chain stiffness in solution increases considerably with increasing molar volume of the solvent when ketones and/or esters used as a solvent.[10] This is likely because solvent molecules tend to form hydrogen bond to the ADMPC chain and thereby restrict internal rotation of the amylosic main chain. It may be considered that hydrogen bonding interactions between ADMPC and small chiral molecules play an important role to recognize the chirality. Therefore, such solvent dependent chain stiffness may be a key factor to elucidate the performance of ADMPC as a chiral stationary phase. Furthermore, immobilized type chiral columns have been recently developed to use a broader variety of organic solvents as a mobile phase.[11,12] The performance however becomes lower with increasing immobilization. It might be due to the structural constraint or change by

multiple fixed points on an ADMPC molecule.

More recently, we successfully synthesized cyclic amylose tris(phenylcarbamate) (cATPC)[13,14] and cyclic amylose tris(*n*-butylcarbamate) (cATBC)[15] to investigate their dilute solution behavior. Some cyclic polymers in solution behave as the wormlike ring with substantially the same wormlike chain parameters, the Kuhn segment length λ^{-1}, and the helix pitch h per residue, as those for the corresponding linear chain. However, cATBC in tetrahydrofuran (THF), for example, has much smaller λ^{-1} with appreciably different local helical structure with larger h as mentioned in Chapter II. Such local conformational difference between linear and cyclic macromolecules has been found only for semiflexible or rigid cATPC and cATBC while it should never be seen for flexible ring polymers.

ADMPC also behaves as a semiflexible or rigid polymer in 4-methyl-2-pentanone (MIBK) for which λ^{-1} is nearly equal to 75 nm and equivalent to that for ATBC in THF because of the hydrogen bonding between ADMPC and MIBK molecules, as mentioned above, although the stiffness of ATBC in THF is mainly due to the intramolecular hydrogen bonding. Solution properties of cyclic polymers with high chain stiffness have not been reported except for some comb-shaped ring polymers[16,17] and cyclic DNA[18,19] though conformational properties for flexible cyclic polymers are widely investigated including cyclic polysaccharides,[20–24] poly(dimethylsiloxane),[25] and polystyrene;[26–30] note that cyclic DNA is not a good example of the rigid cyclic chains because of the supercoiling behavior. Furthermore, if we consider that the difference in the origin of the high stiffness between ADMPC and ATBC, it is necessary from a fundamental point of view to make a detailed

comparison of the dilute solution behavior between ADMPC and its cyclic analogue (cADMPC). From a practical point of view, such a study may make an important contribution to the optimization of the immobilization method for ADMPC as a stationary chiral phase.

We thus prepared cADMPC samples from enzymatically synthesized cyclic amylose (cESA)[23,31] with different molar mass. Their dimensional and local conformational properties in different solvents were analyzed in the manner described in Chapter II using the latest theoretical methods on the basis of the wormlike chain model.[19,32] We chose the three solvents methyl acetate (MEA), MIBK, and THF. We note that the chain stiffness of linear ADMPC in MIBK was reported to be 3 times higher than that in MEA while it is not soluble in THF.[10]

III-2. Experimental

III-2-1. Samples and solvents

3,5-Dimethylphenylcarbamate derivative samples of cyclic amylose were prepared from several cESA samples with different chain length. Synthesis procedure of cADMPC was substantially the same as those for linear ADMPC[10] and similar to the previously reported method for cATPC[13] and cATBC.[15] A typical procedure is as follows. A cESA sample (powder, 2.76 g) and lithium chloride (3.03 g) were dried under vacuum at 100 °C for 3 h in a round-bottom glass flask. An appropriate amount (40 mL) of *N*,*N*-dimethylacetamide (Wako, dehydrated grade) was added to dissolve the cESA sample at 90 °C. Pyridine (90

mL) and 3,5-dimethylphenyl isocyanate (25 g) were added to the solution, and then the mixture was stirred at 110 °C for 3 h. Pyridine was distilled over calcium hydride prior to use. The reaction mixture was poured into methanol at room temperature to precipitate cADMPC. The crude cADMPC sample was dissolved into MEA, and the insoluble part was removed by centrifugation. The soluble part was divided into a few samples by the fractional precipitation procedure with methanol as a precipitant. Appropriate middle fractions—cADMPC14K, cADMPC19K, cADMPC31K, cADMPC49K, and cADMPC91K—were chosen for this study. According to the theoretical prediction by Deguchi *et al*.,[33] knotted rings are rarely formed in good solvent unless the chain length is extremely long. The obtained cADMPC samples have therefore almost no knotted rings because the Kuhn segment number is estimated to be at most 13 for our cESA samples taking the chain stiffness into account.[23] Furthermore, although linear ADMPC is not soluble in THF, the obtained cADMPC samples are well soluble, and no aggregation was found from the following scattering measurements, indicating that a negligibly small amount of linear ADMPC was included in the current cADMPC samples. The degree of substitution was estimated by the elemental analysis to be 3.1 ± 0.2 from the mass ratio of carbon to nitrogen. Full substitution was also confirmed by ^{1}H NMR in deuterated chloroform as in the case of linear ADMPC.[10] As we mention later, two cADMPC samples having relatively wide molar mass distribution were used for infrared absorption (IR) measurements. The three solvents MEA, MIBK, and THF for the following measurements were distilled over calcium hydride other than THF for the SEC measurements.

III-2-2. Online light scattering measurements with size exclusion chromatography (SEC)

The weight-average molar mass M_w and the dispersity index $Đ$ defined as the ratio of M_w to the number-average molar mass for each sample were determined in THF at 25 °C by using SEC measurements with a DAWN DSP multiangle light scattering (MALS) photometer (WYATT) and a refractive index detector (JASCO). Each detector was calibrated with a polystyrene ($M_w = 2.18 \times 10^4$ g mol^{-1} and $Đ = 1.02$) solution. Note that angular dependence of the scattering intensity was not so high as to estimate the gyration radius. A TSK guard column HXL-H and a TSKgel GMH$_{XL}$ column were connected in series. The flow rate was set to be 0.5 mL min^{-1}, and a sample loop with 100 μL was used for this study. A monomodal peak was obtained for each sample. The refractive index increment for cADMPC in THF at 25 °C was determined with a Shultz–Cantow type differential refractometer to be 0.165 cm^3 g^{-1} at the wavelength of 633 nm (under vacuum). The second virial coefficient A_2 (or the finite concentration c of the injected solution) did not appreciably affect the values of M_w so determined (less than 1%) when the A_2 value was estimated from the sedimentation equilibrium and SAXS measurements as described later.

III-2-3. Ultracentrifugation

In order to verify the molar mass determined in the last section, sedimentation equilibrium measurements were made on a Beckman Optima XL-I analytical ultracentrifuge for cADMPC19K in THF at 25 °C to determine M_w, the z-average molar mass M_z, and A_2.

See ref 34 for experimental details and data analysis. The wavelength of the interference detector and the rotor speed were 675 nm and 19000 rpm, respectively. The partial specific volume of cADMPC in THF was determined to be 0.776 $cm^3\ g^{-1}$ from the concentration dependence of solution density which was measured by using an Anton Paar DMA5000 density meter. The obtained A_2 value was 2.3×10^{-4} mol $g^{-2}\ cm^3$, showing this solvent is a good solvent of cADMPC whereas clear solution cannot be obtained for linear ADMPC in THF.

III-2-4. Small-angle X-ray scattering (SAXS) measurements

SAXS measurements were carried out at the BL40B2 beamline in SPring-8 (Hyogo, Japan) and the BL-10C beamline in KEK-PF (Ibaraki, Japan) for the five cADMPC samples in MEA, MIBK, and THF to determine the particle scattering function $P(q)$ and the z-average mean-square radius of gyration $\langle S^2 \rangle_z$. The wavelength, camera length, accumulation time, and the detector were chosen to be 0.10 nm, 3.0 – 4.0 m, 180 s, and a Rigaku R-AXIS VII imaging plate in SPring-8. Those are 0.15 nm, 1.0 m, 120 s, and a Dectris PILATUS2M silicon pixel detector in KEK-PF. The beam center and the accurate camera length were determined from the Bragg reflection of silver behenate. A circular average procedure was examined for each two-dimensional image to obtain the scattering intensity $I(q)$ as a function of the magnitude q of the scattering vector. The intensity $I(q)$ was calibrated by the intensity of the direct beam detected at the lower end of the capillary to take into account both the intensity of incident light and transparency of the sample solution. Solvent and solutions

with four different polymer mass concentration c of which range is from 2×10^{-3} to 1.2×10^{-2} g cm^{-3} were measured in the same capillary to determine the excess scattering intensity $\Delta I(q)$. The obtained $\Delta I(q)$ data were extrapolated to infinite dilution by means of the Guinier plot[35] to determine $P(q)$. The $\Delta I(q)$ data were also extrapolated to $q^2 = 0$ with the Guinier plot to estimate A_2 and $\langle S^2 \rangle_z$.

III-2-5. Atomic force microscopy (AFM)

AFM observations were carried out for cADMPC91K and ADMPC49K ($M_w = 4.88 \times 10^4$ g mol^{-1}).[10] One drop of MEA solution of each sample ($c = 3 \times 10^{-6}$ g cm^{-3}) was dripped on a mica substrate and dried at room temperature. The resultant substrate was observed by the following equipment in the PeakForce Tapping mode. AFM measurements were performed using a Dimension Icon AFM with NanoScope V controller system (Bruker AXS). Silicon nitride cantilevers (SCANASYST-AIR, Bruker AXS) with a nominal spring constants of 0.40 N/m were used. Scanning areas were 3, 1, and 0.3 μm square with 256 × 256 data points, and a scan rate was around 1.0 Hz for each measurement.

III-2-6. Infrared absorption (IR)

IR absorption measurements were made on an FT/IR-4200 (JASCO) spectrometer with a solution cell made of calcium fluoride for two cADMPC samples with M_w of $(4 – 7) \times 10^4$ g mol^{-1} and relatively large $Đ$ (~ 1.3) in THF at 25 °C. The path length of the solution cell and c were set to be 0.05 mm and 2×10^{-2} g cm^{-3}, respectively.

III-2-7. Circular dichroism (CD)

CD spectra were recorded on a J720WO spectropolarimeter (JASCO) with a Peltier thermostated cell holder and a quartz cell of 1 mm to determine molar circular dichroism $\Delta\varepsilon$. The measurements were made for two cADMPC samples, cADMPC19K, and one of the samples used for the above-mentioned solution IR measurements. Polymer mass concentration c of the sample solution and the path length of the cell were set to be 6×10^{-5} g cm^{-3} and 1 mm, respectively.

III-3. Results

III-3-1. Molar mass and dimensional properties

The values of M_w and $Đ$ determined from SEC-MALS measurements for the five cADMPC samples in THF are summarized in Table III-1. The M_w value for cADMPC19K is consistent with that determined from the sedimentation equilibrium. The M_w range of the current samples corresponds to the weight-average degree of polymerization from 23 to 150. The Guinier plot shown in Figure III-1 was utilized to determine $\langle S^2 \rangle_z$. Slight upward deviation in the low q region may be due to the stray X-ray light or the slight aggregation of the cyclic polymer samples in solution. The $\langle S^2 \rangle_z$ value becomes at most 3% larger if we choose lower q range to determine the initial slope. The resultant $\langle S^2 \rangle_z$ data and the corresponding g-factors in different solvents at 25 °C are also listed in Table III-1, where g is defined as the ratio of the $\langle S^2 \rangle_z$ value to that for the linear ADMPC with the same M_w. The g-factor in THF is infeasible to be obtained because of no data for the corresponding linear

chain. The obtained g values range from 0.30 to 0.66 whereas those from theoretical gyration radius for wormlike ring are between 0.3 and 0.5.[36] The large g values for cADMPC31K may be due to the experimental error as well as the locally extended helical structure, which is discussed later with the $P(q)$ data. Molar mass dependencies of $\langle S^2 \rangle_z^{1/2}$ illustrated in Figure III-2 were obeyed roughly by the power low with the exponent of 0.85 – 0.86, suggesting the semiflexible ring nature.[36]

Table III-1. Molecular Characteristics of cADMPC Samples in Methyl Acetate (MEA), 4-Methyl-2-pentanone (MIBK), and Tetrahydrofuran (THF)

Sample	M_w (kg mol^{-1})	$Đ$	in MEA		in MIBK		in THF
			$\langle S^2 \rangle_z^{1/2}$ (nm)	g	$\langle S^2 \rangle_z^{1/2}$ (nm)	g	$\langle S^2 \rangle_z^{1/2}$ (nm)
cADMPC14K	14.1	1.02	1.71	0.55	1.80	0.55	1.90
cADMPC19K	19.4 (19.7)[a]	1.04 (1.07)[b]	2.05	0.45	2.14	0.42	2.19
cADMPC31K	31.2	1.06	3.77	0.66	3.95	0.59	4.17
cADMPC49K	49.4	1.14	5.14	0.57	5.48	0.48	5.05
cADMPC91K	91.1	1.20	7.14	0.43	7.55	0.30	7.55

[a] Sedimentation equilibrium (SE). [b] M_z/M_w from SE.

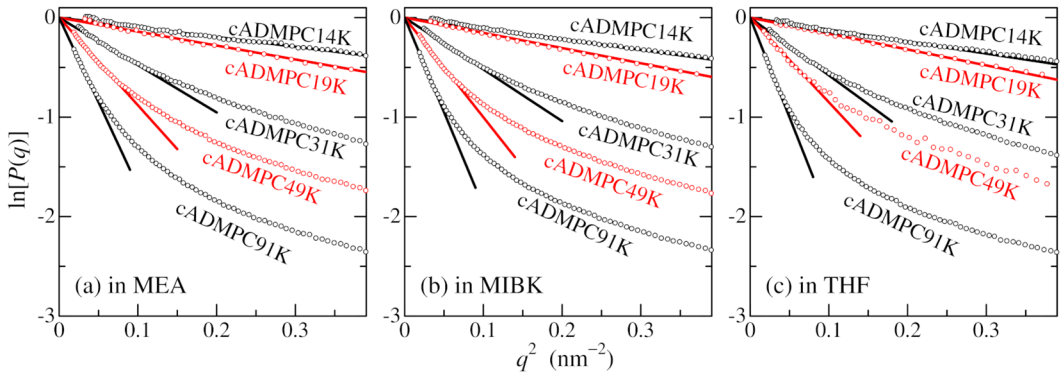

Figure III-1. Guinier plots for the indicated cADMPC samples in (a) methyl acetate (MEA), (b) 4-methyl-2-pentanone (MIBK), and (c) tetrahydrofuran (THF) all at 25 °C.

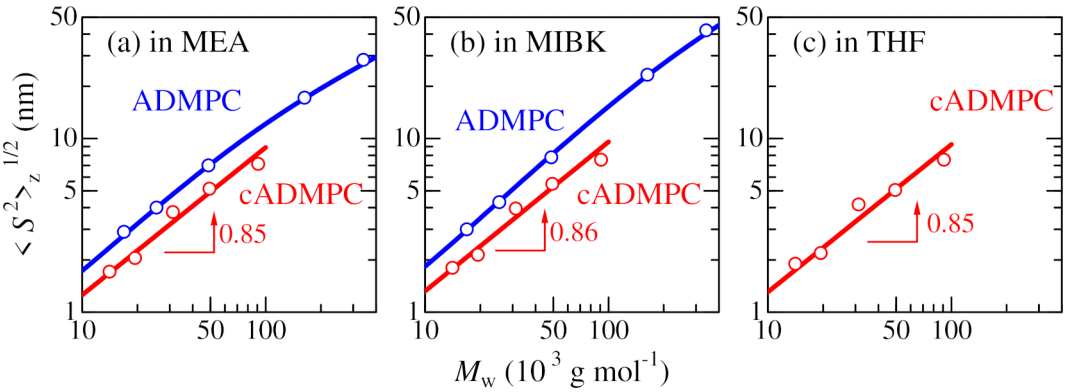

Figure III-2. Double logarithmic plots of the z-average radius of gyration $\langle S^2 \rangle_z$ vs weight-average molar mass M_w for cADMPC in (a) MEA, (b) MIBK, and (c) THF all at 25 °C, along with those for the corresponding linear ADMPC.[10]

The particle scattering function $P(q)$ of the five cADMPC samples in the three solvents are summarized in Figure III-3 in the form of the reduced Holtzer plot. As in the case of other cyclic amylose derivatives,[13–15] the experimental $P(q)$ data have appreciable peak at low-q region and the peak position shifts to large q with lowering M_w. This is a typical feature of the semi-rigid ring polymers as mentioned in Chapter II.

The SAXS measurements were also made for some samples at −80 °C. Substantially

the same $\langle S^2 \rangle_z$ as those at 25 °C were observed as in the case with cATPC in THF,[37] suggesting good solubility of this polymer even at low temperature. We thus further analyze the SAXS data only at 25 °C in this paper.

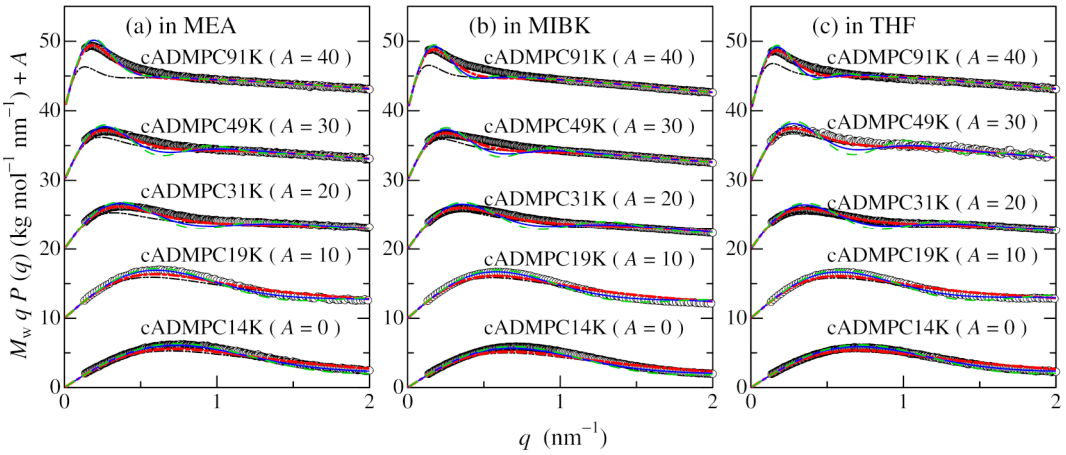

Figure III-3. Reduced Holtzer plots for cADMPC in MEA (a), MIBK (b), and THF (c) at 25 °C. Double-dot-dashed black curves, theoretical values of rigid rings with $Đ$ = 1.20. Curves, theoretical values for wormlike rings with the helix pitch per residue h and the Kuhn segment length λ^{-1} shown in Figure III-8, and $Đ$ = 1.00 (dashed green), 1.05 (solid blue), and 1.20 (dot-dashed red). The ordinate values are shifted by A.

III-3-2. AFM images

To confirm ring shape of the obtained cADMPC, some AFM images were acquired. Figure III-4 shows one of the AFM images for cADMPC91K. Although only linear rodlike chains were observed for ADMPC49K (not shown here), a number of toroidal particles are found with almost no rodlike particles in the figure, suggesting that cyclic chains are successfully obtained. The height of the cyclic chain is about 1.5 – 3 nm, which is consistent

with the previously reported hydrodynamic diameter of 2.1 – 2.6 nm of linear ADMPC,[10] suggesting each toroidal ring consists of a cyclic chain. While the weight-average contour length for cADMPC91K is estimated as 60 nm from M_w, the enlarged ring in the right picture has about 3 times larger circumference (180 nm) and almost no ring smaller than 60 nm were found in the AFM images. This is most likely because longer cyclic chains preferably adsorbed on the mica surface. Furthermore, the adsorbed cyclic chains are seem as rigid toroids whereas the Kuhn segment number N_K is estimated to be 8 from the circumference and the Kuhn segment length for linear ADMPC in MEA (22 nm).[10] The currently obtained cADMPC chains tend to form more extended structure on the mica surface when we choose above-mentioned sample preparation.

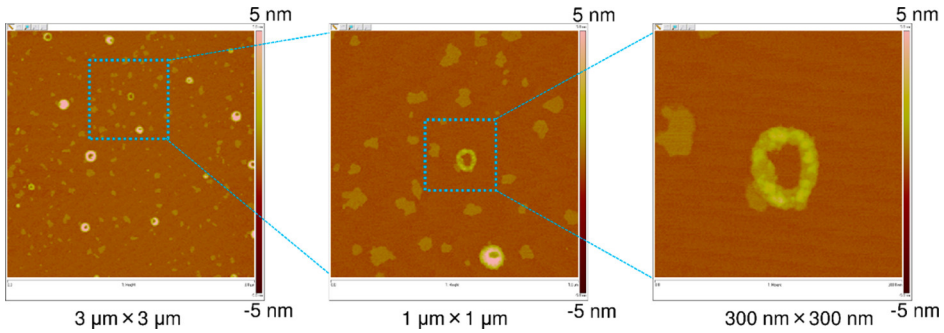

Figure III-4. AFM images for cADMPC91K on a mica surface.

III-3-3. CD and IR spectra in THF

CD spectra for cADMPC samples reflect the helical arrangement of phenyl groups on the side groups. The CD spectra for the adsorption band of the phenyl groups of the two samples having different M_w in Figure III-5 are mostly identical with each other, suggesting

no significant molar mass dependence of the local helical structure. This is also supported by the solution IR spectra. According to Kasat *et al.*,[8] the intramolecular hydrogen bonds can be observed as a split amide I band in the solution IR absorption spectra. Figure III-6 illustrates wavenumber dependence of the molar absorption coefficient ε of the repeat unit for the two cADMPC samples; note that this band cannot be observed in MEA and MIBK because of the significant absorption from the solvent. The amide I peaks at 1756 and 1703 cm^{-1} may be assigned to be free and hydrogen bonding C═O groups of the carbamate group, suggesting that about 40% of C═O groups form intramolecular hydrogen bonds. This is a similar behavior to that for ATPC[34] and amylose-2-acetyl-3,6-bis(phenylcarbamate)[38] in 1,4-dioxane; thus, the hydrogen bonding C═O groups should stiffen the main chain of cADMPC in THF.

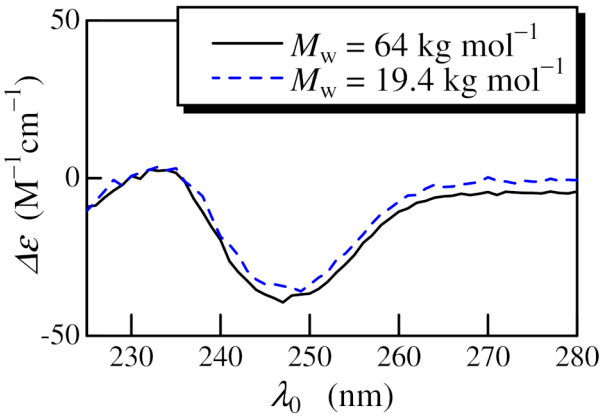

Figure III-5. Solution CD spectra for the two cADMPC samples in THF at 25 °C.

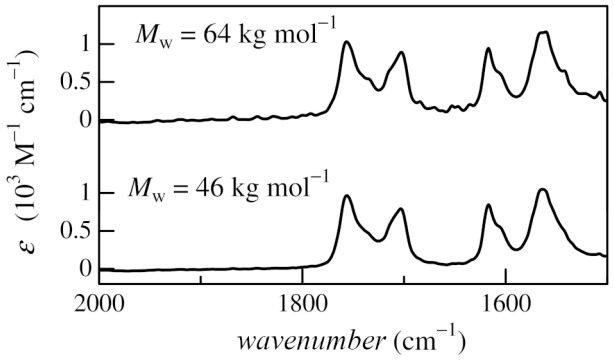

Figure III-6. Solution IR spectra for the two cADMPC samples in THF at 25 °C.

III-4. Discussion

The particle scattering function $P(q)$ data displayed in Figure III-3 were analyzed in terms of the cyclic wormlike chain model. In spite of infeasibility to obtain analytical solution for relatively rigid cyclic chains, a Monte Carlo simulation method[32,39] with a discrete wormlike chain model[40] allows us to calculate the particle scattering function $P_0(q)$ for infinitely thin cyclic wormlike chains with arbitrary chain stiffness and chain length, that is, the Kuhn segment length λ^{-1} (or twice the persistence length) and the contour length L. It should be noted that $P_0(q)$ was calculated originally as a function of $\lambda^{-1}q$ at fixed N_K ($\equiv \lambda L$). Since the chain thickness should be taken into account for actual cyclic polymers, the equation for $P(q)$ of the touched bead chains having finite chain thickness defined as[41,42]

$$P(q) = 9\left(\frac{2}{qd_b}\right)^6 \left(\sin\frac{qd_b}{2} - \frac{qd_b}{2}\cos\frac{qd_b}{2}\right)^2 P_0(q) \qquad \text{(III-1)}$$

is applied to calculate the theoretical values, where d_b denotes the diameter of each bead. We also calculate z-average particle scattering function with assuming the log-normal molar-mass

distribution because the theoretical $P(q)$ values for cyclic chains are more affectable by the chain length distribution than those for linear chains. We note that the three parameters, the helix pitch (or helix rise) per residue h, λ^{-1}, and d_b, are required to calculate theoretical $P(q)$ when we assume an appropriate value of $Đ$. A curve fitting procedure was employed to determine the three wormlike chain parameters. Although all experimental data are well explained by the theoretical values when we choose appropriate λ^{-1}, h, and d_b values as seen from the curves in Figure III-3, the parameter h for the lowest M_w sample cannot be unequivocally determined. This is because the length scale of chain dimensions of such sample is not far from that for d_b. Furthermore, the chain stiffness parameter is determinable only for the two high M_w samples since the theoretical $P(q)$ values so obtained for lower M_w samples are hardly distinguishable from the theoretical values for rigid rings.

The radius of gyration $\langle S^2\rangle_{calc}$ for the wormlike ring having finite chain thickness may be calculated from

$$\left\langle S^2\right\rangle_{calc} = \left\langle S^2\right\rangle_{0,c} + \frac{3{d_b}^2}{20} \qquad \text{(III-2)}$$

The second term may be derived from eq III-1. According to Shimada and Yamakawa,[36] the gyration radius $\langle S^2\rangle_{0,c}$ for infinitely thin wormlike chain can be calculated from the following interpolation formula

$$\begin{aligned}\lambda^2\left\langle S^2\right\rangle_{0,c} &= \frac{N_K^2}{4\pi^2}\left(1-0.1140N_K-0.0055258N_K^2\right.\\ &\qquad \left.+0.0022471N_K^3-0.00013155N_K^4\right) \quad \text{for} \quad N_K \le 6 \qquad \text{(III-3)}\\ &= \frac{N_K}{12}\left\{1-\frac{7}{6N_K}-0.025\exp\left(-0.01N_K^2\right)\right\} \quad \text{for} \quad N_K \ge 6\end{aligned}$$

If we calculate the $\langle S^2 \rangle_{calc}$ values with the same parameters using the theoretical values for $P(q)$ in Figure III-3, the resultant $\langle S^2 \rangle_{calc}$ are fairly close to the experimental $\langle S^2 \rangle_z$ as shown in Figure III-7. Somewhat larger $\langle S^2 \rangle_z$ for the middle M_w samples are likely because molar mass distribution as well as slight aggregation as mentioned in the Section III-3.

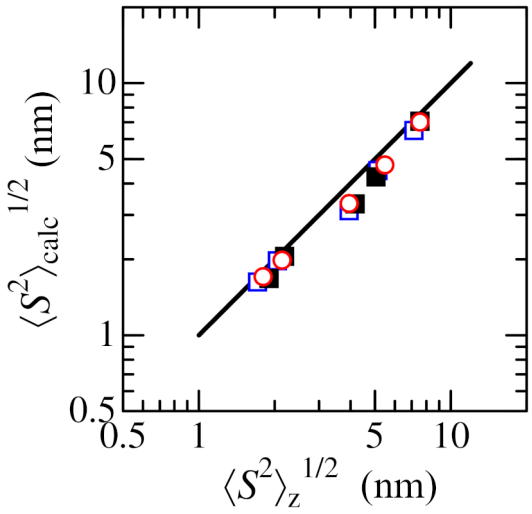

Figure III-7. Comparison between the calculated gyration radii $\langle S^2 \rangle_{calc}^{1/2}$ from eq III-2 with the parameters from $P(q)$ and the experimental $\langle S^2 \rangle_z^{1/2}$ for cADMPC in MEA (unfilled squares), MIBK (circles), and THF (filled squares) at 25 °C. Solid line, $\langle S^2 \rangle_{calc}^{1/2} = \langle S^2 \rangle_z^{1/2}$.

The resultant wormlike chain parameters are summarized in Figure III-8 along with the parameters for the corresponding linear polymers (solid lines); note that no data are shown for THF solution due to lower solubility of linear ADMPC. The obtained h values for the three solvents are substantially independent of M_w whereas the values in MIBK and MEA are appreciably larger than those for the corresponding linear chains. This is most likely because the bent main chain due to the circular topology extends the local helical structure. The difference between linear and cyclic chains is more obvious in the chain stiffness in MIBK.

Though λ^{-1} for linear ADMPC is reported to be 73 nm, those in cyclic chains are about 20 nm. Likewise, λ^{-1} for cADMPC in MEA is also somewhat smaller than that for linear polymer whereas the λ^{-1} values for cADMPC, which are nearly equal to 20 nm, are still quite larger than that for cyclic amylose in aqueous sodium hydroxide.[23] We may thus conclude that since the local helical structure of cADMPC with finite molar mass appreciably extends, hydrogen bonding solvent molecules to the cyclic chains do not stiffen the main chain. Another interesting point is that the h value for cADMPC in MIBK is larger than that for ADMPC whereas the h value for cATPC in MIBK is appreciably smaller than that for ATPC as mentioned in Ref. 14 and Chapter II. This is most likely because the local helical structure of linear ATPC is significantly changed by the hydrogen bonding solvent molecules more easily than that for ADMPC.[10,43]

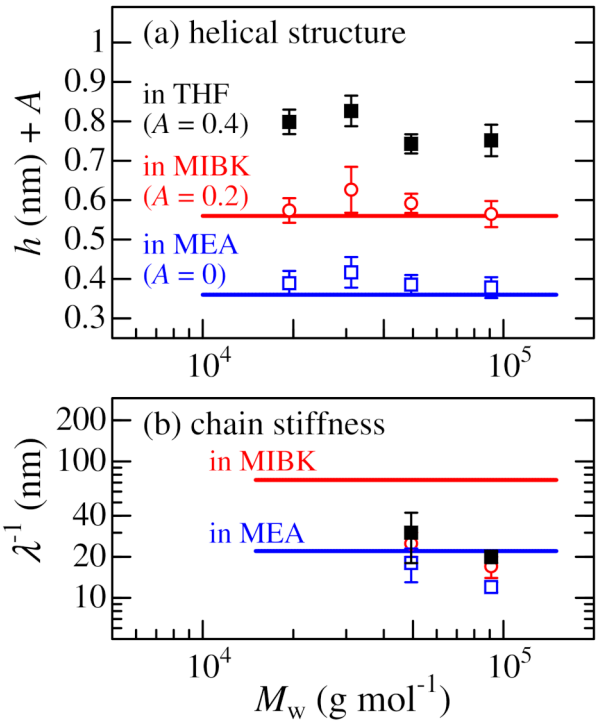

Figure III-8. Plots of h (a) and λ^{-1} (b) against M_w for cADMPC in MEA (unfilled squares), MIBK (circles), and THF (filled squares) at 25 °C. Solid lines indicate the h or λ^{-1} for the corresponding linear chains. In panel (a), the data are shifted by A for clarity.

The difference in the wormlike chain parameters for the linear and cyclic chains can be compared with each other if we use the double-logarithmic plots (Figure III-9) for the Kuhn segment number $N_{K,ring}$ ($\equiv \lambda L$) of ring chains vs those for the corresponding linear chain $N_{K,linear}$, which is calculated from the molar mass of the ring polymer and the wormlike chain parameters for the corresponding linear chains.[10] It should be noted that the data for the two highest M_w samples, cADMPC49K and cADMPC91K, are plotted in the figure since the Kuhn segment length for the other samples are difficult to be determined as mentioned above. This figure includes data for cATPC and cATBC determined in Chapter II. This figure

clearly shows that $N_{K,ring}$ including our new data is fairly close to those for linear chain when $N_{K,linear} > 1.5$. On the contrary, the value ($N_{K,ring}$) becomes much larger in the lower $N_{K,linear}$ range; namely, the chain stiffness of circular chains is much smaller than the corresponding linear chains. The further interesting points are that the boundary $N_{K,linear}$ for cADMPC and cATBC are substantially the same and also that the main chain both of cADMPC and cATBC is more flexible than that for the corresponding linear polymers at such low N_K region although the origins of the chain stiffness for the two derivatives are different from each other as described above. It can be concluded that the topological constraint of cyclic chains softens the main chain when $N_{K,linear} < 1$. This threshold value 1 – 1.5 in N_K is substantially close to that at which the probability to link the both ends (ring closure probability) of the linear wormlike chain significantly decreases with decreasing N_K. This is reasonable because the difference in the chain curvature distribution of cyclic and linear chains becomes much more significant in such small N_K range. According to Shen *et al.*,[12] the number of chemical bonds immobilizing polysaccharide derivatives onto silica particles should be fewer in order to achieve a high chiral recognition. This may be related to the current finding that the topologically constrained polysaccharide chains have quite small chain stiffness and the slightly different local helical structure from the corresponding chains without topological constraints. To confirm this hypothesis, the performance of a chiral stationary phase made from cADMPC should be investigated.

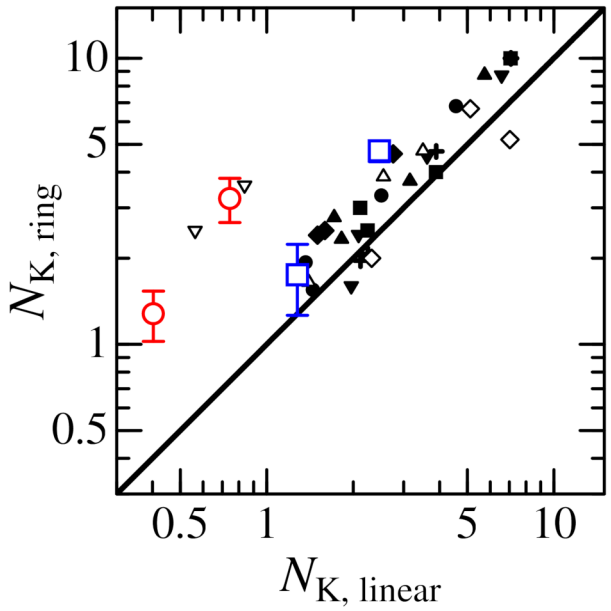

Figure III-9. Double-logarithmic plots of $N_{K,ring}$ against $N_{K,linear}$ for cADMPC in MEA (unfilled squares) and in MIBK (unfilled circles) at 25 °C. The small symbols are the data determined in Chapter II for cATPC in 1,4-dioxane at 25 °C (filled circles), 2-ethoxyethane at 25 °C (filled triangles), MEA at 25 °C (filled squares), ethyl acetate at 33 °C (filled inverted triangles), MIBK at 25 °C (filled diamonds) and 58 °C (crosses), and for cATBC in THF at 25 °C (unfilled inverted triangles), 2-propanol at 35 °C (unfilled triangles) and methanol at 25 °C (unfilled diamonds). The solid line represents $N_{K,ring} = N_{K,linear}$.

III-5. Conclusions

The particle scattering function $P(q)$ of a novel cyclic amylose derivative (cADMPC) of which chain length ranges from 9 to 60 nm was analyzed in terms of the cyclic wormlike chains to determine the Kuhn segment length λ^{-1} and the helix pitch per residue h. While both λ^{-1} and h are mostly independent of the molar mass in the investigated M_w range, the former parameter in MIBK is significantly smaller than those for the corresponding linear

chains. As is the case with cATBC, when the Kuhn segment number becomes less than unity, the cyclic chains behave as much more flexible chain than the corresponding linear chain whereas the origins of the chain stiffness of ADMPC and ATBC are different each other according to our recent research.

Reference

(1) Burchard, V. W.; Husemann, E. *Die Makromol. Chemie* **1961**, *44*, 358–387.

(2) Burchard, W. In *Soft Matter Characterization*; Springer Netherlands: Dordrecht, 2008; pp 463–603.

(3) Okamoto, Y.; Kawashima, M.; Hatada, K. *J. Am. Chem. Soc.* **1984**, *106*, 5357–5359.

(4) Yashima, E. *J. Chromatogr. A* **2001**, *906*, 105–125.

(5) Ikai, T.; Okamoto, Y. *Chem. Rev.* **2009**, *109*, 6077–6101.

(6) Okamoto, Y. *J. Polym. Sci. A Polym. Chem.* **2009**, *47*, 1731–1739.

(7) Yamamoto, C.; Yashima, E.; Okamoto, Y. *J. Am. Chem. Soc.* **2002**, *124*, 12583–12589.

(8) Kasat, R. B.; Zvinevich, Y.; Hillhouse, H. W.; Thomson, K. T.; Wang, N.-H. L.; Franses, E. I. *J. Phys. Chem. B* **2006**, *110*, 14114–14122.

(9) Tsui, H.-W.; Wang, N.-H. L.; Franses, E. I. *J. Phys. Chem. B* **2013**, *117*, 9203–9216.

(10) Tsuda, M.; Terao, K.; Nakamura, Y.; Kita, Y.; Kitamura, S.; Sato, T. *Macromolecules* **2010**, *43*, 5779–5784.

(11) Okamoto, Y.; Ikai, T.; Shen, J. *Isr. J. Chem.* **2011**, *51*, 1096–1106.

(12) Shen, J.; Ikai, T.; Okamoto, Y. *J. Chromatogr. A* **2014**, *1363*, 51–61.

(13) Terao, K.; Asano, N.; Kitamura, S.; Sato, T. *ACS Macro Lett.* **2012**, *1*, 1291–1294.

(14) Asano, N.; Kitamura, S.; Terao, K. *J. Phys. Chem. B* **2013**, *117*, 9576–9583.

(15) Terao, K.; Shigeuchi, K.; Oyamada, K.; Kitamura, S.; Sato, T. *Macromolecules* **2013**, *46*, 5355–5362.

(16) Schappacher, M.; Deffieux, A. *J. Am. Chem. Soc.* **2008**, *130*, 14684–14689.

(17) Doi, Y.; Iwasa, Y.; Watanabe, K.; Nakamura, M.; Takano, A.; Takahashi, Y.; Matsushita, Y. *Macromolecules* **2016**, *49*, 3109–3115.

(18) Bates, A. D.; Maxwell, A. *DNA Topology*; Oxford University Press: New York, U.S.A., 2005.

(19) Yamakawa, H.; Yoshizaki, T. *Helical Wormlike Chains in Polymer Solutions*, 2nd ed.; Springer: Berlin, Heidelberg, 2016.

(20) Kitamura, S.; Isuda, H.; Shimada, J.; Takada, T.; Takaha, T.; Okada, S.; Mimura, M.; Kajiwara, K. *Carbohydr. Res.* **1997**, *304*, 303–314.

(21) Shimada, J.; Kaneko, H.; Takada, T.; Kitamura, S.; Kajiwara, K. *J. Phys. Chem. B* **2000**, *104*, 2136–2147.

(22) Nakata, Y.; Norisuye, T.; Kitamura, S. *Biopolymers* **2002**, *64*, 72–79.

(23) Nakata, Y.; Amitani, K.; Norisuye, T.; Kitamura, S. *Biopolymers* **2003**, *69*, 508–516.

(24) Suzuki, S.; Yukiyama, T.; Ishikawa, A.; Yuguchi, Y.; Funane, K.; Kitamura, S. *Carbohydr. Polym.* **2014**, *99*, 432–437.

(25) Higgins, J. S.; Dodgson, K.; Semlyen, J. A. *Polymer (Guildf).* **1979**, *20*, 553–558.

(26) Ragnetti, M.; Geiserb, D.; Hd, H.; Oberthiir, R. C. *Makromol. Chemie* **1985**, *186*, 1701–1709.

(27) Lutz, P.; McKenna, G. B.; Rempp, P.; Strazielle, C. *Makromol. Chemie, Rapid Commun.* **1986**, *7*, 599–605.

(28) Hadziioannou, G.; Cotts, P. M.; ten Brinke, G.; Han, C. C.; Lutz, P.; Strazielle, C.; Rempp, P.; Kovacs, A. J. *Macromolecules* **1987**, *20*, 493–497.

(29) Takano, A.; Ohta, Y.; Masuoka, K.; Matsubara, K.; Nakano, T.; Hieno, A.; Itakura, M.; Takahashi, K.; Kinugasa, S.; Kawaguchi, D.; et al. *Macromolecules* **2012**, *45*, 369–373.

(30) Gooßen, S.; Brás, A. R.; Pyckhout-Hintzen, W.; Wischnewski, A.; Richter, D.; Rubinstein, M.; Roovers, J.; Lutz, P. J.; Jeong, Y.; Chang, T.; et al. *Macromolecules* **2015**, *48*, 1598–1605.

(31) Takaha, T.; Yanase, Mi.; Takata, H.; Okada, S.; Smith, S. M. *J. Biol. Chem.* **1996**, *271*, 2902–2908.

(32) Tsubouchi, R.; Ida, D.; Yoshizaki, T.; Yamakawa, H. *Macromolecules* **2014**, *47*, 1449–1454.

(33) Deguchi, T.; Tsurusaki, K. *Phys. Rev. E* **1997**, *55*, 6245–6248.

(34) Terao, K.; Fujii, T.; Tsuda, M.; Kitamura, S.; Norisuye, T. *Polym. J.* **2009**, *41*, 201–207.

(35) Glatter, O.; Kratky, O. *Small Angle X-Ray Scattering*; Academic press: London, U.K., 1982.

(36) Shimada, J.; Yamakawa, H. *Biopolymers* **1988**, *27*, 657–673.

(37) Terao, K.; Morihana, N.; Ichikawa, H. *Polym. J.* **2014**, *46*, 155–159.

(38) Tsuda, M.; Terao, K.; Kitamura, S.; Sato, T. *Biopolymers* **2012**, *97*, 1010–1017.

(39) Ida, D.; Nakatomi, D.; Yoshizaki, T. *Polym. J.* **2010**, *42*, 735.

(40) Frank-Kamenetskii, M. D.; Lukashin, A. V.; Anshelevich, V. V.; Vologodskii, A. V. *J. Biomol. Struct. Dyn.* **1985**, *2*, 1005–1012.

(41) Burchard, W.; Kajiwara, K. *Proc. R. Soc. A* **1970**, *316*, 185–199.

(42) Nagasaka, K.; Yoshizaki, T.; Shimada, J.; Yamakawa, H. *Macromolecules* **1991**, *24*, 924–931.

(43) Fujii, T.; Terao, K.; Tsuda, M.; Kitamura, S.; Norisuye, T. *Biopolymers* **2009**, *91*, 729–736.

Chapter IV.

Linear and cyclic amylose derivatives having brush like side groups in solution: Amylose tris(*n*-octadecylcarbamate)s

IV-1. Introduction

Intramolecular interactions between neighboring side groups of polymers play an important role to determine the conformation of polymers in solution. One of the most significant examples is molecular bottlebrushes or polymacromonomers of which main chain becomes stiffer with increasing the side chain length.[1–4] The side-chain dependence of the conformation was also reported for polymers having different alkyl side chains, that is, polymethacrylates[5,6] and polysilanes.[7,8] Synthetic techniques of comb-like polymers were recently extended to non-linear polymers[9,10] such as star,[11] comb,[12] and cyclic[13–16] chains in order to observe their branching structure or topology by the atomic force microscopy (AFM) or to obtain novel functional materials. Solution properties of the semiflexible or rigid nonlinear polymers are however much less investigated than those for linear polymers.[17–20] Indeed, while dilute solution properties were reported for cyclic comb polymers,[14,21] conformational difference between cyclic and the corresponding linear chain were rarely discussed.

Meanwhile, we recently prepared three different cyclic amylose carbamate derivatives with phenyl,[22] *n*-butyl,[23] and 3,5-dimethylphenyl (cf. Chapter III) side groups from enzymatically synthesized cyclic amylose (cESA), which has substantially no linear

contamination.[24,25] If we choose appropriate isocyanate with relatively long alkyl chains, macrocyclic comb-like polymers can be synthesized from cESA. We thus prepared linear and cyclic amylose tris(*n*-octadecylcarbamate) (ATODC and cATODC, Figure IV-1) from enzymatically synthesized linear amylose (ESA) and cESA, respectively. Light and small-angle X-ray scattering measurements were performed to obtain the weight-average molar mass M_w, the particle scattering function $P(q)$, the z-average mean square radius of gyration $\langle S^2 \rangle_z$, and the second virial coefficient A_2 to determine their conformational properties of macrocyclic comb chains in solution.

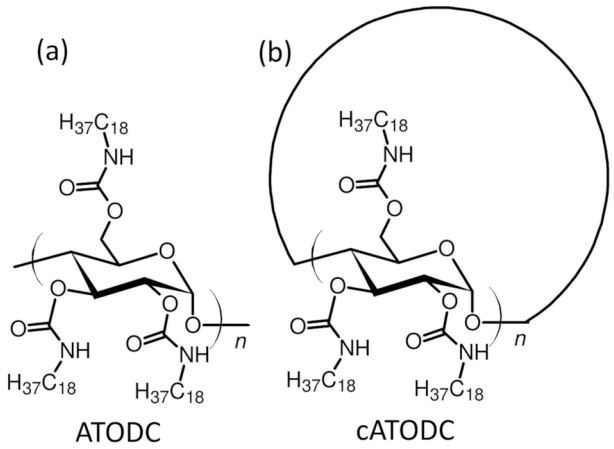

Figure IV-1. Chemical structures of ATODC (a) and cATODC (b).

Cyclic or ring polymers are much less investigated than the linear polymers owing to the difficulty to synthesize suitable model polymers. Chain conformation of cyclic DNA,[17,26] cyclic polysaccharides,[25,27,28] polystyrene,[29–34] and polydimethylsiloxane[35] were reported other than above mentioned macrocyclic comb polymers. Only cyclic DNA behaves as rather rigid ring polymers while the other cyclic macromolecules have quite

flexible main chain in solution. On the other hand, cyclic amylose tris(phenylcarbamate) (cATPC),[22,36] cyclic amylose tris(*n*-butylcarbamate) (cATBC),[23] and cyclic amylose tris(3,5-dimethylphenylcarbamate) (cADMPC) discussed in Chapter III have relatively high chain stiffness in solution since the corresponding linear amylose derivatives behave as semiflexible or rigid chain of which chain stiffness depends significantly on the intramolecular hydrogen bonds[37–40] (H-bonds) and/or H-bonding interactions between polymer and solvent molecules.[41,42] A further surprising finding was that the chain stiffness and/or the local helical structure are not always the same as the corresponding linear chain as described in the literature[36] and previous chapters (II and III). It is however still unclear whether this topologically originated conformational difference depend on the chemical structure of the side groups.

IV-2. Experimental

IV-2.1. Preparation of ATODC and cATODC samples

ATODC and cATODC samples were synthesized from five ESA and two cESA samples with different chain length, respectively, in the manner reported in our previous studies.[22,23,39,40,42] A typical procedure is as follows.

An ESA sample (1.69 g) and lithium chloride (3.07 g) were dried in a reaction flask under vacuum at 100 °C for 6 h. *N,N*-Dimethyl acetamide (40 mL) was added to dissolve them at 110 °C under argon atmosphere. Pyridine (100 mL) and *n*-octadecyl isocyanate were added to the mixture and stirred for 7 h at 105 °C. After toluene (100 mL) was added

into the reaction mixture to dissolve gel-like precipitation, it was kept at 105 °C overnight. The resultant brown viscous solution was poured into excess amount of methanol to precipitate the crude sample. It was further purified by successive reprecipitation using THF or toluene as a solvent and methanol or acetone as a precipitant.

The samples thus obtained were divided into several fractions by means of the fractional precipitation with THF and methanol as the solvent and the precipitant, respectively. Appropriate fractions, seven ATODC and seven cATODC samples listed in Table IV-2, were used in this study.

^{1}H NMR, infrared (IR) absorption, and elemental analysis measurements were performed for the all samples to confirm the chemical structure in the same manner as reported previously.[39] The obtained weight ratio w_N/w_C of nitrogen to carbon ranges between 0.056 and 0.060, which is similar to that for the theoretical value (0.056). The NMR and IR charts are illustrated in Figure IV-2 and Figure IV-3, respectively. Substantially the same signals for all samples support the full substitution. It should be noted that the degree of substitution cannot be determined properly from w_N/w_C because of the low weight fraction of nitrogen atoms comparing to those with shorter alkyl side chain.[39] While the original cESA samples were characterized by the MALDI-TOF-MS measurements to confirm substantially no linear amylose contaminant, the method cannot be applied for the cATODC samples owing to insufficiently substituent in each sample. Very high molar mass linear ATODC samples (> 10^6 g mol^{-1}) obtained from ESA, and furthermore, specific solubility only for cyclic amylose derivative supports high purity of cyclic chains.

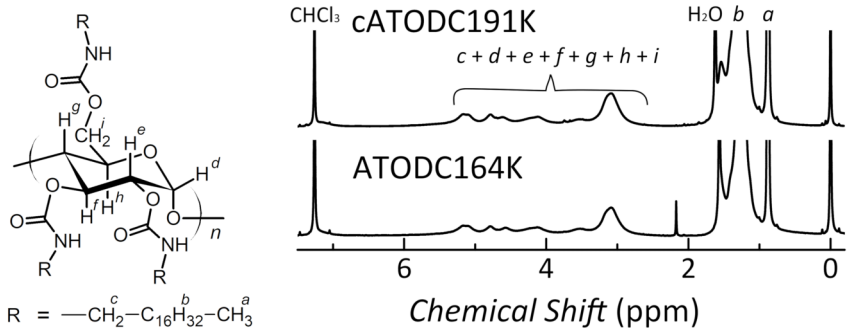

Figure IV-2. ^{1}H NMR spectra for **cATODC191K** and **ATODC164K** in $CDCl_3$ at 25 °C.

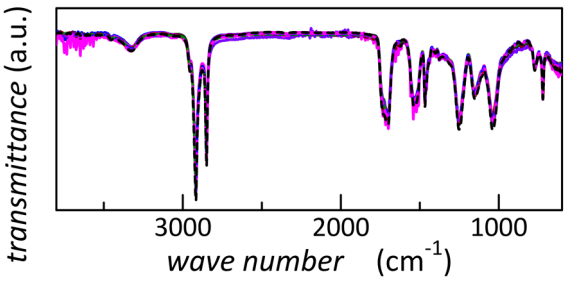

Figure IV-3. Infrared adsorption spectra for **ATODC25K** (solid red), **ATODC38K** (solid brown), **ATODC102K** (solid green), **ATODC164K** (solid blue), **ATODC284K** (solid purple), **ATODC852K** (solid pink), **ATODC1510K** (solid black), **cATODC36K** (dashed red), **cATODC55K** (dashed brown), **cATODC74K** (dashed green), **cATODC77K** (dashed blue), **cATODC110K** (dashed purple), **cATODC120K** (dashed pink), and **cATODC190K** (dashed black).

While previously investigated amylose tris(ethylcarbamate) (ATEC), amylose tris(*n*-butylcarbamate) (ATBC), and amylose tris(*n*-hexylcarbamate) (ATHC) are soluble not only in THF and chloroform but also some alcohols,[40,43] ATODC was not soluble in alcohols as shown in Table VI-1. We thus chose THF, 2-octanone (MHK), and *tert*-butyl methyl ether (MTBE) as solvents for the following measurements. As preliminary experiments, we

found both ATODC and cATODC form liquid crystal phase in concentrated solution, suggesting high chain stiffness in these solvent systems.

Table VI-1. Solubility of amylose alkylcarbamates (ATACs) at room temperature

solvent	ATEC[a]	ATBC[b]	ATHC[a]	ATODC
n-hexane	I	I	I	I
2-octanone (MHK)	I	S	S	S
tert-butyl methyl ether (MTBE)	I	S	I	S
tetrahydrofuran (THF)	S	S	S	S
chloroform	S	S	S	S
toluene	I	S	I	S
acetone	S	S	S	I
1-propanol (1PrOH)	S	S	S	I
2-propanol (2PrOH)	S	S	I	I
methanol (MeOH)	S	S	I	I

S: soluble. I: insoluble. [a] Refs. 40,44 [b] Refs. 39,43,44

IV-2.2. Size-exclusion chromatography with multi-angle light scattering (SEC-MALS)

SEC-MALS measurements were performed for all ATODC and cATODC samples with a DAWN DSP multi-angle light scattering photometer and a refractive index detector in a JASCO GPC-900 liquid chromatography system to determine M_w, the dispersity index $Đ$, and $\langle S^2 \rangle_z$ in THF at 25 °C; note that $Đ$ is defined as the ratio of M_w to the number-average molar mass M_n. A TSKguardcolumn HXL-H column and a TSKgel HXL column were

connected in series. A sample loop with 100 μL was used, the flow rate was set to be 0.5 mL min^{-1}, the polymer mass concentration c of the injected solution was chosen to be between 4×10^{-4} and 3×10^{-3} g cm^{-3}, and the temperature of the column oven was set to be 40 °C. The scattering intensity at different scattering angles were recorded as a function of the elusion volume V_E. The refractive index increment $\partial n/\partial c$ at the wavelength λ_0 in vacuum of the light scattering photometer ($\lambda_0 = 633$ nm) was determined to be 0.0790 cm^3 g^{-1} for ATODC852K with a Shultz-Cantow type differential refractometer. Molar masses were calculated taking into account A_2 estimated from SAXS measurements as described below. Note that the M_w value was underestimated about 0.4 – 3% when A_2 was ignored. The obtained M_w and $Đ$ values are listed in Table IV-2.

Table IV-2. Weight-average molar mass M_w and dispersity index $Đ$ ($\equiv M_w/M_n$) of ATODC or cATODC samples

sample	M_w (kg mol^{-1})	$Đ$
ATODC25K	24.6	1.08
ATODC38K	37.7	1.08
ATODC102K	102	1.10
ATODC164K	164	1.18
ATODC284K	284	1.32
ATODC852K	852	1.51
ATODC1510K	1510	1.47
cATODC36K	36.1	1.16
cATODC55K	54.7	1.09
cATODC74K	74.2	1.07
cATODC77K	77.1	1.15
cATODC115K	115	1.10
cATODC122K	122	1.22
cATODC191K	191	1.15

IV-2.3. Small angle X-ray scattering (SAXS) measurements

SAXS measurements were performed at the BL-10C and BL-6A (for preliminary measurements) beamlines in KEK-PF (Ibaraki, Japan) and at the BL40B2 beamline in SPring-8 (Hyogo, Japan) for all ATODC and cATODC samples in THF, in MTBE, and in MHK at 25 °C to determine $P(q)$ and $\langle S^2 \rangle_z$ except for some high M_w samples of ATODC. The camera length, λ_0, the irradiation time, and the detector were chosen to be 2.0 – 3.0 m, 0.10 – 0.15 nm,

180 – 300 s, and a Dectris PILATUS2M silicon pixel detector in KEK-PF. Those in SPring-8 were chosen to be 4.0 m, 0.10 nm, 180 – 300 s, and a Rigaku R-AXIS VII imaging plate. The beam center and the accurate camera length were determined from the Bragg reflection of silver behenate. The scattering intensity data were corrected for the incident-light intensity and the transmittance of the solution by using the ion chamber installed upper and lower ends of the capillary. A circular-average procedure was employed for each two-dimensional intensity data to obtain the scattering intensity $I(q)$ as a function of the magnitude q of the scattering vector. Solvent and solutions with four or three different polymer mass concentrations c ranging from 1×10^{-3} to 2×10^{-2} g cm^{-3} were measured using exactly the same capillary to obtain the excess scattering intensity $\Delta I(q)$ from the solute. The obtained $\Delta I(q)$ for ATODC were extrapolated to infinite dilution by means of the Zimm plot to determine $[c/\Delta I(q)]_{c=0}$. The resultant $[c/\Delta I(q)]_{c=0}$ data were further extrapolated to $q^2 = 0$ with the Berry plot to determine $P(q)$ and $\langle S^2 \rangle_z$ (Figure VI-4). It should be noted that the data in THF were more fluctuated owing to the lower electron density contrast than those in the other two solvents. Similarly, the $\Delta I(q)$ data for cATODC were analyzed by means of the Guinier plot to obtain $P(q)$ and $\langle S^2 \rangle_z$ (Figure VI-5). The A_2 data in the three solvents were also evaluated by means of the method reported elsewhere[45] to be 5×10^{-5} – 4×10^{-4} mol cm^3 g^{-2} for ATODC and 5×10^{-5} – 3×10^{-4} mol cm^3 g^{-2} for cATODC, indicating these are good solvents both for ATODC and cATODC at 25 °C.

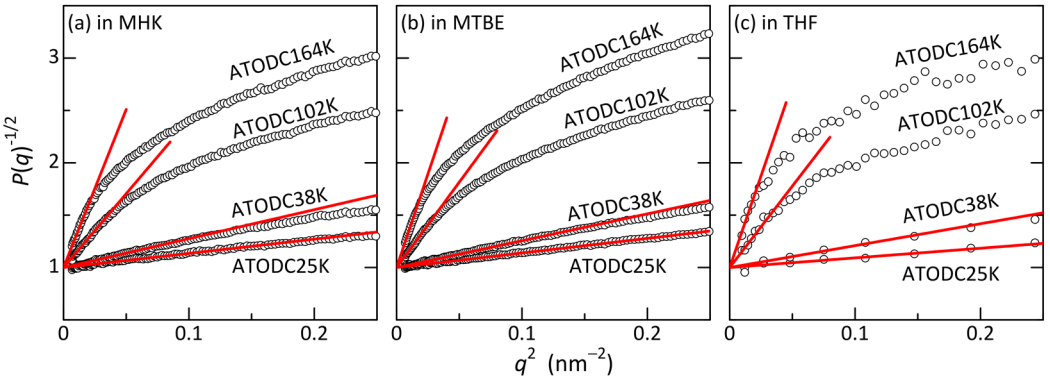

Figure IV-4. Berry plots for ATODC in MHK (a), in MTBE (b), and in THF (c) at 25 °C.

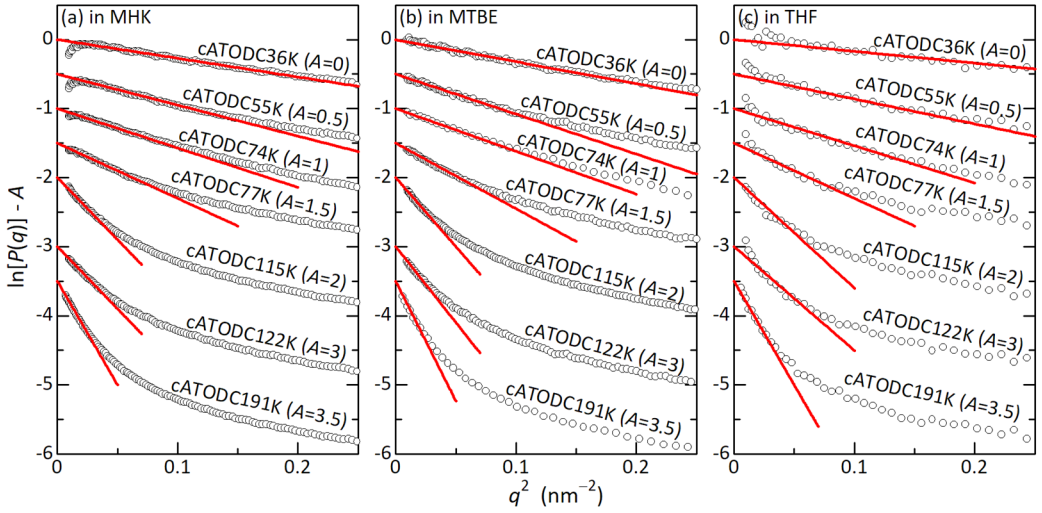

Figure IV-5. Guinier plots for cATODC in MHK (a), in MTBE (b), and in THF (c) at 25 °C. The ordinate values are shifted by *A*.

IV-2.4. Viscometry

Solvent and solution viscosity measurements were made for ATODC25K, ATODC38K, ATODC102K, ATODC164K, ATODC852K, and ATODC1510K in THF, MTBE, and MHK

at 25 °C by using Ubbelohde type viscometers. The intrinsic viscosity [η] and the Huggins constant k' were determined from the Huggins plot, the Fuoss-Mead plot, and the Billmeyer plot. The obtained k' values were 0.35 – 0.78 in MHK, 0.36 – 0.86 in MTBE and 0.38 – 0.69 in THF. This result is consistent with the above mentioned A_2. The measurements were not carried out for cATODC samples due to the limitation of sample quantity.

IV-2.5. Infrared (IR) absorption spectroscopy

IR absorption spectra were recorded for ATODC164K, cATODC36K, and cATODC191K in MTBE and THF at 25 °C with a FT/IR-4200 (JASCO) spectrometer and a solution cell made of CaF_2 with a path length of 0.05 mm (c ~ 0.03 g cm^{-3}). We note that MHK is not a suitable solvent to detect H-bonding of the carbamate groups because of the significant absorption of the solvent at the corresponding wavelength.

IV-3. Results

IV-3.1. Dimensional and hydrodynamic properties in solution

Double logarithmic plots of $\langle S^2 \rangle_z^{1/2}$ against M_w are shown in Figure IV-6. Data points for ATODC in the low M_w range obey a straight line with a slope of 0.85 – 0.95 and the slope for ATODC in THF decreases with increasing M_w. This is a typical behavior of semi-flexible polymers in solution. Data points for cATODC are appreciably smaller than those for ATODC at the same M_w. The shrinking factor g_s is defined as

$$g_s = \frac{\langle S^2 \rangle_c}{\langle S^2 \rangle_l} \qquad \text{(IV-1)}$$

where $\langle S^2 \rangle_c$ and $\langle S^2 \rangle_l$ are the gyration radius of cyclic and linear chains with the same molar mass, respectively. Except for the two lowest M_w samples, the calculated g_s values were between 0.34 and 0.51, which is substantially between $3/\pi^2$ and 1/2 for rigid and flexible rings, respectively, suggesting semiflexible nature of the higher M_w samples. The appreciably larger g_s values for the low M_w samples are most likely due to the different local helical structure as described in the following sections.

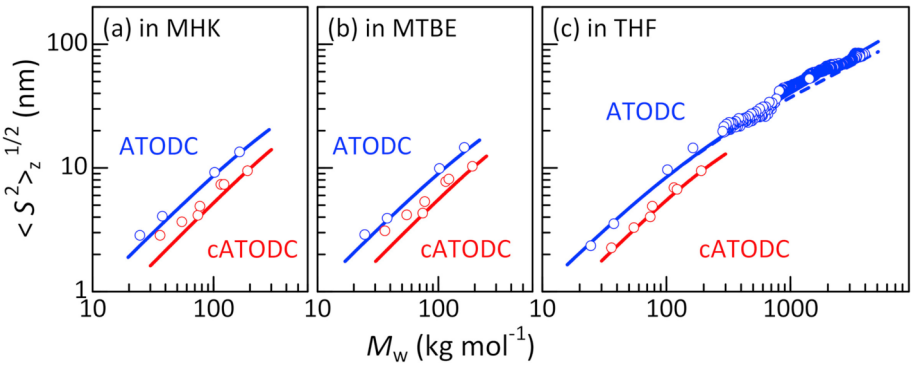

Figure IV-6. Double logarithmic plots of the radius of gyration $\langle S^2 \rangle_z^{1/2}$ against M_w for ATODC (unfilled circles) and cATODC (filled circles) in MHK (a), in MTBE (b), and in THF (c) at 25 °C. Blue solid and dashed curves, theoretical values for the wormlike chains with and without the excluded-volume effect. Red solid curves, theoretical values for the wormlike rings.

The $P(q)$ data for the linear ATODC samples are illustrated in Figure IV-7 in the form of the Holtzer plot. As in the case of other polysaccharide carbamate derivatives,[40] the $qP(q)$ data have a plateau region between $q = 0.4 - 1.9$ nm^{-1} and decrease with increasing q in MHK

and MTBE. This is a typical feature of the rod-like chain with finite chain thickness. An upward curvature for ATODC in THF is most likely due to the multilayered electron density profile. Indeed, similar behavior was also seen for ATBC in ethyl lactate[46] and cellulose tris(*n*-octadecylcarbamate) (CTODC) in THF.[44]

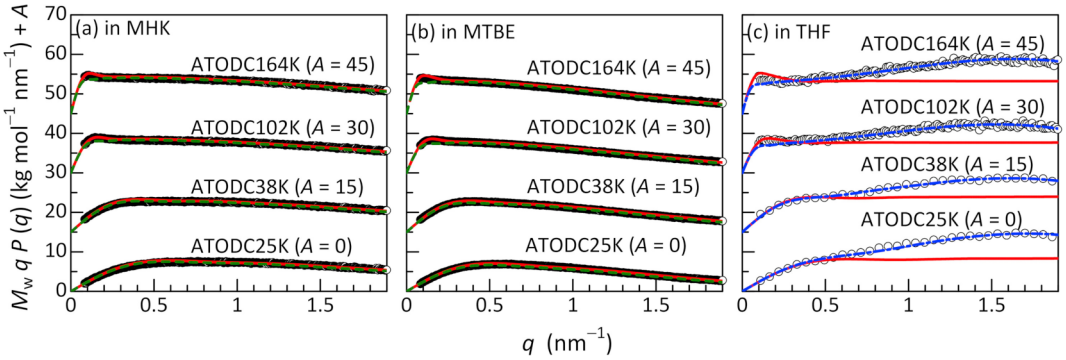

Figure IV-7. Reduced Holtzer plots for ATODC in MHK (a), in MTBE (b), and in THF (c) at 25 °C. Solid red curves, theoretical values for the wormlike cylinder. Dashed green curves, theoretical values for the cylindrical rod. Dot-dashed blue curves, theoretical values of the concentric double cylinder. The ordinate values are shifted by *A*.

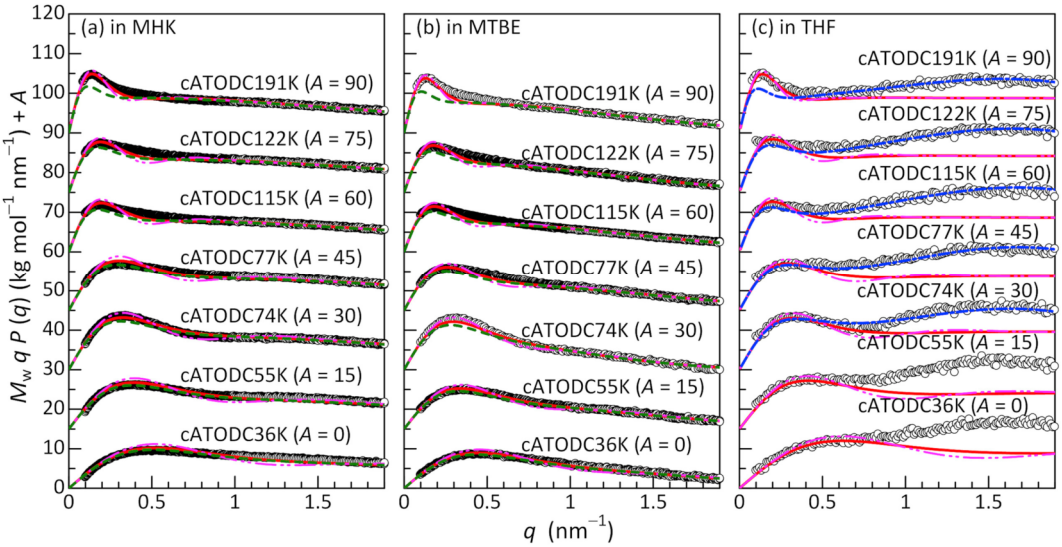

Figure IV-8. Reduced Holtzer plots for cATODC in MHK (a), in MTBE (b), and in THF (c) at 25 °C. Solid red and double dot-dashed magenta curves, theoretical values for the touched-bead wormlike ring with log-normal distribution with $Đ = 1.20$ and 1.05, respectively. Dashed green curves, theoretical values for the rigid limit with $Đ = 1.20$. Dot-dashed blue curves, theoretical values of the concentric double cylindrical toroid with $Đ = 1.20$. The ordinate values are shifted by A.

The reduced Holtzer plot was also constructed for the cATODC samples as displayed in Figure IV-8. While the shape of the plot in a high q region of each sample is substantially similar to that for the corresponding linear chain, a significant peak is found at the low-q range only for the cyclic chain. Similar peaks on Holtzer plots were also found for other cyclic amylose carbamates.[22,23,36]

Molar-mass dependence of $[\eta]$ is shown in Figure IV-9 for linear ATODC samples in the three solvents. The S-shaped curve with the relatively large slope is typical for rigid polymer chains.

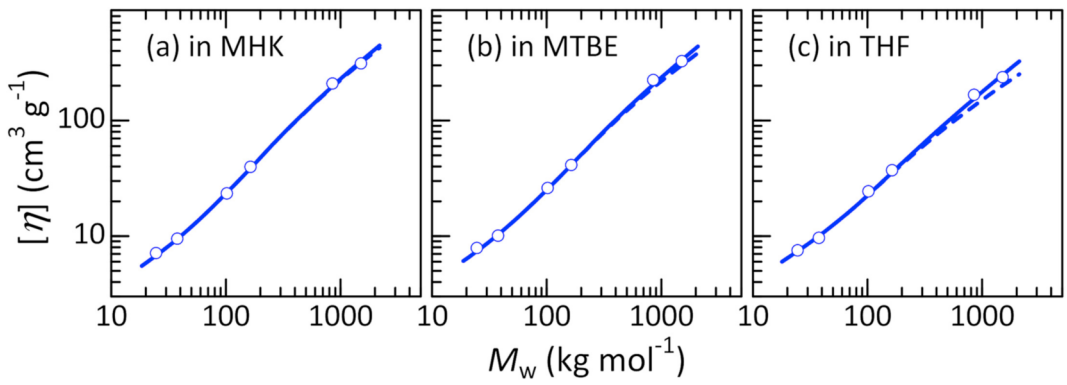

Figure IV-9. Double logarithmic plots of the intrinsic viscosity $[\eta]$ against M_w for ATODC in MHK (a), in MTBE (b), and in THF (c) at 25 °C. Solid and dashed curves, theoretical values for the wormlike cylinders with and without excluded volume effects.

IV-3.2. Solution infrared (IR) absorption spectra

The IR spectra for ATODC and cATODC in MTBE and THF are shown in Figure IV-10. A split amide I band is found around 1720 cm^{-1}. The two peaks at 1740 cm^{-1} and 1700 cm^{-1} may be assigned to be free and intramolecular H-bonding C=O groups, respectively, as in the case of amylose tris(3,5-dimetylphenylcarbamate) (ADMPC)[47] and ATBC.[39] Since the double peak is well fitted by two Gaussian distributions, we obtained the number fraction f_{hyd} of H-bonding C=O groups for the three samples in the three solvents, that is, $f_{hyd} = 0.53 \pm 0.02$ for all the systems investigated. This value is the highest in the other amylose tris(alkylcarbamate) (ATAC) samples in various solvents. It indicates that repulsion force between side groups are negligibly effectible to the intramolecular H-bonding of the ATODC and cATODC chains. Furthermore, the f_{hyd} value is almost independent of the solvent while those for previously investigated ATACs significantly depend on the

solvents. This may be because currently investigated MTBE and THF do not have enough polarity to significantly break the intramolecular H-bonds.

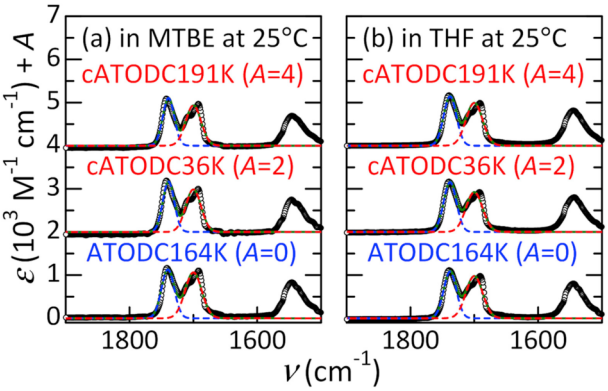

Figure IV-10. Solution IR spectra for indicated samples in MTBE (a) and THF (b) at 25 °C. The ordinate values are shifted by *A*.

IV-4. Discussion

IV-4.1. Analyses in terms of the linear wormlike chain: ATODC

The particle scattering function $P(q)$ of linear wormlike chains can be calculated in terms of the Nakamura-Norisuye expression for the wormlike cylinder.[48,49] The theoretical $P(q)$ can be calculated by their equation with the contour length L, the Kuhn segment length λ^{-1} (or twice the persistence length), and the chain diameter d. The parameter L is proportional to M_w as follows,

$$L = \frac{hM_w}{M_0} \qquad \text{(IV-2)}$$

with M_0 being the molar mass of the repeat unit ($M_0 = 1049$ g mol^{-1}) and h the helix pitch (or

rise) per residue. A curve fitting procedure was employed for ATODC samples in MHK and MTBE. Two parameters, h and d, were uniquely determined to be $h = 0.36$ nm and $d = 1.5$ nm in MHK and $h = 0.39$ nm and $d = 2.3$ nm in MTBE while λ^{-1} cannot be determined since the obtained theoretical values are substantially the same as the rod limiting value as illustrated in Figure IV-7. If we assume the λ^{-1} value determined from $[\eta]$ described below, the theoretical $P(q)$ quantitatively explains the experimental data. Upward curvature for ATODC in THF may not, however, be explained by the theory. This is most likely because the side alkyl groups have lower electron density than the core region and solvent. According to our recent study,[44] experimental data for CTODC, which has the same side group as ATODC, were well fitted by the theoretical values for the concentric double cylinder, of which $P(q)$ can be expressed as,[50]

$$P(q) = \int_0^{\pi/2} \left[\frac{d_o^2 G\left(q, \beta, \frac{d_o}{2}, \frac{L}{2}\right) + f d_i^2 G\left(q, \beta, \frac{d_i}{2}, \frac{L}{2}\right)}{d_o^2 + f d_i^2} \right]^2 \sin\beta \, \mathrm{d}\beta \qquad \text{(IV-3)}$$

$$G(q, \beta, a, b) = \frac{\sin(qb\cos\beta)\, 2J_1(qa\sin\beta)}{q^2 ab \sin\beta \cos\beta} \qquad \text{(IV-4)}$$

$$f = \frac{\Delta\rho_i - \Delta\rho_o}{\Delta\rho_o} \qquad \text{(IV-5)}$$

when the chain flexibility is negligible. Here, d_i and d_o are the diameter of the inner and outer cylinders, $\Delta\rho_i$ and $\Delta\rho_o$ are the corresponding excess electron densities, and J_1 is a first-order Bessel function of the first kind. We estimated h, d_i, d_o, and f to be 0.40 nm, 2.5 nm,

3.2 nm, and −2.2, respectively, to fit the experimental data as shown in Figure IV-7. It should be noted that the experimental data for ATODC in MHK and MIBK may be explained by the same d_i and d_o with $f = -2.9$, and −6.0, respectively. The obtained theoretical values for high molar mass ATODC in THF at low q region somewhat underestimate the experimental data which can be reproduced by the thin wormlike chain when we choose λ^{-1} determined from $[\eta]$ described later (solid red curves in Figure IV-7c).

Theoretical intrinsic viscosity $[\eta]_0$ formulated by Yamakawa et al.[17,51,52] for the wormlike cylinder can be calculated with the three parameters, L, λ^{-1}, and d. When we assume h from $P(q)$, the remaining two parameters, λ^{-1} and d, were unequivocally determined to be $\lambda^{-1} = 45 \pm 4$ nm and $d = 4.0$ nm in MHK, $\lambda^{-1} = 37 \pm 4$ nm and $d = 3.9$ nm in MTBE, and $\lambda^{-1} = 30 \pm 2$ nm and $d = 4.0$ nm in THF. It should be noted that the d values are not consistent with those from $P(q)$ because $P(q)$ reflects electron density profile of the polymer chain as described above. Since the three solvent systems are good solvents, the viscosity expansion factor α_η defined as

$$\alpha_\eta^{\,3} = \frac{[\eta]}{[\eta]_0} \tag{IV-6}$$

may not be negligible. We thus estimated $\alpha_\eta^{\,3}$ in terms of the Barrett function[53] and the quasi-two-parameter (QTP) theory[17,54,55] with the parameters, that is, L, λ^{-1}, and the excluded volume strength B. When we approximately estimated the last parameter B from the above mentioned A_2 with the QTP scheme with a method as reported elsewhere,[45] α_η was substantially close to unity for ATODC in MHK and MTBE in the current M_w range while the

theoretical [η] quite overestimated the data in THF. Theoretical values with somewhat smaller λ^{-1} of 24 nm reproduce the experimental data as shown in Figure IV-9.

Likewise, theoretical gyration radii $\langle S^2\rangle_0$ for the unperturbed wormlike chain can be calculated from the following Benoit-Doty equation[56] as

$$\lambda^2 \left\langle S^2 \right\rangle_0 = \frac{N_K}{6} - \frac{1}{4} + \frac{1}{4N_K} - \frac{1}{8N_K^2}\left[1 - \exp\left(-2N_K\right)\right] \qquad \text{(IV-7)}$$

where N_K is the Kuhn segment number defined as $N_K \equiv \lambda L$. The gyration-radius expansion factor α_s defined as $\alpha_s^2 \equiv \langle S^2\rangle/\langle S^2\rangle_0$ with $\langle S^2\rangle$ being the gyration radius taking the excluded-volume effects into consideration can be estimated in terms of the Domb-Barrett function[57] in the QTP scheme.[17,54,55] Two wormlike chain parameters, h and λ^{-1}, were uniquely determined for ATODC in THF when assuming B from A_2 as in the case of [η]. The experimental $\langle S^2\rangle_z$ data in the other two solvents can be explained by the same model with the parameters determined by $P(q)$ and [η] while each wormlike chain parameter was infeasible to be determined unequivocally. We note that the chain thickness was negligible for $\langle S^2\rangle$ if we consider it as $\langle S^2\rangle = \langle S^2\rangle_0 + d^2/8$. The resultant parameters summarized in Table IV-3 are consistent with each other, indicating that the wormlike chain is a good model for ATODC in the three solvents.

Table IV-3. Wormlike chain parameters for linear ATODC in solution

solvent	method	h (nm)	λ^{-1} (nm)	B (nm)	d (nm)
MHK	$\langle S^2\rangle_z$	0.36[a]	45[a]	2.6[b]	
	$P(q)$	0.36 ± 0.02	45[a]		1.5
	$[\eta]$	0.36[a]	45 ± 4	2.6[b]	4.0
MTBE	$\langle S^2\rangle_z$	0.39[a]	37[a]	5.6[b]	
	$P(q)$	0.39 ± 0.01	37[a]		2.2
	$[\eta]$	0.39[a]	37 ± 4	5.6[b]	3.9
THF	$\langle S^2\rangle_z$	0.40 ± 0.03	24 ± 2	5.8[b]	
	$P(q)$	0.40 ± 0.03	31[a]		3.2[c]
	$[\eta]$	0.40[a]	24 ± 2	5.8[b]	4.0

[a] Assumed. [b] Estimated from A_2 and the QTP theory (see text). [c] d_o.

IV-4.2. Chain characteristics of linear ATODC

Table IV-4 summarizes the obtained wormlike chain parameters for ATODC along with other ATACs[39,40,43,46] and cellulose alkylcarbamates (CTACs).[44] Although ATODC (alkyl side chain length $n = 18$) has the highest f_{hyd} in the investigated n range (2, 4, 6, and 18), the chain stiffness parameter (λ^{-1}) is appreciably smaller than those for ATBC ($n = 4$) and ATHC ($n = 6$) as illustrated in Figure IV-11, while the h value reflecting the local helical structure is longer than them. This indicates that repulsive forces between neighboring side chains of ATODC inhibit the formation of a tightly wound local helical structure. The chain stiffness is not only determined by intramolecular H-bonds but also by the difference in the local helical structure. Recently investigated CTACs seem to have similar tendency while the n dependence is less significant (Figure IV-11). On the other hand, the chain stiffness of

ATODC in MHK and MTBE is quite higher than that in THF while they have almost the same h value and f_{hyd} (in MTBE). Similar solvent dependent chain stiffness was also found for an amylose carbamate derivative having bulky side groups, that is, ADMPC[42] and ATPC,[41] in Figure IV-12 whereas the wormlike chain parameters for ATACs with shorter side groups significantly depends on f_{hyd}.[39,40,43] This suggests that H-bonding MHK and MTBE molecules may hinder the internal rotation of ATODC main chain. Taking into account the excellent ability of ADMPC[58,59] (and ATPC)[60] as the chiral stationary phase, ATODC may have a potential use as the chiral separation agent.

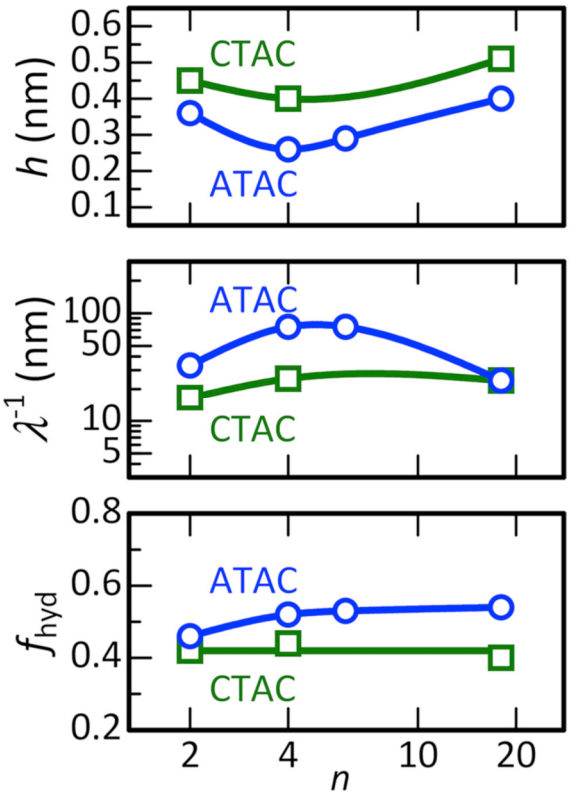

Figure IV-11. Side-chain length (n) dependence of the h, λ^{-1}, and f_{hyd} for ATACs (circles) and CTACs (squares)[44] in THF.

Table IV-4. Values of h, λ^{-1}, and the number fraction f_{hyd} of intramolecular H-bonding C=O groups for ATACs and cellulose tris(alkylcarbamate)s (CTACs)

polymer	solvent	T (°C)	h (nm)	λ^{-1} (nm)	f_{hyd}	Ref.
ATODC	MHK	25	0.36 ± 0.02	45 ± 4		This work
ATODC	MTBE	25	0.39 ± 0.01	37 ± 4	0.55	This work
ATODC	THF	25	0.40 ± 0.03	24 ± 2	0.54	This work
ATHC	THF	25	0.29 ± 0.02	75 ± 5	0.53	40
ATHC	1PrOH	25	0.39 ± 0.02	30 ± 3	0.34	40
ATBC	THF	25	0.26 ± 0.01	75 ± 5	0.52	39
ATBC	$_{D}$-EL	25	0.26 ± 0.01	49 ± 4		46
ATBC	2BuOH	45	0.25 ± 0.01	40 ± 5	0.41	43
ATBC	2EE	25	0.25 ± 0.01	38 ± 4	0.39	43
ATBC	$_{DL}$-EL	25	0.26 ± 0.01	38 ± 3		46
ATBC	$_{L}$-EL	25	0.26 ± 0.01	32 ± 2		46
ATBC	1PrOH	40	0.28 ± 0.01	25 ± 2	0.33	43
ATBC	2PrOH	35	0.29 ± 0.01	20 ± 2	0.29	43
ATBC	MeOH	25	0.32 ± 0.01	11 ± 2	0	39
ATEC	THF	25	0.36 ± 0.02	33 ± 3	0.46	40
ATEC	$_{D}$-EL	25	0.35 ± 0.02	27 ± 2		40
ATEC	$_{L}$-EL	25	0.38 ± 0.02	15 ± 2		40
ATEC	2ME	25	0.38 ± 0.02	14 ± 2	0.26	40
ATEC	MeOH	25	0.38 ± 0.02	9 ± 1	0	40
CTODC	THF	25	0.51 ± 0.03	24 ± 1	0.40	44
CTBC	THF	25	0.40 ± 0.02	25 ± 1	0.44	44
CTEC	THF	25	0.45 ± 0.02	16.5 ± 1	0.42	44

2BuOH: 2-butanol. 2EE: 2-rthoxyethanol. EL: ethyl lactate. 2ME: 2-methoxyethanol. CTEC: cellulose tris(ethylcarbamate). CTBC: cellulose tris(*n*-butylcarbamate).

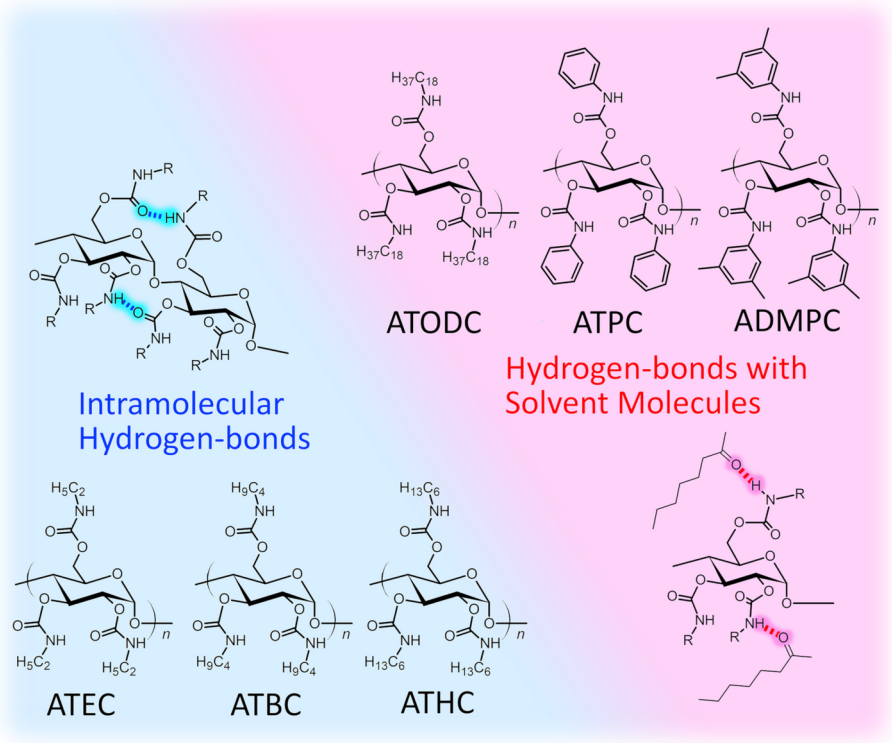

Figure IV-12. Schematic representation of the origin of the chain stiffness of amylose carbamates investigated.

IV-4.3. Analyses in terms of the cyclic wormlike chain: cATODC

According to Shimada and Yamakawa,[61] gyration radii $\langle S^2 \rangle_c$ of the wormlike ring may be calculated as

$$\lambda^2 \left\langle S^2 \right\rangle_c = \frac{N_K^2}{4\pi^2}\left(1 - 0.1140N_K - 0.0055258N_K^2 + 0.0022471N_K^3 - 0.00013155N_K^4\right) \quad \text{for} \quad N_K \le 6 \qquad \text{(IV-8)}$$

$$= \frac{N_K}{12}\left\{1 - \frac{7}{6N_K} - 0.025\exp\left(-0.01N_K^2\right)\right\} \quad \text{for} \quad N_K \ge 6$$

Solid red curves in Figure IV-6 are the calculated values of eq IV-8 with the parameters (h and λ^{-1}) for the corresponding linear ATODC listed in Table IV-3. They only reproduce the $\langle S^2\rangle_z$ data for high M_w region and deviate upward with lowering M_w in MHK and in MTBE, suggesting that the wormlike chain parameters of the cyclic chain are different from those for the corresponding linear chain and/or they may depend on the chain length as depicted in the literature[36] and previous chapters (II and III). It should be noted that the chain thickness effect is insignificant in the M_w range investigated if we estimate it as the touched-bead model of which the contribution can be estimated as $\langle S^2\rangle = \langle S^2\rangle_c + 3d_b^2/20$ with d_b being the bead diameter estimated from the $P(q)$ described below.

Analyses of $P(q)$ allow us to determine the wormlike chain parameters for each sample. This is an effective method when the wormlike chain parameters may depend on the chain length. While $P(q)$ of the wormlike ring cannot be calculated analytically, Tsubouchi et al.[62] developed a Monte Carlo simulation method to calculate the particle scattering function $P_c(q)$ of thin wormlike ring. Furthermore, if the chain thickness is taken into account by the touched-bead model as follows,

$$P(q) = 9\left(\frac{2}{qd_b}\right)^6\left(\sin\frac{qd_b}{2} - \frac{qd_b}{2}\cos\frac{qd_b}{2}\right)^2 P_c(q) \qquad \text{(IV-9)}$$

we reported that the resultant $P(q)$ successfully reproduced the experimental data for the three amylose derivatives, that is, cATPC, cATBC, and cADMPC (cf. Chapter II and Chapter III). A curve fitting procedure was examined assuming log-normal molar-mass distribution with $Đ = 1.05$ and 1.20. The resultant theoretical values well explain the experimental data for

cATODC in MHK and MTBE as illustrated in Figure IV-8. While the obtained d_b values are consistent with the corresponding linear chains, that is, $d_b = 1.5 \pm 0.3$ nm in MHK and $d_b = 2.8 \pm 0.6$ nm in MTBE, appreciably M_w-dependent h values were evaluated. The parameter λ^{-1} was only determined for the highest M_w sample because the theoretical $P(q)$ for the wormlike ring with the corresponding λ^{-1} and lower M_w is substantially the same as those for the rigid ring.

Since the specific behavior in the $P(q)$ data for cATODC in THF cannot be analyzed by the above mentioned touched-bead model, the concentric cylindrical ring model was utilized to analyze the data for lower M_w samples. The particle scattering function $P(q)$ can be expressed as

$$P(q) = \int_0^{\pi/2} \left[\frac{d_o^2 F\left(q, \beta, \frac{d_o}{2}, \frac{L}{2\pi}\right) + f d_i^2 F\left(q, \beta, \frac{d_i}{2}, \frac{L}{2\pi}\right)}{d_o^2 + f d_i^2} \right]^2 \sin\beta \, \mathrm{d}\beta \qquad \text{(IV-10)}$$

$$F\left(q, \beta, a, b\right) = \frac{\int_{b-a}^{b+a} 2 r J_0\left(qr \sin\beta\right) \sin\left[q \cos\beta \sqrt{a^2 - \left(r-b\right)^2} \right] dr}{\pi a^2 b q \cos\beta} \qquad \text{(IV-11)}$$

where J_0 is the Bessel function of zeroth order. This equation can be readily evaluated from the scattering function of torus[63] and the above mentioned procedure for the concentric cylinder[50] or for the concentric spheres.[64] The z-average $P(q)$ were calculated assuming log-normal distribution of L with $Đ = 1.20$. The parameter h may uniquely be determined for five samples except for the two lowest M_w samples. This difficulty to analyze the data of the low M_w samples is probably because the length scale of the gyration radii is similar to that

for the chain thickness. We note that d_i, d_o, and f were substantially the same as those for the linear chain. Assuming the obtained h value, we also attempted to estimate λ^{-1} in terms of the thin wormlike ring to fit the data point at the low q region (see solid red curves in Figure IV-8c). The parameter could only be estimated for the highest M_w sample as in the case of the other solvents systems.

To check the validity of the estimated parameters, we compared the experimental $\langle S^2 \rangle_z$ and the calculated $\langle S^2 \rangle_c$ from eq IV-8 with the parameters obtained for each sample in Figure IV-13. Good agreement but slightly larger $\langle S^2 \rangle_z$ are most likely due to the molar mass distribution which is only considered for $P(q)$. Indeed, if we calculate the z-average values with log-normal distribution, they reproduce the experimental data almost quantitatively.

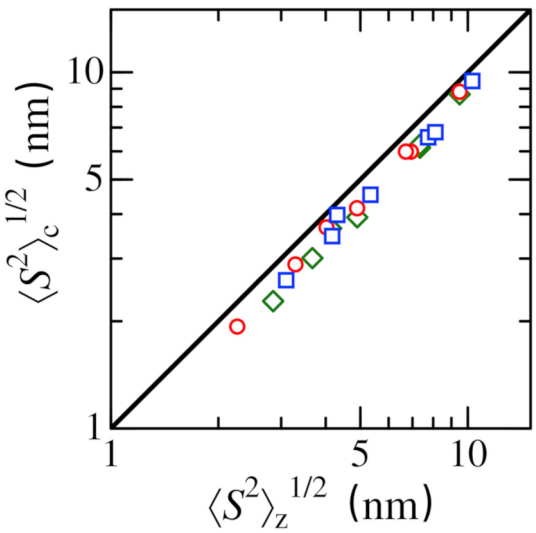

Figure IV-13. Comparison between theoretical $\langle S^2 \rangle_c^{1/2}$ from eq IV-8 and experimental $\langle S^2 \rangle_z^{1/2}$ for cATODC in MHK (green diamonds), in MTBE (blue squares), and in THF (red circles). A solid line, $\langle S^2 \rangle_c^{1/2} = \langle S^2 \rangle_z^{1/2}$.

IV-4.4. Comparison between cATODC and ATODC

The obtained h values for cATODC are plotted against M_w in Figure IV-14. While the parameter h for the highest M_w sample is substantially the same as that in the corresponding solvent, it gradually deviates upward with decreasing M_w. This molar mass dependent crossover behavior is firstly observed in our knowledge because the molar mass range for the previously investigated cyclic amylose derivatives did not match the crossover range. While almost the same h values as that for the corresponding linear chain were obtained for the highest M_w sample, cATODC191K, the obtained λ^{-1} is somewhat smaller than that for the linear polymer in the same solvent, that is, $\lambda^{-1} = 25 \pm 5$ nm, 24 ± 5 nm, and 25 ± 5 nm in MHK, MTBE, and THF, respectively. Recently, we showed that the Kuhn segment number of the ring polymer becomes larger with lowering N_K for the corresponding linear chain. The current N_K data are plotted along with the results for cATBC, cATPC (cf. Chapter II), and cADMPC (cf. Chapter III) in Figure IV-15. While the λ^{-1} values for cATODC tends to deviate with lowering $N_{K,linear}$, they are still fairly close to that for $N_{K,linear}$ and therefore they are fitted by the previous data for other cyclic amylose derivatives. This is reasonable because the $N_{K,linear}$ data of the current cATODC samples is higher than the previously determined threshold value of 1 – 1.5 at which the ring closure probability of the wormlike chains abruptly decreases with lowering $N_{K,linear}$.[17] We may thus concluded that drastic conformational difference can only be observed when $N_{K,linear} < 1 - 1.5$, but it is still negligible in the higher $N_{K,linear}$ range. Even though the linear contaminant is not negligible, the 'real' h value for cATODC should be more different from the linear chain and the λ^{-1} value

should be lower, indicating above mentioned conclusion may not be an artifact of contamination.

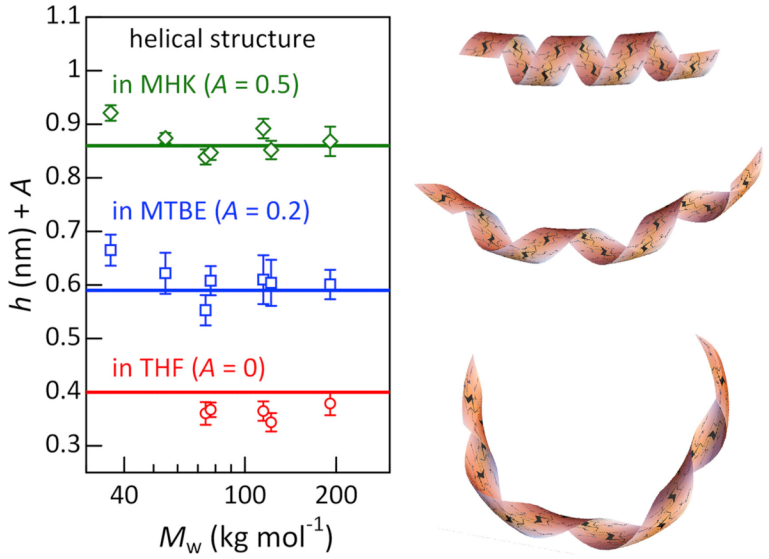

Figure IV-14. Comparison of h for cATODC (symbols) with those for linear ATODC (solid lines) in MHK (green diamonds), in MTBE (blue squares), and in THF (red circles). The ordinate values are shifted by A.

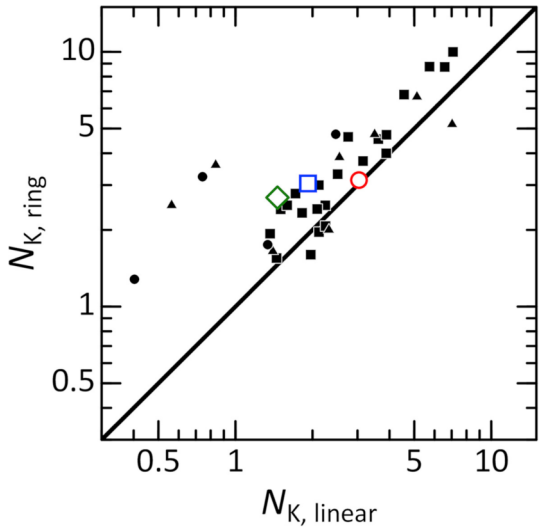

Figure IV-15. Double logarithmic plots of $N_{K,ring}$ against $N_{K,linear}$ for cATODC in MHK (a green diamond), in MTBE (a blue square), and in THF (a red circle). The other symbols are the values for cADMPC (filled circles), cATPC (filled squares), and cATBC (filled triangles) reported in Chapter II and Chapter III. A solid line, $N_{K,ring} = N_{K,linear}$.

IV-5. Conclusion

Linear and cyclic amylose carbamate derivatives (ATODC and cATODC) having relatively long alkyl ($C_{18}H_{37}$) groups are successfully prepared from the corresponding enzymatically synthesized amylose. Chain stiffness of the linear chain is appreciably lower than those with shorter alkyl (butyl or hexyl) side chains, while the main chain of many brush like polymers tends to be stiffened with increasing side chain length. The alkyl side chains of ATODC mainly extend the amylosic helix in THF and the resultant weakly wounded local helical structure retains the lower chain stiffness.

As in the case of our recent study for cyclic amylose derivatives, more extended local helical structure and somewhat less chain stiffness were observed for the cATODC samples

in solution. This indicates that brush-like ring polymers may show similar behavior as those for the other semiflexible ring polymers. Both ATODC and cATODC may be good models of stiff polymers since they have good solubility in common organic solvents and indeed they form lyotropic liquid crystallinity in semi-concentrated solutions.

IV-6. Appendix

Table IV-A1. Radius of Gyration for ATODC in MHK, MTBE, and THF at 25 °C

Sample Name	$\langle S^2 \rangle_z^{1/2}$ (nm)		
	in MHK	in MTBE	in THF
ATODC25K	2.85	2.89	2.35
ATODC38K	4.07	3.92	3.54
ATODC102K	9.20	9.89	9.66
ATODC164K	13.5	14.6	14.5

Table IV-A2. Radius of Gyration for cATODC in MHK, MTBE, and THF at 25 °C

Sample Name	$\langle S^2 \rangle_z^{1/2}$ (nm)		
	in MHK	in MTBE	in THF
cATODC36K	2.85	3.10	2.26
cATODC55K	3.67	4.17	3.29
cATODC74K	4.14	4.31	4.02
cATODC77K	4.90	5.34	4.90
cATODC115K	7.35	7.75	6.93
cATODC122K	7.35	8.12	6.71
cATODC191K	9.49	10.3	9.49

Table IV-A3. Intrinsic Viscosity for ATODC in MHK, MTBE and THF

Sample Name	$[\eta]$ (cm^3g^{-1})		
	in MHK	in MTBE	in THF
ATODC25K	7.1	7.9	7.5
ATODC38K	9.5	10.1	9.7
ATODC102K	23.4	26.1	24.4
ATODC164K	39.7	41.2	37.1
ATODC852K	209	224	167
ATODC1510K	312	326	237

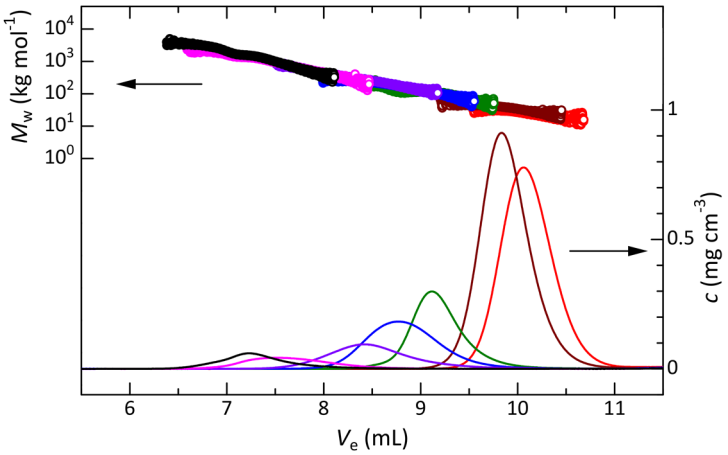

Figure IV-A1. Retention volume V_e dependence of the weight-average molar mass M_w (circles) and the polymer mass concentration c (solid curves) for ATODC25K (red), ATODC38K (brown), ATODC102K (green), ATODC164K (blue), ATODC284K (purple), ATODC852K (pink), and ATODC1510K (black) separated by size exclusion chromatograph in THF.

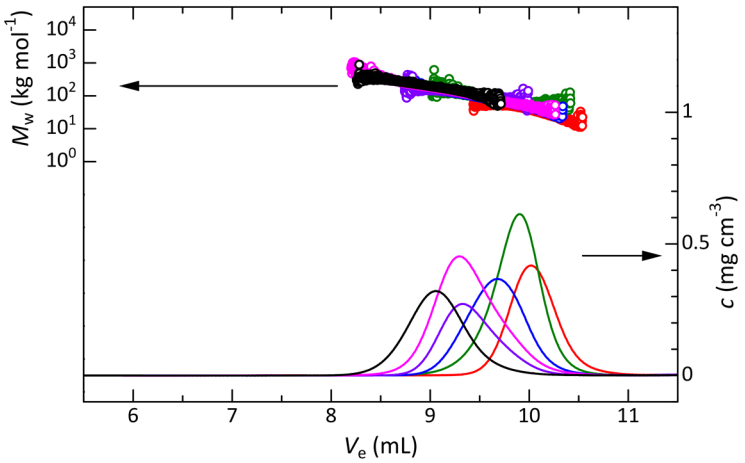

Figure IV-A2. Retention volume dependence of the weight-average molar mass Mw (circles) and the polymer mass concentration *c* (solid curves) for cATODC36K (red), cATODC74K (green), cATODC77K (blue), cATODC110K (purple), cATODC120K (pink), and cATODC190K (black) separated by size exclusion chromatograph in THF.

Reference

(1) Wintermantel, M.; Gerle, M.; Fischer, K.; Schmidt, M.; Wataoka, I.; Urakawa, H.; Kajiwara, K.; Tsukahara, Y. *Macromolecules* **1996**, *29*, 978–983.

(2) Terao, K.; Nakamura, Y.; Norisuye, T. *Macromolecules* **1999**, *32*, 711–716.

(3) Zhang, B.; Gröhn, F.; Pedersen, J. S.; Fischer, K.; Schmidt, M. *Macromolecules* **2006**, *39*, 8440–8450.

(4) Sugiyama, M.; Nakamura, Y.; Norisuye, T. *Polym. J.* **2008**, *40*, 109–115.

(5) Xu, Z.; Hadjichristidis, N.; Fetters, L. J. *Macromolecules* **1984**, *17*, 2303–2306.

(6) Mays, J. W.; Hadjichristidis, N. *J. Macromol. Sci. Part C Polym. Rev.* **1988**, *28*, 371–401.

(7) Kato, H.; Sasanuma, Y.; Kaito, A.; Tanigaki, N.; Tanabe, Y.; Kinugasa, S. *Macromolecules* **2001**, *34*, 262–268.

(8) Chung, W.; Shibaguchi, H.; Terao, K.; Fujiki, M.; Naito, M. *Macromolecules* **2011**, *44*, 6568–6573.

(9) Sheiko, S. S.; Sumerlin, B. S.; Matyjaszewski, K. *Prog. Polym. Sci.* **2008**, *33*, 759–

785.

(10) Yuan, J.; Müller, A. H. E.; Matyjaszewski, K.; Sheiko, S. S. In *Polymer Science: A Comprehensive Reference*; Elsevier, 2012; Vol. 6, pp 199–264.

(11) Schappacher, M.; Deffieux, A. *Macromolecules* **2005**, *38*, 4942–4946.

(12) Schappacher, M.; Deffieux, A. *Macromolecules* **2005**, *38*, 7209–7213.

(13) Schappacher, M.; Deffieux, A. *Science (80-.).* **2008**, *319*, 1512–1515.

(14) Schappacher, M.; Deffieux, A. *J. Am. Chem. Soc.* **2008**, *130*, 14684–14689.

(15) Xia, Y.; Boydston, A. J.; Grubbs, R. H. *Angew. Chemie - Int. Ed.* **2011**, *50*, 5882–5885.

(16) Zhang, K.; Tew, G. N. *React. Funct. Polym.* **2014**, *80*, 40–47.

(17) Yamakawa, H.; Yoshizaki, T. *Helical Wormlike Chains in Polymer Solutions*, 2nd ed.; Springer: Berlin, Heidelberg, 2016.

(18) Norisuye, T. *Prog. Polym. Sci.* **1993**, *18*, 543–584.

(19) Nakamura, Y.; Norisuye, T. In *Polymer Science: A Comprehensive Reference*; Elsevier, 2012; Vol. 2, pp 5–32.

(20) Hasegawa, H.; Nagata, Y.; Terao, K.; Suginome, M. *Macromolecules* **2017**, *50*, 7491–7497.

(21) Doi, Y.; Iwasa, Y.; Watanabe, K.; Nakamura, M.; Takano, A.; Takahashi, Y.; Matsushita, Y. *Macromolecules* **2016**, *49*, 3109–3115.

(22) Terao, K.; Asano, N.; Kitamura, S.; Sato, T. *ACS Macro Lett.* **2012**, *1*, 1291–1294.

(23) Terao, K.; Shigeuchi, K.; Oyamada, K.; Kitamura, S.; Sato, T. *Macromolecules* **2013**, *46*, 5355–5362.

(24) Takaha, T.; Yanase, Mi.; Takata, H.; Okada, S.; Smith, S. M. *J. Biol. Chem.* **1996**, *271*, 2902–2908.

(25) Nakata, Y.; Amitani, K.; Norisuye, T.; Kitamura, S. *Biopolymers* **2003**, *69*, 508–516.

(26) Bates, A. D.; Maxwell, A. *DNA Topology*; Oxford University Press: New York, U.S.A., 2005.

(27) Kitamura, S.; Isuda, H.; Shimada, J.; Takada, T.; Takaha, T.; Okada, S.; Mimura, M.; Kajiwara, K. *Carbohydr. Res.* **1997**, *304*, 303–314.

(28) Shimada, J.; Kaneko, H.; Takada, T.; Kitamura, S.; Kajiwara, K. *J. Phys. Chem. B* **2000**, *104*, 2136–2147.

(29) Ragnetti, M.; Geiserb, D.; Hd, H.; Oberthiir, R. C. *Makromol. Chemie* **1985**, *186*,

1701–1709.

(30) Lutz, P.; McKenna, G. B.; Rempp, P.; Strazielle, C. *Makromol. Chemie, Rapid Commun.* **1986**, *7*, 599–605.

(31) Hadziioannou, G.; Cotts, P. M.; ten Brinke, G.; Han, C. C.; Lutz, P.; Strazielle, C.; Rempp, P.; Kovacs, A. J. *Macromolecules* **1987**, *20*, 493–497.

(32) Takano, A.; Ohta, Y.; Masuoka, K.; Matsubara, K.; Nakano, T.; Hieno, A.; Itakura, M.; Takahashi, K.; Kinugasa, S.; Kawaguchi, D.; et al. *Macromolecules* **2012**, *45*, 369–373.

(33) Gooßen, S.; Brás, A. R.; Pyckhout-Hintzen, W.; Wischnewski, A.; Richter, D.; Rubinstein, M.; Roovers, J.; Lutz, P. J.; Jeong, Y.; Chang, T.; et al. *Macromolecules* **2015**, *48*, 1598–1605.

(34) Jeong, Y.; Jin, Y.; Chang, T.; Uhlik, F.; Roovers, J. *Macromolecules* **2017**, *50*, 7770–7776.

(35) Higgins, J. S.; Dodgson, K.; Semlyen, J. A. *Polymer (Guildf).* **1979**, *20*, 553–558.

(36) Asano, N.; Kitamura, S.; Terao, K. *J. Phys. Chem. B* **2013**, *117*, 9576–9583.

(37) Bittiger, H.; Keilich, G. *Biopolymers* **1969**, *7*, 539–556.

(38) Burchard, W. In *Soft Matter Characterization*; Springer Netherlands: Dordrecht, 2008; pp 463–603.

(39) Terao, K.; Murashima, M.; Sano, Y.; Arakawa, S.; Kitamura, S.; Norisuye, T. *Macromolecules* **2010**, *43*, 1061–1068.

(40) Terao, K.; Maeda, F.; Oyamada, K.; Ochiai, T.; Kitamura, S.; Sato, T. *J. Phys. Chem. B* **2012**, *116*, 12714–12720.

(41) Fujii, T.; Terao, K.; Tsuda, M.; Kitamura, S.; Norisuye, T. *Biopolymers* **2009**, *91*, 729–736.

(42) Tsuda, M.; Terao, K.; Nakamura, Y.; Kita, Y.; Kitamura, S.; Sato, T. *Macromolecules* **2010**, *43*, 5779–5784.

(43) Sano, Y.; Terao, K.; Arakawa, S.; Ohtoh, M.; Kitamura, S.; Norisuye, T. *Polymer (Guildf).* **2010**, *51*, 4243–4248.

(44) Jiang, X.; Ryoki, A.; Terao, K. *Polymer (Guildf).* **2017**, *112*, 152–158.

(45) Jiang, X.; Terao, K.; Chung, W.; Naito, M. *Polymer (Guildf).* **2015**, *68*, 221–226.

(46) Arakawa, S.; Terao, K.; Kitamura, S.; Sato, T. *Polym. Chem.* **2012**, *3*, 472–478.

(47) Kasat, R. B.; Wee, S. Y.; Loh, J. X.; Wang, N.-H. L.; Franses, E. I. *J. Chromatogr. B*

2008, *875*, 81–92.

(48) Nakamura, Y.; Norisuye, T. *J. Polym. Sci. Part B Polym. Phys.* **2004**, *42*, 1398–1407.

(49) Nakamura, Y.; Norisuye, T. In *Soft Matter Characterization*; Springer Netherlands: Dordrecht, 2008; pp 235–286.

(50) Livsey, I. *J. Chem. Soc., Faraday Trans. 2* **1987**, *83*, 1445–1452.

(51) Yamakawa, H.; Fujii, M. *Macromolecules* **1974**, *7*, 128–135.

(52) Yamakawa, H.; Yoshizaki, T. *Macromolecules* **1980**, *13*, 633–643.

(53) Barrett, A. J. *Macromolecules* **1984**, *17*, 1566–1572.

(54) Yamakawa, H.; Stockmayer, W. H. *J. Chem. Phys.* **1972**, *57*, 2843–2854.

(55) Shimada, J.; Yamakawa, H. *J. Chem. Phys.* **1986**, *85*, 591–600.

(56) Benoit, H.; Doty, P. *J. Phys. Chem.* **1953**, *57*, 958–963.

(57) Domb, C.; Barrett, A. J. *Polymer (Guildf).* **1976**, *17*, 179–184.

(58) Okamoto, Y.; Aburatani, R.; Fukumoto, T.; Hatada, K. *Chem. Lett.* **1987**, *16*, 1857–1860.

(59) Ikai, T.; Okamoto, Y. *Chem. Rev.* **2009**, *109*, 6077–6101.

(60) Okamoto, Y.; Kawashima, M.; Hatada, K. *J. Am. Chem. Soc.* **1984**, *106*, 5357–5359.

(61) Shimada, J.; Yamakawa, H. *Biopolymers* **1988**, *27*, 657–673.

(62) Tsubouchi, R.; Ida, D.; Yoshizaki, T.; Yamakawa, H. *Macromolecules* **2014**, *47*, 1449–1454.

(63) Kawaguchi, T. *J. Appl. Crystallogr.* **2001**, *34*, 580–584.

(64) Cebula, D. J.; Goodwin, J. W.; Ottewill, R. H.; Jenkin, G.; Tabony, J. *Colloid Polym. Sci.* **1983**, *261*, 555–564.

Chapter V.

Does chain topology affect the chiral recognition ability of an amylose derivative? Comparison between linear and cyclic amylose tris(3,5-dimethylphenylcarbamate)

V-1. Introduction

In the preceding chapters, we found from analyses of the particle scattering function and the z-average mean-square radius of gyration for cADMPC that the local helical structure is somewhat extended compared with the linear chain in the same solvent and the main chain of cADMPC is appreciably flexible. If we consider that quite different polymer-solvent interactions was found for linear and cyclic ATPC[1] and furthermore dimensional properties of ATBC and ATEC are appreciably affected by the solvent chirality if we choose $_{D}$- and $_{L}$-ethyl lactate as solvents,[2,3] this conformational difference between linear and cyclic chains (Figure V-1) may cause an appreciable difference in the chiral separation ability of ADMPC, which is one of the most abundantly used chiral selectors.[4] Although chiral separation mechanism of ADMPC has been investigated from a molecular mechanics calculations[5] or spectroscopic techniques[6], the relationship between the performance of chiral stationary phases (CSPs) and the local helical structure is still unclear. On the other hand, according to Okamoto *et al.*,[7] the performance of γ-cyclodextrin tris(3,5-dimethylphenylcarbamate) is substantially different from that of the ADMPC columns.

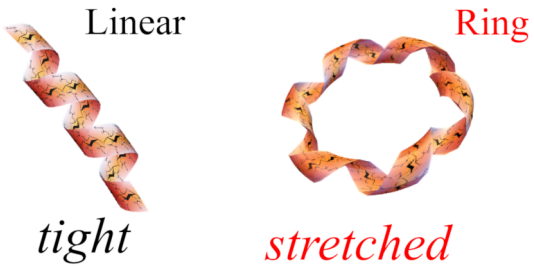

Figure V-1. Schematic illustration of the difference in the helical structure between ADMPC and cADMPC.

We thus prepared two types of chiral stationary phases (CPSs), that is, physically coated and chemically immobilized CSPs with cADMPC (Figure V-2A) and cADMPC with 3-(triethoxysilyl)propyl linkers (cADMPCi, Figure V-2B), respectively. CSPs were also prepared for linear ADMPC (Figure V-2C) and ADMPCi (Figure V-2D) samples with the same method to compare the chiral separation ability. The performance of CSPs was characterized with 8 racemates with a mobile phase consisting of *n*-hexane and 2-propernol. Samples with different chain lengths were also prepared to clarify the chain length effect including the chain end effect. The precursor materials of the immobilized columns were also characterized in dilute methylacetate (MEA) solution to confirm the conformational difference.

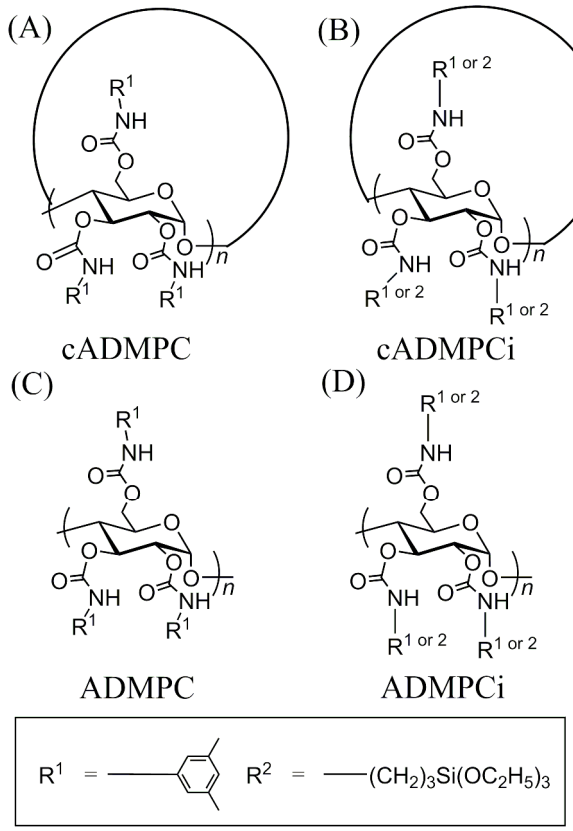

Figure V-2. Chemical structure of cADMPC (A), cADMPCi (B), ADMPC (C) and ADMPCi (D).

V-2. Experimental

V-2-1. Chemical reagents

A wide-pore silica gel (Daiso gel SP-1000-7) with a mean particle diameter of 7 μm and a mean pore size of 100 nm was purchased from Osaka Soda. Toluene (Fujifilm Wako Pure Chemical), pyridine (Fujifilm), and MEA (Kishida Chemical) were distilled over calcium hydride (Nacalai Tesque) before use. 3-Aminopropyltriethoxysilane, 3,5-

dimethylphenyl isocyanate, 3-(triethoxysilyl)propyl isocyanate, and chlorotrimethylsilane (TCI chemical), and *N*,*N*-dimethylformamide-d_7 (Sigma-Aldrich) , *N,N*-Dimethylacetamide (dehydrated grade), lithium chloride, acetone, methanol, *n*-hexane, *n*-tetradecane, and 2-propanol (Fujifilm) were used without further purification. We chose HPLC grade 2-propanol (Fujifilm) for the eluents of the HPLC measurements. Racemate samples, *trans*-stilbene oxide (Sigma), Tröger's base (Fujifilm), 2,2,2-trifluoro-1-(9-anthryl)ethanol (TCI), flavanone (TCI), tris(2,4-pentanedionato)cobalt(III) (TCI), benzoin (Fujifilm), 1,1'-bi-2-naphthol (TCI), and 1-(2-Naphthyl)ethanol (TCI), and reference materials, spectrochemical-analysis grade benzene (Fujifilm) and 1,3,5-tri-*tert*-butylbenzene (TCI), for HPLC measurements were purchased and used without further purification.

V-2-2. Cyclic and linear amylose carbamate samples

Three cADMPC samples (cf. Chapter III), cADMPC19K, cADMPC49K, and cADMPC91K, and two ADMPC samples,[8] ADMPC25K and ADMPC49K were used for this study. The weight-average molar mass M_w is summarized in Table V-1. Their dispersity index $Đ$, the ratio of M_w to the number-average molar mass, was estimated to be from 1.04 to 1.20 and the degree of substitution DS_{R1} determined from the ultimate analysis to be 2.9 – 3.3 (cf. Chapter III and Ref. 8). Another ADMPC sample, ADMPC90K, was newly synthesized form an enzymatically synthesized amylose sample, ESA50K, of which M_w is 50 kg mol^{-1} determined from viscometry[9] in the manner reported previously.[8] The obtained crude sample was dissolved in MEA to remove the insoluble impurity and reprecipitated into

methanol. The chemical structure of the purified ADMPC90K sample was confirmed by ^{1}H NMR in deuterated chloroform and the ultimate analysis was made to determine DS_{R1} to be 3.1. The M_w value was estimated from the intrinsic viscosity [η] (= 36.0 mL g^{-1}) in MEA at 25 °C with the [η] – M_w relationship.[8]

Table V-1. Weight-average molar masses M_w and degrees of substitution DS_{R2} of amylose carbamate samples used for the chiral stationary phase, and conditions of the chiral separation experiment

samples	M_w (kg mol^{-1})	DS_{R2}	eluent used for the chiral separation experiment (see Subsection V-2-5)	
			n-hexane/2-propanol (9/1)	*n*-hexane/2-propanol (99/1)
cADMPC19K[a]	19.4[c]	0	-[g]	**a**–**e** and **h**[h]
cADMPC49K[a]	49.4[c]	0	**a**–**h**	**a**–**e** and **h**[h]
cADMPC91K[a]	91.1[c]	0	**a**–**h**	**a**–**e** and **h**[h]
ADMPC25K[a]	25.4[d]	0	-[g]	**a**–**e** and **h**[h]
ADMPC49K[a]	48.8[d]	0	**a**–**h**	**a**–**e** and **h**[h]
ADMPC90K[a]	90[e]	0	**a**–**h**	**a**–**e** and **h**[h]
cADMPCi31K[b]	31[f]	0.30	**a**–**h**	
ADMPCi18K[b]	18[e]	0.14	-	**a**–**e** and **h**[h]
ADMPCi20K[b]	20[e]	0.23	**a**–**h**	
ADMPCi130K[b]	130[e]	0.24	**a**–**h**	**a**–**e** and **h**[h]

[a] For coated-type columns. [b] For immobilized-type columns. [c] Chapter III [d] Ref. 8 [e] From [η]. [f] From SAXS. [g] Not applicable due to the slightly higher solubility of the polymer. [h] Solubility of racemates **f** and **g**, being too poor.

A cADMPCi sample was prepared in the manner reported in elsewhere.[10] The procedure is as follows. An enzymatically synthesized cyclic amylose sample (cESA9K, M_w = 9 kg mol^{-1}, 2.1 g, 13 mmol of the repeat unit) and lithium chloride (2.1 g) were dried in a vacuum at 100 °C for 6 h. *N*,*N*-Dimethylacetamide (40 mL) was added to them and stirred at 90 °C under Ar atmosphere to dissolve both amylose and lithium chloride. Pyridine (80 mL) and 3,5-dimethylphenyl isocyanate (5.0 mL, 35 mmol) were added to the reaction mixture. The mixture was stirred at 80 °C for 6 h. After 3-(triethoxysilyl)propyl isocyanate (1.3 mL, 5.3 mmol) was added, the mixture was stirred at 80 °C overnight. In order to diminish residual hydroxyl groups on the glucosidic ring, we further added 3,5-dimethylphenyl isocyanate (5.0 mL) to the resultant solution and stirred at 80 °C for 6 h. The crude product was poured into an excess amount of methanol at room temperature to purify the polymer sample as a precipitant. The chemical structure of the obtained sample designated to be cADMPCi31K was confirmed by the ^{1}H NMR spectrum in fully deuterated *N*,*N*-dimethylformamide at 80 °C. We did not further purify the samples to protect the linker group. Possible impurity, amine and urethane, was estimated to be at most 1 – 7 wt% in each sample. This may not substantially affect the performance of CSPs because the chiral columns will be washed with large amount of eluent before use. The degree of substitution DS_{R2} of the 3-(triethoxysilyl)propyl carbamate group (R^2) of cADMPCi31K was determined from the peak area ratio of the protons of SiH_2 group on R^2 to the aromatic protons on the 3,5-dimtheylcarbamate group (R^1). The M_w value was determined to be 31 kg mol^{-1} form SAXS measurements as described later.

We have also prepared three ADMPCi samples, ADMPCi18K, ADMPCi20K, and ADMPCi130K from two enzymatically synthesized amylose samples, ESA6K and ESA50K, in the similar manner as that for cADMPCi31K. The chemical structures of the samples were also confirmed by the ultimate analysis and ^{1}H NMR. Viscosity measurements were made for the three samples in MEA at 25 °C to determine $[\eta]$ to be 7.45, 7.75, and 44.2 mL g^{-1} and the Huggins constant to be 0.82, 0.77, and 0.43 for ADMPCi18K, ADMPCi20K, and ADMPCi130K, respectively. Assuming $[\eta]M_0$ for the ADMPCi samples with M_0 being average molar mass per monosaccharide unit are the same as that for ADMPC with the same M_w/M_0, the M_w values for the three ADMPCi samples were estimated from the known relationship between $[\eta]$ and M_w for ADMPC[8] as listed in Table V-1 along with DS_{R1} and DS_{R2}. This is reasonable because the wormlike chain parameters discussed later is substantially close to those for the ADMPC in the same solvent.

V-2-3. Small-angle X-ray scattering (SAXS) of dilute solution

In order to compare the conformation of the amylose carbamates samples with or without triethoxysilyl groups, synchrotron-radiation SAXS measurements were made for cADMPCi31K and ADMPCi130K in MEA at 25 °C at the BL40B2 beamline in SPring-8 to determine the excess scattering intensity $\Delta I(q)$ as functions of the magnitude q of the scattering vector and the polymer mass concentration c. Solvent and the four solutions of which c ranged between 2.2 and 11 mg mL^{-1} were measured with the same quartz capillary cell to precisely extrapolate $\Delta I(q)/c$ to infinite dilution. The scattered light was detected by

a Dectris PILATUS2M detector for 120 s for each sample. The wavelength of the incident light and the camera length were set to be 0.1 nm and 4 m, respectively. The beam center on the detector and the actual camera distance were determined from the Bragg reflection of silver behenate.[11] Data analysis for the cADMPCi and ADMPCi samples were substantially the same as those for cADMPC (cf. Chapter III) and ADMPC[8] to determine the z-average mean-square radius of gyration $\langle S^2 \rangle_z$ and the particle scattering function $P(q)$. We also estimated M_w of cADMPCi31K from the doubly extrapolated scattering intensity $[\Delta I(0)/c]_{c \to 0}$ to both $c = 0$ and $q = 0$ by using that for ADMPCi130K assuming the excess electron density of the two samples are equivalent.

V-2-4. Preparation of chiral stationary phases (CSPs) and chiral columns

We prepared 10 CSPs from the samples in Table V-1, that is, six coated-type CSPs and four immobilized-type CSPs. All chiral stationary phases (CSPs) were made from the same macroporous silica gel (Daiso gel SP-1000-7) to compare the chiral recognition ability among the polysaccharide derivative samples. The detailed procedure is as follows.

Preparation of Coated-type Stationary Phases. Six coated-type CSPs were prepared from ADMPC25K, ADMPC49K, ADMPC90K, cADMPC18K, cADMPC49K, and cADMPC91K in the manner reported by Okamoto *et al.*[12] A typical procedure is as follows. The silica gel (25 g) was dried under vacuum at 100 °C overnight and mixed with toluene (240 mL) in a two-necked flask at 80 °C under Ar atmosphere. A mixture of 3-aminopropyltriethoxysilane (51 g) and toluene (40 mL) was dropped into the silica-gel

suspension. The resultant suspension was kept at 80 °C for 5 h to complete the reaction to obtain 3-amynopropyltriethoxisilinized silica gel (A-silica),[13,14] which was washed four times with toluene (100 mL each) and four times with methanol (100 mL each). The resultant crude sample was dispersed into a mixture of water (100 mL) and methanol (100 mL) by sonication for 2 min. The suspension was kept at room temperature for 2 h to eliminate the remaining ethoxy groups.[14] The obtained A-silica sample was washed three times by methanol (100 mL each) and dried under reduced pressure. An MEA solution (11 mL) of cADMPC49K (0.23 g) was mixed with the A-silica sample (0.92 g) and the solvent was evaporated in an eggplant flask. The obtained CSP was dried in a vacuum overnight.

Preparation of Immobilized-type Stationary Phases. Four immobilized-type CSPs were synthesized from cADMPCi31K, ADMPCi18K, ADMPCi20K, and ADMPCi130K with the cross-linking method on silica particles following the procedure reported by Ikai *et al*.[10] A sample, cADMPCi31K (0.70 g), was dissolved in pyridine (8 mL) and mixed with the silica gel (Daiso gel SP-1000-7, 2.8 g). The solvent was evaporated from the mixture and the resultant sample was dried in a vacuum overnight to physically coat cADMPCi31K on silica particles. The obtained product (1.95 g) was mixed with ethanol (18 mL), water (4.5 mL), and chlorotrimethylsilane (0.3 mL). The mixture was kept under reflux condition at 110 °C for 10 min to immobilize the polymer chains. The obtained CSP was washed with an excess amount of acetone and MEA to remove impurities including free cADMPCi31K molecules. Thermogravimetric analyses showed that about 90% of ADMPCi20K, and ADMPCi130K or 70% of cADMPCi31K and ADMPCi18K were immobilized on the silica surface.

Preparation of Chiral Columns. Each stationary phase was packed in a stainless steel column (Senshu Scientific) with 2.1 mm of the inner diameter and 250 mm of the length by using a slurry method. 2-Propanol was chosen as an eluent to pack CSPs with cADMPC49K, cADMPC91K, ADMPC49K, ADMPC90K, cADMPCi31K, ADMPCi18K, ADMPCi20K, and ADMPCi130K. Tetradecane including 2% 2-propanol (volume fraction) was chosen as the eluent to fill the CSPs of cADMPC19K and ADMPC25K due to slight solubility of the polysaccharide derivatives in 2-propanol. A typical procedure is as follows. A CSP of cADMPC49K (0.9 g) was sonicated in 2-propanol (30 mL) to be dispersed. The obtained suspension was filtered with a stainless steel mesh (270 mesh) and incubated at room temperature for 1h to precipitate the CSP, which was washed with 2-propanol (30 mL) again. The resultant CSP was dispersed in 2-propanol (30 mL) and filled into the column with a specially designed column packer and an HPLC pump. The flow rate was set to be 1.0 mL min^{-1} to achieve the back pressure of 32 MPa for about 4 h.

V-2-5. High-performance liquid chromatography (HPLC) of the CSPs

Chiral separation performance of the ten columns prepared from the CSPs listed in Table V-1 were tested with the following racemates, *trans*-stilbene oxide (**a**), Tröger's base (**b**), 2,2,2-trifluoro-1-(9-anthryl)ethanol (**c**), flavanone (**d**), tris(2,4-pentanedionato)cobalt(III) (**e**), benzoin (**f**), 1,1'-bi-2-naphthol (**g**), and 1-(2-Naphthyl)ethanol (**h**) of which chemical structures are summarized in Figure V-3. Tröger's base **b** contains two bridgehead stereogenic nitrogen atoms, there are two enantiomers for the cobalt complex **e**, and 1,1'-bi-

2-naphthol **g** has axial chirality of which two enantiomers are stable toward racemization.

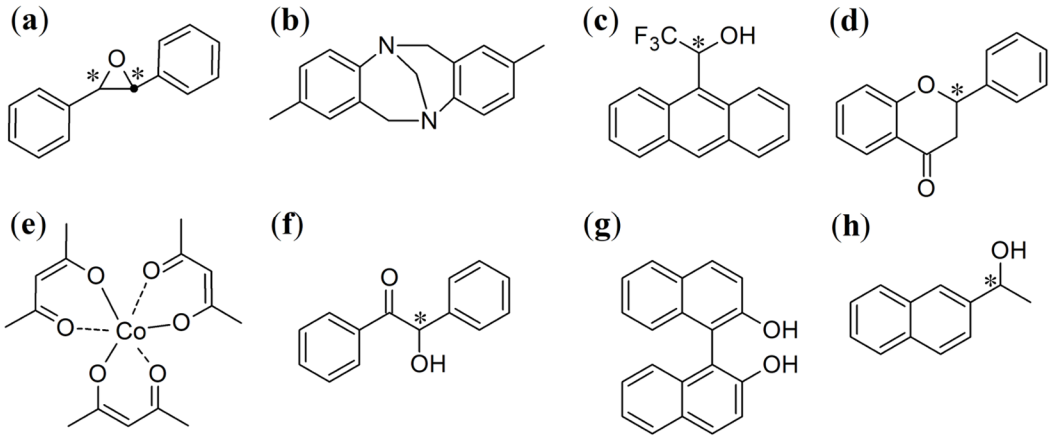

Figure V-3. Chemical structures of the racemates (**a**-**h**) investigated.

Each column was installed into an HPLC system equipped with a Chromaster 5160 pump (Hitachi), a Rheodyne 7125 injector with a 20 μL sample loop, an online UV absorption detector with the wavelength λ_0 in a vacuum being 254 nm, and an Advantech SF-3120 fraction collector. The column temperature was controlled to be 25.0 ± 0.1 °C using a thermostated water bath. As listed in Table V-1, the 7 columns, made of cADMPC49K, cADMPC91K, ADMPC49K, ADMPC90K, cADMPCi31K, ADMPCi20K, and ADMPCi130K were tested with the mobile phase of hexane/2-prppanol (9/1) at the flow rate of 0.05 and 0.1 mL min^{-1} to separate all the 8 racemates. The 8 columns, made of cADMPC19K, cADMPC49K, cADMPC91K, ADMPC25K, ADMPC49K, ADMPC90K, ADMPCi18K, and ADMPCi130K were tested with hexane/2-propanol (99/1) at 0.1 and 0.2 mL min^{-1} to separate **a–e** and **h**. Noted that cADMPC19K and ADMPC25K are not applicable for the former mobile phase due to the slightly higher solubility and the solubility

of the two racemates, **f** and **g**, was poor to the latter eluent.

The plate number N and the dead volume V_0 of the columns were estimated from the peak shape of benzene and 1,3,5-tri-*tert*-butylbenzene, respectively. While the latter was evaluated to be $V_0 = 0.6 – 0.7$ mL and mostly independent both of the eluent and the flow rate investigated, the former was estimated to be between $N = 350$ and 2300 and appreciably decreased with increasing the flow rate when the flow rate exceeded 0.1 mL min^{-1}. When we obtained two peaks in the chromatogram, each fraction was characterized by circular dichroism (CD) spectra in the ultraviolet region ($\lambda_0 = 210 – 350$ nm) except for **h** which does not show appreciable CD signal. One of the fractions having negative CD signal at the highest λ_0 was designated to be E− and the other was named E+; see Figure V-4 for the CD spectra. Retention volumes V_{E-} and V_{E+} were determined to as the peak-top positions for each chromatogram.

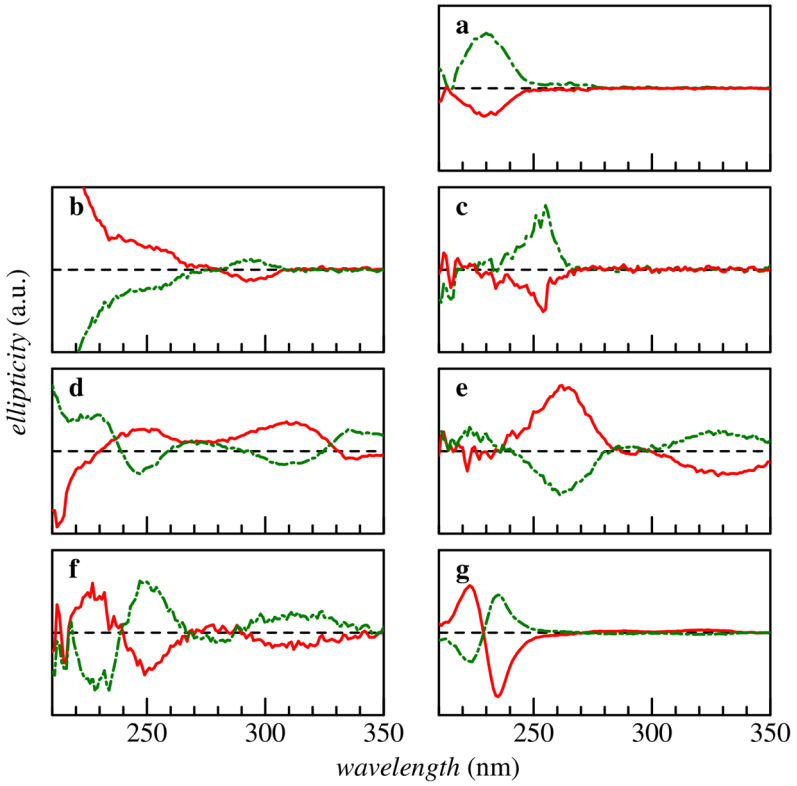

Figure V-4. CD spectra for the enantiomers separated from racemates (**a**-**g**). Red solid lines and green dashed lines indicate spectra for E− and E+, respectively, for each racemate.

V-3. Results and discussion

V-3-1. Conformation of cADMPCi and ADMPCi in MEA

Figure V-5 shows that the $\langle S^2 \rangle_z^{1/2}$ data for ADMPCi130K and cADMPCi31K in MEA at 25 °C plotted against M_w/M_0, where M_0 is the average molar mass of the repeat unit (M_0 = 0.628 kg mol^{-1} for ADMPCi130K and M_0 = 0.634 kg mol^{-1} for cADMPCi31K), are substantially the same as that for the corresponding chains without the linkers, that is,

ADMPC and cADMPC, respectively.

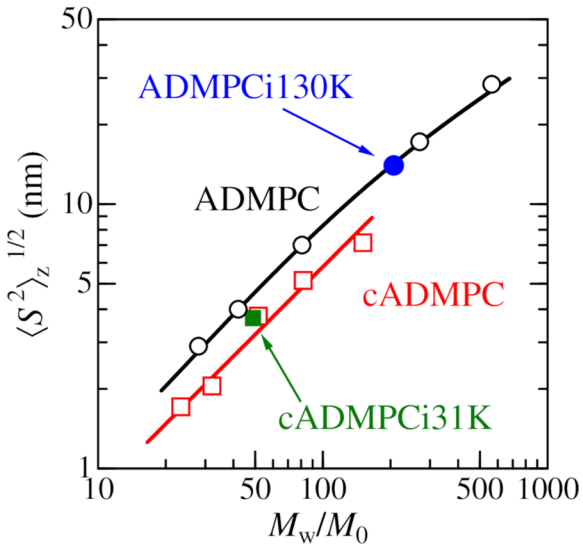

Figure V-5. The *z*-average radius of gyration $\langle S^2\rangle_z^{1/2}$ for cADMPCi31K (a filled green square) and ADMPCi130K (a filled blue circle) in MEA at 25 °C plotted against M_w/M_0 along with the literature data for cADMPC in Chapter III (unfilled red squares) and ADMPC[8] (unfilled black circles).

Figure V-6 illustrates the Holtzer plot for ADMPCi130K in MEA at 25 °C. Since the shape is typical for the wormlike chain with finite thickness, the data was analyzed in terms of the wormlike cylinder model[15] as in the case of ADMPC in the same solvent.[8] A curve fitting procedure was employed to determine the Kuhn segment length λ^{-1}, the contour length per residue h, and the chain diameter d as 20 ± 4 nm, 0.39 ± 0.03 nm, and 1.6 ± 0.2 nm, respectively, in which the second parameter was calculated from $h = LM_0/M_w$, where L is the contour length. The theoretical solid curve in Figure V-6 well explains the experimental data. The obtained parameters are essentially the same as those for ADMPC in the same solvent,

that is, $\lambda^{-1} = 22 \pm 2$ nm, $h = 0.36 \pm 0.02$ nm, and $d = 1.3 \pm 0.1$ nm, indicating the conformation of ADMPCi130K in MEA is substantially the same as those for the ADMPC chain with the same chain length.

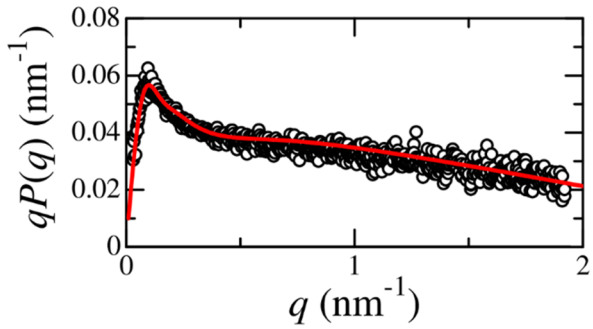

Figure V-6. Holtzer plots for ADMPCi130K in MEA at 25 °C. A solid curve indicates theoretical values for the wormlike cylinder model[15] with the parameters of $\lambda^{-1} = 20$ nm, $L = 80$ nm, and $d = 1.6$ nm.

The $P(q)$ data for cADMPCi31K in MEA are shown in Figure V-7, which is similar to that for cADMPC (cf. Chapter III) with substantially the same chain length. The data was analyzed in terms of the touched-bead wormlike ring model which is characterized by λ^{-1}, L, and the bead diameter d_b as is the case with our recent research for cADMPC as described in Chapter III. The detailed procedure including the computer program developed by Ida *et al.*[16] was described in Chapter II. If we choose $\lambda^{-1} = 13$ nm, $L = 20$ nm, and $d_b = 1.7$ nm, the theoretical dot-dashed curve in Figure V-7 significantly fluctuates. A reason for the disagreement is due to the molar mass distribution. Indeed, if we assume $Đ = 1.2$, the resultant theoretical solid curve in the figure satisfactory reproduce the experimental data. Since M_0 was calculated to be 0.634 kg mol^{-1}, we thus determined $h = 0.38 \pm 0.04$ nm and d_b

= 1.8 ± 0.2 nm from the curve fitting method. It should be noted that we estimated the lowest limit of λ^{-1} to be 13 nm since the theoretical rigid limiting value (dashed curve) is substantially close to that for the wormlike ring. Nevertheless, the obtained parameters are consistent with those for cADMPC31K of which chain length is essentially close to that for the current cADMPCi31K, indicating substantially the same conformation between the two samples.

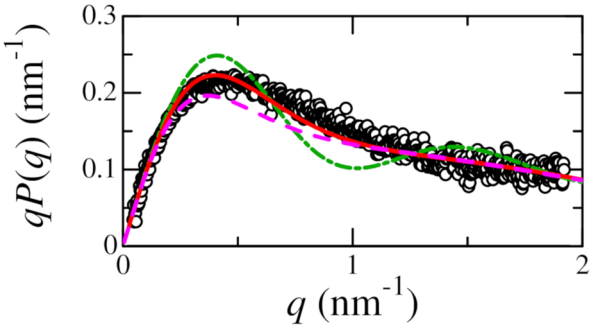

Figure V-7. Holtzer plots for cADMPCi31K in MEA at 25 °C. A solid red curve indicates theoretical $P(q)$ values for the touched-bead wormlike ring model (cf. Chapter II) with λ^{-1} = 13 nm, L = 20 nm, d_b = 1.7 nm, and $Đ$ = 1.20 (red solid). A dot-dashed green curve, theoretical values for the monodisperse wormlike ring. A dashed magenta curve, theoretical values for touched-bead rigid ring with $Đ$ = 1.20.

V-3-2. Chiral separation behavior in *n*-hexane/2-propanol (9/1)

Some examples of the HPLC chromatograms are shown in Figure V-8 in which *n*-hexane/2-propanol (9/1) was used as the mobile phase. The column made of cADMPC49K clearly separates **d** while the ADMPC49K column for which the chain length of the polysaccharide derivative is substantially the same as the cyclic chain shows a single peak

with no chiral separation. On the other hand, if we test **f**, only linear-chain column separates the racemate. These results indicate that cADMPC and ADMPC have appreciably different chiral separation ability. Similar differences in chiral separation ability were observed also for other racemates.

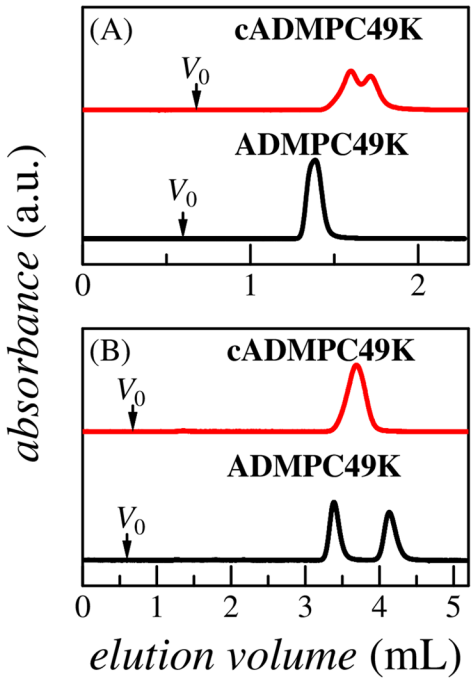

Figure V-8. Chromatograms of the racemates **d** (A) and **f** (B) on indicated CSPs using hexane/2-propanol (9/1) as the eluent. Arrows indicate the dead volume (V_0) of the column.

For quantitative discussion on the adsorption ability of the stationary phases for the enantiomers, the following separation factor α is conventionally used,

$$\alpha \equiv \frac{k_{E+}}{k_{E-}} \quad \text{for } k_{E-} \le k_{E+}$$
$$\alpha \equiv \frac{k_{E-}}{k_{E+}} \quad \text{for } k_{E-} > k_{E+} \tag{V-1}$$

where the retention factors k_{E-} and k_{E+} are related to the dead volume V_0 and the retention volumes V_{E-} and V_{E+} for the enantiomer showing negative and positive CD signal at the highest λ_0, respectively (cf. Figure V-4), by

$$k_{E-} = (V_{E-} - V_0)/V_0$$
$$k_{E+} = (V_{E+} - V_0)/V_0 \tag{V-2}$$

In this study, we utilized the modified separation factor α' instead of α to clarify the difference in the elution order among the investigated CSPs, that is,

$$\alpha' \equiv \frac{k_{E+}}{k_{E-}} \tag{V-3}$$

We chose α for the racemate **h** because each enantiomer cannot be recognized by the CD spectra. The obtained α' data (or α for **h**) are plotted against M_w in Figure V-9. We plotted $\alpha' = \alpha = 1$ when only single peak was found in the chromatogram. According to the plate theory,[17] when $k_{E-} \sim k_{E+}$ and the N value is the same both for E− and E+, the resolution factor R_s may be written as

$$R_s = \frac{1}{4}(\alpha - 1)\sqrt{N}\left(\frac{k_{E-}}{1 + k_{E-}}\right) \tag{V-4}$$

To recognize two species included in the analyte, R_s is at least 0.6.[17,18] When we assume the maximum R_s is 0.5 for the single peak chromatograms with the N for benzene, the possible errors are shown in the figure.

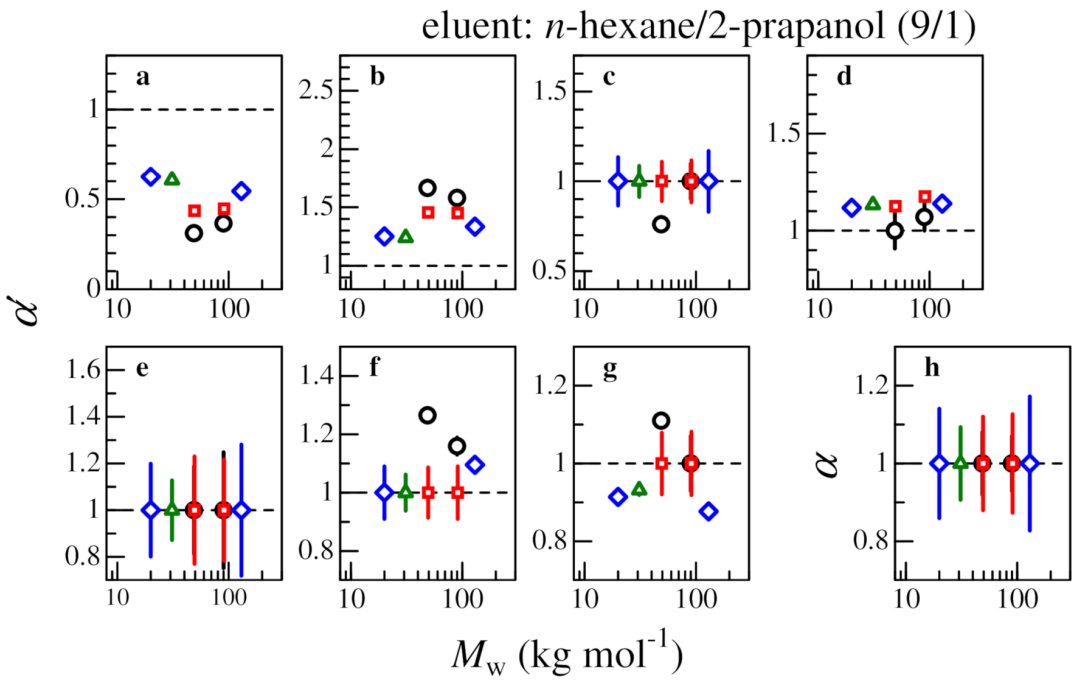

Figure V-9. M_w dependence of α' or α for the indicated racemates (**a**-**h**) separated on ADMPC columns (black circles), cADMPC columns (red squares), cADMPCi column (green triangles) and ADMPCi columns (blue diamonds), with *n*-hexane/2-propanol (9/1) as the eluent.

While the ADMPC columns (black circles) appreciably separated **a**-**d**, **f**, and **g** as shown in Figure V-9, significant resolution for the cADMPC columns (red squares) was found only for **a**, **b**, and **d** of which the elution order is the same as that for the linear chain. Interestingly, the resolution of **d** is however better for the cADMPC columns than that for the ADMPC whereas the ADMPC column has higher resolution for the other racemates. This difference in the chiral separation clearly indicates that the topology of the polymer chains affects the chiral recognition of CSPs.

Another important point is the molar mass dependence of the resolution. The α'

value for the ADMPC column systematically decreases and becomes close to that for the cADMPC chain with increasing M_w for **a**, **b**, **c**, **f**, and **g**. When a polymer chain is adsorbed on the silica gel in the physically coating process to form loops, trains, and tails,[19–22] the conformational fluctuation may be restricted for the loop and train chains. The restriction for the loop chain of ADMPC may be rather similar to that for the cADMPC chain, and the fraction of the loop chains should increase with increasing the molecular weight of ADMPC. According to Chapter III for the dilute solution properties, the local helical structure of cADMPC is more extended than that for the linear chain. The current result of the chromatograms suggests that the local helical structure in the CSPs may play an important role for the chiral separation.

Next, we compare the chiral separation behavior for the coated-type columns with those for immobilized columns. The α values obtained from eq. V-1 for **a**, **b**, **c**, and **f** for ADMPCi and cADMPCi samples are appreciably smaller than those for ADMPC while an opposite behavior is found for **d**. This tendency is quite similar to those for the cADMPC columns but the difference is more significant. Another interesting point is that the chiral separation behavior between ADMPCi and cADMPCi are quite similar. Furthermore, opposite elution order was found for **g**. The α values for ADMPCi are similar to the previous report.[10] Taking into consideration that the current ADMPCi and cADMPCi have relatively large amount of linker unit, the part chain between two adjacent linkers may bend more significantly and/or the local helical structure may be stretched more than the physically coated cADMPC chains. The difference in the linear and cyclic topology of the immobilized

chain is consequently no more important for the local helical structure.

The chiral separation ability of the stationary phase for each racemate is characterized by the excess molar Gibbs energy ($\Delta\Delta G_{E-,E+}$) of adsorption between the two enantiomers, E– and E+. It is related to the capacity factors for E– (k_{E-}) and E+ (k_{E+}) by using the following equation,[23]

$$\frac{\Delta\Delta G_{E-,E+}}{RT} = -\ln\left(\frac{k_{E+}}{k_{E-}}\right) = -\ln\alpha' \qquad \text{(V-5)}$$

where R and T denote the gas constant and the absolute temperature, respectively. Taking thickly covered amylose carbamate layer on the silica surface into account, the interaction between the racemates and the silica gel surface may be negligible. If so, the value of $\Delta\Delta G_{E-,E+}$ mainly reflects the interaction energy difference between the polymer chains and the two enantiomers in a specific mobile phase. The absolute value is calculated from the α' value to be at most 4 kJ mol^{-1}. The difference in $\Delta\Delta G_{E-,E+}$ for linear and ring chains is the same order as that for each value, strongly suggesting that the local chain conformation is quite important for the chiral separation.

V-3-3. Chiral separation behavior in *n*-hexane/2-propanol (99/1)

The α' value for **a**-**e**, and **h** for the CPSs made of ADMPC, cADMPC, and ADMPCi in *n*-hexane/2-propanol (99/1) are plotted against M_w in Figure V-10. Relatively high chiral separation performance was observed for all the tested racemates including **e** and **h**, for which no appreciable resolution of the enantiomers was found in the former mobile phase, *n*-

hexane/2-propanol (9/1). The elusion order from the racemates does not depend on the investigated CSPs. Figure V-10 shows that the α' values of cADMPC are somewhat closer to α' =1 than those of ADMPC for **a** and **b**. For **c** and **h**, however, α' (α) for cADMPC is slightly larger than that for ADMPC. Interestingly, the difference in α' between cADMPC and ADMPC CSPs for **a**-**c** becomes the most significant for the middle M_w sample. This seemingly complex M_w dependence suggests that not only the chain end effect but also the local conformational difference plays an important role for the chiral separation since the end effects generally increase monotonically with lowering M_w. The α' values of **d** and **e** for cADMPC and ADMPC are substantially close to each other whereas somewhat difference is found for the lowest M_w sample. This is reasonable because the local helical structure of cADMPC becomes more different from ADMPC with lowering M_w.

Let us compare the α' (α) data with those for the immobilized CSPs. The α values of ADMPCi is lower than that of ADMPC for **a**-**d** and slightly larger than those of ADMPC for **e** and **h** while the α' values of ADMPCi are quite similar to those of cADMPC except for **c**. This similarity between ADMPCi and cADMPC is comparable to the former result in *n*-hexane/2-propanol (9/1). The elution order of the enantiomers for **c** in *n*-hexane/2-propanol (99/1) is opposite to that in hexane/2-propanol (9/1) and similar behavior with changing alcohol content was also reported in some previous studies.[24–26]

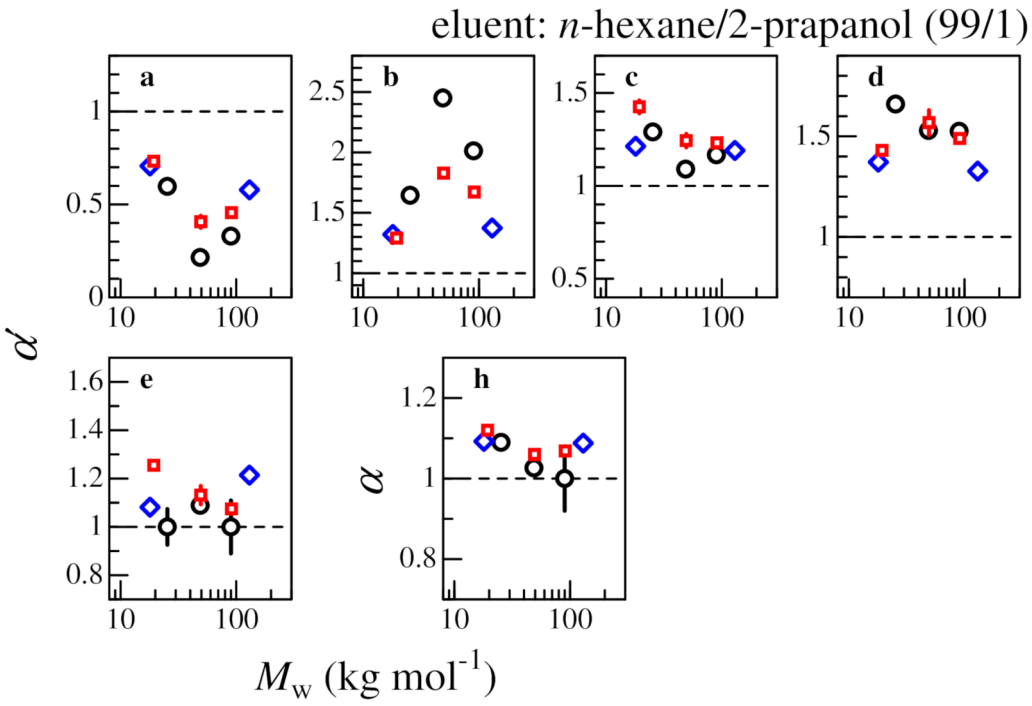

Figure V-10. M_w dependence of α' or α for the indicated racemates (**a**-**e** and **h**) separated on ADMPC columns (black circles), cADMPC columns (red squares), and ADMPCi columns (blue diamonds), with *n*-hexane/2-propanol (99/1) as the eluent.

V-3-4. Adsorption of analytes to the stationary phases

The geometric average [$\bar{k} = (k_{E-}\, k_{E+})^{1/2}$] of the capacity factors may be associated with the mean of molar Gibbs energy of adsorption for the E– (ΔG_{E-}) and E+ (ΔG_{E+}) by the following equation,[23]

$$\ln \bar{k} = \frac{\ln k_{E-} + \ln k_{E+}}{2} = -\frac{1}{RT}\left(\frac{\Delta G_{E-} + \Delta G_{E+}}{2}\right) + \ln \phi \qquad \text{(V-6)}$$

where ϕ denotes the volume ratio of the stationary to the mobile phase. The obtained $\bar{k}$ shown in Figures V-11 and V-12 is substantially independent of the stationary phase while it

significantly depends on the analyte, suggesting that local helical conformation of polysaccharide derivative molecules does not cause appreciable difference in the adsorption behavior of the racemates. In other words, chiral separation of the current stationary phases utilizes slight difference in the adsorption ability to polysaccharide derivative molecules between the enantiomers. The direct estimate of this adsorption ability (the preferential adsorption) for each pair of the polysaccharide derivative and the enantiomer is desirable to clarify the detailed mechanism. According to Arakawa *et al.*,[2] the preferential adsorption difference between $_{D}$- and $_{L}$-ethyl lactates to amylose tris(*n*-butylcarbamate) was detected by the isothermal calorimetry measurement.

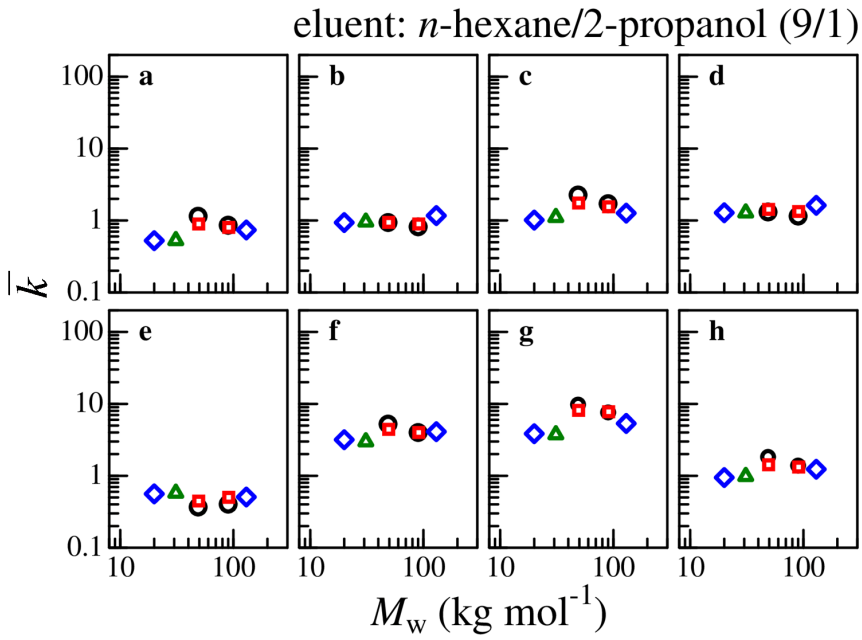

Figure V-11. Geometric-mean capacity factors ($\bar{k}$) of the E– and E+ for the indicated racemates (**a**-**h**) separated on cADMPC (red squares), ADMPC (black circles), cADMPCi (green triangles), and ADMPCi (blue diamonds) columns using *n*-hexane/2-propanol (9/1) as the eluent plotted against the M_w of the amylose carbamates of the corresponding columns.

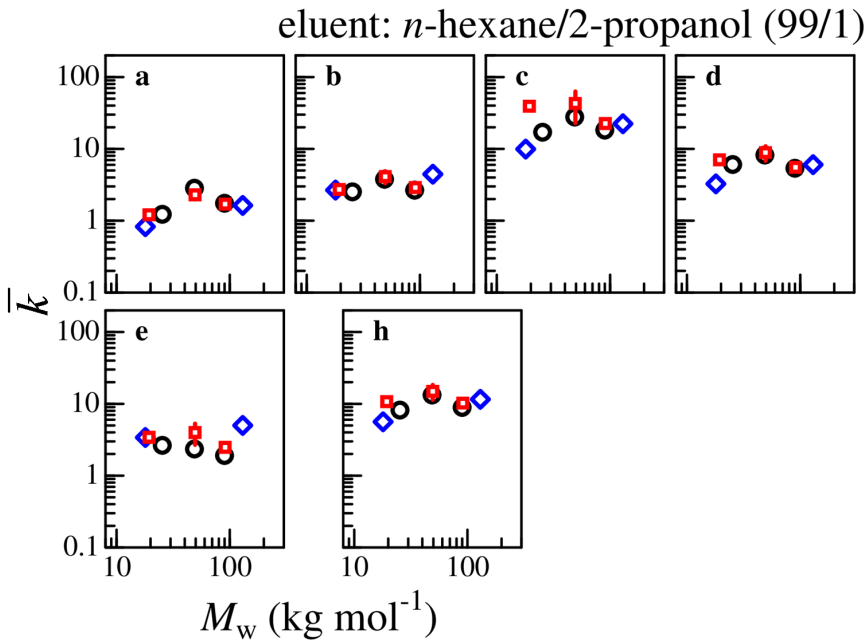

Figure V-12. Geometric-mean capacity factors ($\bar{k}$) of the E– and E+ for the indicated racemates (**a**-**e**, **h**) separated on cADMPC (red squares), ADMPC (black circles), ADMPCi (blue diamond), columns using *n*-hexane/2-propanol (99/1) as the eluent plotted against the M_w of the amylose carbamates of the corresponding columns.

V-4. Conclusions

Both coated and immobilized type chiral stationary phases (CSPs) consisting of cyclic amylose tris(3,5-dimethylphenylcarbamate) (cADMPC) were successfully prepared while their linear analogues were also prepared as standard columns. Some racemates were well separated on the CSPs, using *n*-hexane/2-propanol (9/1) and *n*-hexane/2-propanol (99/1) as the eluents. The chiral separation ability of the coated-type cADMPC CSPs is appreciably different from that for ADMPC, indicating local helical structure difference between the cyclic and linear amylose derivatives is substantially important for the performance as CSPs.

On the other hand, the CSPs made of cADMPC have quite similar chiral separation behavior as those for the immobilized-type cADMPCi and ADMPCi columns, suggesting that the local helical structure of the immobilized polysaccharide chains is rather similar to that for cADMPC. These results indicate that the local conformation of the polysaccharide derivatives plays an important role for the chiral separation behavior.

V-5. Appendix

The values of $\bar{k}$ and α' (or α for **h**) are listed in Table V-A1 and V-A2.

Table V-A1. Geometric-average capacity factor $\bar{k}$ and modified separation factor α' for the racemates (**a**-**f**) separated on ADMPC, cADMPC, ADMPCi, and cADMPCi columns with hexane/2-prapanaol (9/1) as the eluent

	ADMPC49K		ADMPC90K		cADMPC49K		cADMPC91K	
Racemate	$\bar{k}$	α'	$\bar{k}$	α'	$\bar{k}$	α'	$\bar{k}$	α'
a	1.15	0.311	0.86	0.366	0.89	0.435	0.80	0.446
b	0.94	1.67	0.82	1.58	0.94	1.46	0.89	1.45
c	2.26	0.760	1.71	~1	1.75	~1	1.55	~1
d	1.31	~1	1.15	1.07	1.42	1.13	1.33	1.18
e	0.37	~1	0.40	~1	0.45	~1	0.50	~1
f	5.23	1.27	3.99	1.16	4.42	~1	4.00	~1
g	9.75	1.11	7.58	~1	8.11	~1	7.76	~1
h	1.83	~1[a]	1.38	~1[a]	1.42	~1[a]	1.32	~1[a]

	ADMPCi20K		ADMPCi130K		cADMPCi31K	
Racemate	$\bar{k}$	α'	$\bar{k}$	α'	$\bar{k}$	α'
a	0.52	0.625	0.74	0.545	0.53	0.607
b	0.94	1.25	1.17	1.33	0.96	1.24
c	1.01	~1	1.27	~1	1.11	~1
d	1.28	1.12	1.62	1.14	1.28	1.13
e	0.56	~1	0.51	~1	0.58	~1
f	3.17	~1	4.10	1.10	2.99	~1
g	3.84	0.91	5.34	0.88	3.74	0.93
h	0.94	~1[a]	1.23	~1[a]	0.99	~1[a]

[a] The values for α.

Table V-A2. Geometric-average capacity factor $\bar{k}$ and modified separation factor α' for the racemates (**a**-**e** and **h**) separated on ADMPC, cADMPC, and ADMPCi columns with hexane/2-prapanaol (99/1) as the eluent

	ADMPC25K		ADMPC49K		ADMPC90K		cADMPC19K	
Racemate	$\bar{k}$	α'	$\bar{k}$	α'	$\bar{k}$	α'	$\bar{k}$	α'
a	1.23	0.597	2.83	0.215	1.74	0.329	1.21	0.733
b	2.52	1.65	3.77	2.45	2.66	2.01	2.72	1.29
c	17.0	1.29	27.7	1.09	18.2	1.17	39.2	1.43
d	6.04	1.66	8.18	1.53	5.36	1.53	7.04	1.43
e	2.63	~1	2.34	1.09	1.90	~1	3.42	1.26
h	8.15	1.09[a]	13.2	1.03[a]	8.89	~1[a]	10.7	1.12[a]
	cADMPC49K		cADMPC91K		ADMPCi18K		ADMPCi130K	
Racemate	$\bar{k}$	α'	$\bar{k}$	α'	$\bar{k}$	α'	$\bar{k}$	α'
a	2.29	0.407	1.70	0.456	0.83	0.707	1.63	0.579
b	4.10	1.83	2.89	1.67	2.67	1.32	4.43	1.37
c	42.8	1.24	22.5	1.23	9.91	1.21	22.4	1.19
d	8.86	1.57	5.54	1.49	3.26	1.37	6.01	1.33
e	3.98	1.13	2.47	1.07	3.40	1.08	4.99	1.21
h	14.9	1.06[a]	10.2	1.07[a]	5.60	1.09[a]	11.5	1.09[a]

[a] The values for α.

Reference

(1) Asano, N.; Kitamura, S.; Terao, K. *J. Phys. Chem. B* **2013**, *117*, 9576–9583.

(2) Arakawa, S.; Terao, K.; Kitamura, S.; Sato, T. *Polym. Chem.* **2012**, *3*, 472–478.

(3) Terao, K.; Maeda, F.; Oyamada, K.; Ochiai, T.; Kitamura, S.; Sato, T. *J. Phys. Chem. B* **2012**, *116*, 12714–12720.

(4) Okamoto, Y. *J. Polym. Sci. A Polym. Chem.* **2009**, *47*, 1731–1739.

(5) Yamamoto, C.; Yashima, E.; Okamoto, Y. *J. Am. Chem. Soc.* **2002**, *124*, 12583–12589.

(6) Kasat, R. B.; Zvinevich, Y.; Hillhouse, H. W.; Thomson, K. T.; Wang, N.-H. L.; Franses, E. I. *J. Phys. Chem. B* **2006**, *110*, 14114–14122.

(7) Aburatani, R.; Okamoto, Y.; Hatada, K. *Bull. Chem. Soc. Jpn.* **1990**, *63*, 3606–3610.

(8) Tsuda, M.; Terao, K.; Nakamura, Y.; Kita, Y.; Kitamura, S.; Sato, T. *Macromolecules* **2010**, *43*, 5779–5784.

(9) Jiang, X.; Kitamura, S.; Sato, T.; Terao, K. *Macromolecules* **2017**, *50*, 3979–3984.

(10) Ikai, T.; Yamamoto, C.; Kamigaito, M.; Okamoto, Y. *J. Chromatogr. A* **2007**, *1157*, 151–158.

(11) Shimizu, N.; Yatabe, K.; Nagatani, Y.; Saijyo, S.; Kosuge, T.; Igarashi, N. In *AIP Conference Proceedings*; 2016; Vol. 1741, p 050017.

(12) Okamoto, Y.; Aburatani, R.; Fukumoto, T.; Hatada, K. *Chem. Lett.* **1987**, *16*, 1857–1860.

(13) Shen, J.; Ikai, T.; Okamoto, Y. *J. Chromatogr. A* **2010**, *1217*, 1041–1047.

(14) Shimizu, I.; Yoshino, A.; Okabayashi, H.; Nishio, E.; O'Connor, C. J. *J. Chem. Soc. Faraday Trans.* **1997**, *93*, 1971–1979.

(15) Nakamura, Y.; Norisuye, T. *J. Polym. Sci. Part B Polym. Phys.* **2004**, *42*, 1398–1407.

(16) Tsubouchi, R.; Ida, D.; Yoshizaki, T.; Yamakawa, H. *Macromolecules* **2014**, *47*, 1449–1454.

(17) Meyer, V. R. *Practical High-Performance Liquid Chromatography*, 3rd ed.; John Wiley & Sons: New York, U.S.A., 1998.

(18) Christian; Gary D. *Analytical Chemistry*, 6th ed.; John Wiley & Sons: Hoboken, N.J., 2004.

(19) Khokhlov, A. R.; Ternovsky, F. F.; Zheligovskaya, E. A. *Die Makromol. Chemie, Theory Simulations* **1993**, *2*, 151–168.

(20) Kramarenko, E. Y.; Winkler, R. G.; Khalatur, P. G.; Khokhlov, A. R.; Reineker, P. *J. Chem. Phys.* **1996**, *104*, 4806–4813.

(21) Kampmann, T. A.; Kierfeld, J. *J. Chem. Phys.* **2017**, *147*, 014901.

(22) Hall, A. R.; Geoghegan, M. *Reports Prog. Phys.* **2018**, *81*, 036601.

(23) Lämmerhofer, M. *J. Chromatogr. A* **2010**, *1217*, 814–856.

(24) Xiang, C.; Liu, G.; Kang, S.; Guo, X.; Yao, B.; Weng, W.; Zeng, Q. *J. Chromatogr. A* **2011**, *1218*, 8718–8721.

(25) Ma, S.; Shen, S.; Lee, H.; Eriksson, M.; Zeng, X.; Xu, J.; Fandrick, K.; Yee, N.; Senanayake, C.; Grinberg, N. *J. Chromatogr. A* **2009**, *1216*, 3784–3793.

(26) Matarashvili, I.; Chankvetadze, L.; Fanali, S.; Farkas, T.; Chankvetadze, B. *J. Sep. Sci.* **2013**, *36*, 140–147.

Chapter VI.

Summary and Conclusions

This dissertation has been concerned with conformational properties of four cyclic amylose derivatives and their chiral separation behavior. Cyclic amylose tris(phenylcarbamate) (cATPC), cyclic amylose tris(*n*-butylcarbamate) (cATBC), cyclic amylose tris(3,5-dimethylphenylcarbamate) (cADMPC), and cyclic amylose tris(*n*-octadecylcarbamate) (cATODC) were investigated in some solvent systems to determine the local helical structure and chain stiffness, which are appreciably different from the corresponding linear chain (Chapter II – IV). Chiral columns were also prepared for cADMPC and the linear analogue with the two method to elucidate that the chain architecture may play a significant role for the chiral recognition behavior (Chapter V).

In Chapter II, previous $P(q)$ data with the magnitude q of the scattering vector for the 6 cATPC and 8 cATBC samples of which the weight-average degree of polymerization N_w from 20 to 300 were reanalyzed in terms of a novel simulation method based on the Kratky-Porod wormlike chain model to determine the wormlike chain parameters, that is, the helix pitch (or helix rise) per residue h and the Kuhn segment length λ^{-1} (the stiffness parameter or twice the persistence length) as a function of N_w. Although the obtained h and λ^{-1} values for relatively long flexible cyclic chains are almost the same as those for the corresponding linear polymers, an appreciable decrease in λ^{-1} and slightly larger h was found for cyclic chains with a higher chain stiffness. The difference in the wormlike chain parameters between the cyclic and linear chains cannot be realized in the previously

reported molar mass dependence of the radius of gyration. This suggests that analyses of $P(q)$ are decisively important to understand the conformational properties of rigid and/or semiflexible cyclic chains in solution if the molar mass range of the cyclic polymer samples is limited.

In Chapter III, 5 cADMPC samples ranging in N_w from 23 to 150 were prepared from enzymatically synthesized cyclic amylose samples. Light scattering (LS) and small-angle X-ray scattering (SAXS) measurements were made on the samples to determine N_w, $P(q)$, and the z-average mean-square radius of gyration $\langle S^2 \rangle_z$ in methyl acetate (MEA), 4-methyl-2-pentanone (MIBK), and tetrahydrofuran (THF) at 25 °C. The obtained $P(q)$ and $\langle S^2 \rangle_z$ data were analyzed on the basis of the cyclic wormlike chain model to determine h and λ^{-1} as a function of N_w. Although λ^{-1} for the corresponding linear polymer was reported to be 22 and 73 nm in MEA and MIBK, respectively, those for cADMPC in the three solvents were determined to be about 20 nm, this value being still significantly larger than that for cyclic amylose in aqueous sodium hydroxide. On the other hand, h is somewhat larger than those for the linear ADMPC. The extended main chain of cADMPC by the topological constraint does not retain the chain stiffness as high as the corresponding linear chain.

In Chapter IV, 7 linear amylose tris(*n*-octadecylcarbamate) (ATODC) samples ranging in N_w from 23 to 1400 and their 7 cyclic analogues (cATODC) of which N_w is from 34 to 180 were prepared to characterize their conformation in THF, in 2-octanone (MHK), and in *tert*-butyl methyl ether (MTBE). LS, SAXS, and viscosity measurements in dilute

solution were employed to determine the $P(q)$, $\langle S^2 \rangle_z$, and the intrinsic viscosity $[\eta]$. The obtained data were analyzed in terms of the wormlike chain model mainly to determine h and λ^{-1}. The parameters indicate that linear ATODC has an appreciably extended local helical structure and high chain stiffness while the latter parameter λ^{-1} in THF is lower than those for amylose alkylcarbamates with shorter side chains. This is most likely due to the repulsion between relatively long side groups. This chain extension and less stiff main chain were more significantly observed for the cyclic chains. Lyotropic liquid crystallinity in concentrated solutions supports the high rigidity of ATODC and cATODC chains in solution.

In Chapter V, coated-type chiral stationary phases (CSPs) for high-performance liquid chromatography (HPLC) were prepared from 3 cADMPC samples of which N_w ranges from 31 to 150, and 3 linear ADMPC samples ranging in N_w from 41 to 140. Immobilized-type CSPs were also prepared from enzymatically synthesized cyclic and linear amylose samples with 3-(triethoxysilyl)propyl linkers (cADMPCi and ADMPCi) of which of which N_w is from 30 to 210. Both coated-type and immobilized-type CSPs of cyclic samples showed appreciably different chiral separation ability comparing with those for coated-type CSPs of the corresponding linear chain, while those were fairly close to the immobilized-type CSPs when we chose a mixed eluent of hexane and 2-propanol. This suggests that the local helical structure of the immobilized polysaccharide chains is rather similar to that for cADMPC. These results indicate that the local conformation of the polysaccharide derivatives plays an important role for the chiral separation behavior.

List of Publications

The contents of this thesis have been published or will be published in following papaers:

(1) Ryoki, A.; Ida, D.; Terao, K. Scattering Function of Semi-Rigid Cyclic Polymers Analyzed in Terms of Worm-like Rings: Cyclic Amylose Tris(Phenylcarbamate) and Cyclic Amylose Tris(*n*-Butylcarbamate). *Polym. J.* **2017**, *49*, 633–637. DOI: 10.1038/pj.2017.27. (Chapter II)

(2) Ryoki, A.; Yokobatake, H.; Hasegawa, H.; Takenaka, A.; Ida, D.; Kitamura, S.; Terao, K. Topology-Dependent Chain Stiffness and Local Helical Structure of Cyclic Amylose Tris(3,5-Dimethylphenylcarbamate) in Solution. *Macromolecules* **2017**, *50*, 4000–4006. DOI: 10.1021/acs.macromol.7b00706. (Chapter III)

(3) Ryoki, A.; Kim, D.; Kitamura, S.; Terao, K. Linear and Cyclic Amylose Derivatives Having Brush like Side Groups in Solution: Amylose Tris(*n*-Octadecylcarbamate)s. *Polymer* **2018**, *137*, 13–21. DOI: 10.1016/j.polymer.2017.12.063. (Chapter IV)

(4) Ryoki, A.; Kimura, Y.; Kitamura, S.; Terao, K. Does Chain Topology Affect the Chiral Recognition Ability of an Amylose Derivative? Comparison between Linear and Cyclic Amylose Tris(3,5-dimethylphenylcarbamate) *in preparation.* (Chapter V)

Related Papers

(5) Jiang, X. Y.; Ryoki, A.; Terao, K. Dimensional and Hydrodynamic Properties of Cellulose Tris(Alkylcarbamate)s in Solution: Side Chain Dependent Conformation in Tetrahydrofuran. *Polymer* **2017**, *112*, 152–158. DOI: 10.1016/j.polymer.2017.02.012.

(6) Terao, K.; Ryoki, A. Novel Synthesis of Rigid Cyclic Polymers and Their Molecular Conformation and Intermolecular Interactions in Solution. *Kobunshi Ronbunshu* **2016**, *73*, 505–513. DOI: 10.1295/koron.2016-0037.

(7) Terao, K.; Jiang, X. Y.; Ryoki, A.; Hasegawa, H. Molecular Conformation and Intermolecular Interactions of Linear, Cyclic, and Branched Polymers in Solution by Means of Synchrotron-Radiation Small-Angle X-Ray Scattering. *Kobunshi Ronbunshu* **2018**, *75*, 254–264. DOI: 10.1295/koron.2017-0088.